

COSSERAT ANALYSIS OF MICRO-SCALE STRUCTURES

By

Sravya Kosaraju

Thesis submitted to the Faculty of the Graduate School of the
University of Maryland, College Park, in partial fulfillment
of the requirements for the degree of
Master of Science

2008

Advisory Committee:
Professor Balakumar Balachandran, Advisor / Chair
Professor Mohamad Al-Sheikhly,
Assistant Professor Teng Li

© Copyright by
Sravya Kosaraju
2008

Dedication

To my Father.

Acknowledgements

My sincere thanks and immense gratitude to my teacher and guide – Prof. Balakumar Balachandran. To him I owe everything I learnt in Mechanical Engineering and with out his support, patience and kindness, this research would have been an unfulfilled dream.

I would like to express my thanks to Prof. Mohamad Al-Sheikhly and Asst.Prof. Teng Li, for sparing their invaluable time to be a part of my thesis committee.

Support received for this work through ARO Grant No. W911NF0510076 is gratefully acknowledged.

I would like to thank my friends- Bargava, Jishnu, Srikanth and who have always been by my side and supported me in everything, my work included.

I thank my cousin-Tbava, who has done everything and more than I could have ever asked for, to make me feel at home, away from home.

Last but not the least I thank my parents, and my sister who have always supported me, and have had immense faith in me, and sacrificed these years that I have been away from them, so I find my own path.

Acknowledgements.....	iii
LIST OF FIGURES.....	vi
CHAPTER 1: INTRODUCTION.....	1
1.1 Literature Review	1
1.1.1 Cosserat Elasticity	1
1.1.2 Cosserat Theory: Shells, Rods, and Points	2
1.1.3 Cosserat Shells.....	3
1.1.4 Cosserat Rod.....	7
1.1.5 Cosserat Point	12
1.2 Microelectromechanical systems (MEMS) and applications	14
1.2.1 Microresonators and Applications.....	15
1.2.2 MEMS Gyroscopes and Applications	19
1.3 Objectives of Thesis work	21
1.4 Organization of Thesis.....	22
CHAPTER 2: COSSERAT MECHANICS OF ROD	23
2.1 Cosserat description of a curve in space.....	23
2.1.1 Convention and Nomenclature	23
2.1.2 Description.....	24
2.2 Governing Equations of Motion	26
2.3 The Rotation Matrix – Parameterization	27
2.4 Generic Parameterization (methods) preferred for Cosserat formulation	29
2.4.1 Direction Cosine Matrix (DCM): (Greenwood, 1988).....	29
2.4.3 Quaternion (as discussed by Hoffmann, 2002).....	32
2.4.4 Other Methods	33
2.6 Energy Expressions and the Extended Hamilton Principle	41
CHAPTER 3: LINEAR ANALYSIS OF MICRO-SCALE STRUCTURES.....	43
3.1 Motivation.....	43
3.2 Micro-scale structures of interest.....	43
3.3 Cosserat Cantilever Analysis.....	46
3.3.1 Shape functions.....	47
3.3.2 System Energy	49
3.3.4 Cosserat beam solution.....	52
3.4 Comparisons with Euler Bernoulli Theory and Remarks.....	56
CHAPTER 4: TETHER SUSPENDED MICROMACHINED GYROSCOPE	57
4.1 Motivation.....	57
4.2 Gyroscope Model.....	58
4.2.1 Nonlinear Tether modeling.....	59
4.3 Perturbation analysis using the rotation angle as a gauge parameter	63

4.4 Free Body Diagrams and Torque.....	66
4.5 Perturbation analysis using an arbitrary book keeping parameter as a gauge parameter	69
CHAPTER 5: MICRORESONATOR.....	70
5.1 Motivation.....	71
5.2 Model of a Typical Micro Resonator.....	71
5.2.1 Nonlinear Beam modeling.....	73
5.2.2 System Energy	77
5.2.3 Cosserat beam solution.....	78
CHAPTER 6: SUMMARY AND SUGGESTIONS FOR FUTURE WORK.....	79
6.1 Thesis Summary	79
6.2 Conclusions	80
6.3 Recommendation for future work.....	80
BIBLIOGRAPHY.....	100

LIST OF FIGURES

1.1	E. Cosserat (1866-1931) [source: the complete biography; St. Andrews University].	1
1.2	A shell-like structure in its reference configuration. A set of unit vectors along with components of the position vector to one of the points in the shell	3
1.3	A simple Cosserat rod. Two sets of unit vectors along with position vectors to the points on the cross-sections of the endpoints are shown.	7
1.4	Sketch of the I th element with deformed values of the director vectors characterizing the cross-sections I and $I + 1$, as shown in Rubin (2000).	9
1.5	A simulated strand of surgical suture that can twist and curl during manipulation of the needle during laparoscopic surgery, as discussed by Pai (2002).	10
1.6	Orbit plane and orientation of a space tether, as discussed by Valverde <i>et al.</i> (2006).	11
1.7	A sophisticated MEMS Thermal Actuator, as discussed by Li (2006).	14
1.8	Scanning Electron Micrograph (SEM) of a 71.49-MHz free-free beam micromechanical resonator, as shown in the work of Wang et al. (2000).	17
1.9(a)	SEM of a 50 μm PZT micro-resonator	18
1.9(b)	schematic showing the details of the device structure , as shown in the work of Kumar, Li, Calhoun, Boudreaux(2004), and DeVoe (2001).	18
1.10	Classical gyroscope and Coriolis effect, as shown in the work of Herbert Classical Mechanics (1952).	19
1.11	Polysilicon surface-micro machined vibrating wheel gyroscope designed at the Berkeley Sensors and Actuators Center	20
2.1	Illustration of Cosserat rod.	25
2.2	Two Cartesian coordinate systems with a common origin and an arbitrary	30

orientation relative to each other.

2.3	Illustration of principal line.	32
3.1	Schematic of micro-scale system studied by Wang et al. (2004).	45
3.2	Illustration of a cantilever structure.	45
3.3	Cantilever beam bending	45
3.4	Cantilever beam undergoing twisting motions.	45
3.5	frequency variation with increase in aspect ratio of the beam	55
3.6	Cosserat and Euler frequency difference plotted against aspect ratio	56
4.1	Scanning electron micrograph of a rotation-based micromachined gyroscope	57
4.2	Two geometries of tether suspensions of interest: (a) inside suspended ring and (b) outside suspended ring.	57
4.3	Reference configuration (B) and present configuration (B*) of a Cosserat	58
4.4	The tether geometry and the reference configuration for the Cosserat rod. The axial centerline of the rod coincides with the reference configuration of the material curve C of the Cosserrat rod and $D_3 = e_3$.	59
4.5	Schematic of a proof mass (rotor) suspended by four identical tethers of length L.	62
4.6	Free-body diagram of an inside suspended ring	66
4.7	Free-body diagram of an outside suspended ring	66
5.1	Model of a representative microresonator	70
5.2	Position vector along the cosserat curve C of the beam.	73

CHAPTER 1: INTRODUCTION

In this introductory chapter, the history and use of Cosserat mechanics is briefly reviewed, micro-scale and macro-scale applications where they can be used are discussed, the thesis objectives are stated, and the organization of this thesis is described.



Figure 1.1: *E. Cosserat (1866-1931) [source: the complete biography; St. Andrews University].*

In developing a three-dimensional continuum theory, it is observed that a position vector describing the location of each material point, as function of time is necessary to define the motion of the chosen continuum. In pure mechanics, one uses the laws of conservation of mass and linear momentum to define the mass and the position, and in Cosserat mechanics, one uses continuum directors and imposes mass and linear momentum balance laws as restrictions on equations of continuum.

The concept of a directed media was introduced by Duhem (1893), and the two French brothers E. Cosserat and F. Cosserat (1909) were the first to present a systematic development of theories for directed continua, and hence the name “Cosserat theory”.

1.1 Literature Review

1.1.1 Cosserat Elasticity

The Cosserat theory of elasticity incorporates a local rotation of *points* as well as the translation assumed in classical elasticity; and a couple stress (torque per unit area) as

well as the force stress (force per unit area). The force stress is referred to simply as “stress” in classical elasticity in which there is no other kind of stress. The idea of a couple stress can be traced to Voigt (1887, 1894), who was active during the formative period of the theory of elasticity. In more recent years, theories incorporating couple stresses have been developed by using the full capabilities of modern continuum mechanics (Ericksen and Truesdell, 1958; Grioli, 1960; Aero and Kuvshinskii, 1960; Toupin, 1962; Mindlin and Tiersten, 1962; Mindlin, 1965; Eringen, 1968; Nowacki, 1970).

A survey of the interrelationship between generalized continuum analysis and material defects, dislocations and other inhomogeneities was presented by Kunin (1982, 1983). Eringen (1968) incorporated micro-inertia and renamed Cosserat elasticity as “micro-polar elasticity”. For an isotropic Cosserat solid, there are six associated elastic constants, in contrast to a classical elastic solid with which there are two associated elastic constants.

1.1.2 Cosserat Theory: Shells, Rods, and Points

Cosserat theory is meant to be a geometrically exact, dynamic, continuum theory for structures that undergo large deformations in space through flexure, torsion, extension, and shear. In three-dimensional modeling, the motion of the directed continuum is characterized by a position vector as well as the additional vector quantities called “directors” at each material point. Hence, for different flexural structures, one has to consider different formulations. To fully understand and appreciate this, one has to consider the three main geometrical shapes, namely, shells, rods, and points. It is noted

that for each of them, as per Cosserat theory, the directors have direct physical interpretation since they are oriented along material fibers along specific directions.

1.1.3 Cosserat Shells

A shell is a three-dimensional structure (Figure 1.2) that is thin along one of its dimensions; this can be interpreted as a curved plane with a small thickness.

A shell can be characterized by its major surfaces, namely, its bottom and top surfaces and lateral surfaces. Another way of looking at it is that a shell is a three-dimensional body with surface S and a finite thickness bounded by major surfaces. If the surface S is flat, then a shell becomes a plate.

Green and Naghdi (1973) formulated a two-dimensional theory for the propagation of fairly long water waves, by using a three-dimensional Cosserat shell theory and mapping to two-dimensional computations for analyzing wave propagation. Jog (2004) used the Cosserat shell theory, for carrying out topology optimization of shell structures, rather

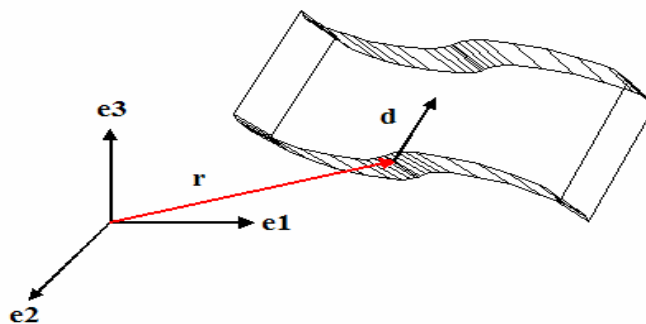


Figure 1.2: A shell-like structure in its reference configuration. A set of unit vectors along with components of the position vector to one of the points in the shell.

than elements based on the degenerated solid approach, since the shell thickness appears explicitly in the formulation, thereby greatly simplifying the sensitivity analysis. One of the well-known shell elements based on the Cosserat shell theory is the four-node element presented by Simo and Fox (1989). Although one could use this element, the use of lower-order elements often results in instabilities (such as the “checkerboard” instability) in the resulting topologies. Implementation details for six-node and seven-node triangular, and nine-node quadrilateral shell elements have also been reported in the literature.

Sansour and Bednarczyk (1999) relying on the concept of a Cosserat continuum, reduced the three-dimensional equations of a shell body to two-dimensions in a direct manner by considering the Cosserat continuum to be a two-dimensional surface. A non-linear shell theory, including transverse shear strains, with exact description of the kinematical fields is derived. The strain measures were taken to be the first and the second Cosserat deformation tensors allowing for an explicit use of a three parameter, rotation tensor. This allows for inclusion of in-plane rotations also called as drilling degrees of freedom in a natural way.

Neff (2004) examined a consistent formal dimensional reduction of a previously introduced finite-strain three-dimensional Cosserat micro-polar elasticity model to the two-dimensional situation of thin plates and shells. Contrary to the direct modeling of a shell as a Cosserat surface with additional directors, the shell model from the Cosserat bulk model, which already includes a triad of rigid directors, is used. The reduction is achieved by assumed kinematics, quadratic through the thickness. The three-dimensional transverse boundary conditions were evaluated analytically in terms of the assumed

kinematics and two unknown coefficients were determined. Further simplifications were obtained through subsequent analytical integration through the thickness. The reduced model includes size-effects, transverse shear resistance, drilling degrees of freedom, and this helps account implicitly for the thickness extension and asymmetric shift of the mid-surface.

The formal thin shell “membrane” limit without the classical h^3 -bending term is non-degenerate due to the additional Cosserat curvature stiffness and control of drill rotations. In the present formulation, the drill-rotations are strictly related to the size-effects of the bulk model and not introduced artificially for numerical convenience. Upon linearization with the zero Cosserat couple modulus $\mu_c = 0$, one recovers the well known infinitesimal-displacement Reissner-Mindlin model without size-effects and without drill-rotations. It is shown that the dimensionally reduced Cosserat formulation is well-posed for positive Cosserat couple modulus $\mu_c > 0$ by means of the direct methods of variations that follow the same line of argument used to show the purposefulness of the three-dimensional Cosserat bulk model.

Circular cylindrical shells are commonly used in engineering structures, such as planes, missiles, silos, and tanks. During their service life, these structures are subjected to loadings of various types. Ramsey (1989) investigated the stability of elastic isotropic cylindrical shells under axial compression, and examined elastic axis symmetric axial buckling of infinitely long shells by using the Cosserat surface theory. Elastic buckling analysis of glass-reinforced plastic cylindrical shells by using the finite element code NONL5 were reported by Lusher and Abu-Farsakh (1985).

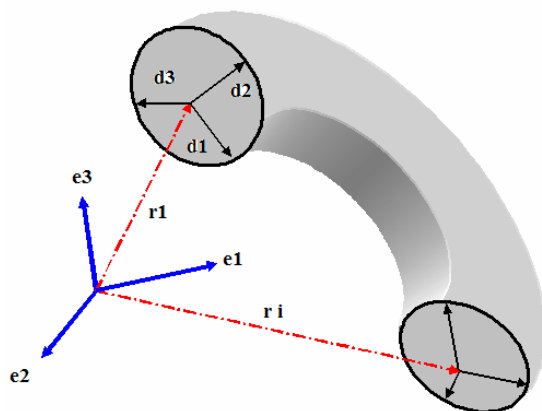
Hansen (1994) investigated the effect of random imperfections on the elastic buckling of circular cylindrical shells. Liu and Li (1991) used a stress hybrid shallow shell element to examine the influences of initial ovality and lack of straightness on the elastic buckling stress of cylindrical shells. The imperfection sensitivity of elastic axial buckling was adopted to solve some other related problems. Krishnakumar and Foster (1990) experimentally studied the influence of imposed diamond local dimples on the buckling loads of isotropic epoxy shells.

The buckling behavior of elasto-plastic circular cylindrical shells under axial compression was investigated analytically and experimentally by Lin and Yeh (1994). For analysis, a finite element code based on the updated Lagrangian formulation was established to analyze the axial buckling problem by considering nonlinear geometric and material properties.

Rubin and Benveniste (2003) studied the modelling of interfaces in elastic media in general, and in composite materials, in particular. The aim was to replace a boundary value problem consisting of a three-phase configuration, say that of a fiber–interface–matrix, by a simpler problem that involved only the fiber and matrix, plus certain matching conditions that simulated the interface. They derived the Cosserat shell model of the interface, which successfully models the original interface in a unified manner, for the full range of its material parameters relative to those of the neighbouring media. The model is derived in the setting of three-dimensional linear elasticity with small deformations and displacements. Comparisons with an existing exact solution of a coated fiber in an infinite matrix show that the solution of the reduced model shows good correspondence even for moderately thick interfaces.

It is challenging to obtain solutions of boundary value problems for shells with a general linear geometry, commonly encountered in problems of heat conduction. Rubin (1985) showed that the formulation of such problems can be simplified by using linear Cosserat theory of rigid heat conducting shells. In this theory, it is ensured that the Cosserat equations produce exact steady-state solutions for Fourier conduction with an arbitrary constant temperature gradient for all shell geometries including variable thickness. Constitutive equations, which satisfy these restrictions, are proposed and example problems of a plate and circular cylindrical and spherical shells are solved to examine the accuracy of Cosserat theory. The results of these examples show that Cosserat theory is accurate for moderately thick shells and moderately strong variation of the temperature field through the shell's thickness. In particular, the Cosserat solution converges smoothly to the exact solution as the shell becomes thin. In contrast, two other theories considered are shown to predict incorrect slopes at the thin shell limit.

1.1.4 Cosserat Rod



A rod is a three-dimensional body that is considered to be thin along two of its dimensions (Figure 1.3). In particular, the rod is characterized by its ends and its lateral surface.

Figure 1.3: A simple Cosserat rod. Two sets of unit vectors along with position vectors to the points on the cross-sections of the endpoints are shown.

The analyses of large deformations and large rotations of rods is of continued interest, since such structures can be used to model flexible robotic arms, helicopter blades, DNA strands, polymer chains, and so on. A rod-like structure is a three-dimensional body that is essentially a space curve with “small” cross-sectional areas. The non-linear elastic deformations of rods have been analyzed by using different approximations of the deformations of the cross-section and of axial extensibility.

Green and Nagdhi (1979) developed equations which are based on the theory of a Cosserat curve. Specifically, this theory allows for the following six types of deformations: (a) bending, (b) torsion, (c) axial extension, (d) tangential (transverse) shear deformation, (e) normal cross-sectional extension, and (f) normal cross-sectional shear deformation. A hierarchy of constrained theories of rods that eliminates combinations of the deformations (c)–(f) has been discussed by Nagdhi and Rubin (1986).

In the classical studies of Kirchhoff and Euler (1744), a simple rod called an “elastica” is considered. This structure has an inextensible reference curve with rigid cross-sections that remain normal to the deformed reference curve. Antman (1972) considered a more general rod theory that included extensibility of the reference curve and allowed for tangential shear deformation while retaining rigid cross-sections. References to a number of related works can be found in Antman (1972).

Recently, Rubin (2000) developed a numerical formulation to find the solution of the dynamical motion of non-linear elastic rods. In this formulation, a Cosserat rod element is used. This element takes into account all of the deformations included in the general

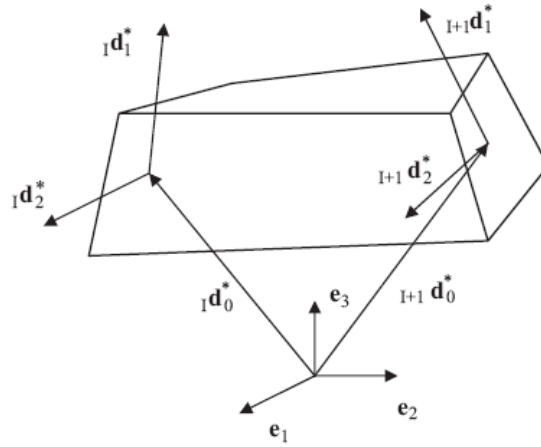


Figure 1.4: Sketch of the I^{th} element with deformed values of the director vectors characterizing the cross-sections I and $I + 1$, as shown in Rubin (2000).

rod theory of Green and Nagdhi (1979). Specifically, this rod element has 18 degrees of freedom which are determined by two sets of three director vectors ${}_I d^*_i$ and ${}_{I+1} d^*_i$ ($i = 1, 2, 3$) that characterize the cross-sections of the element (Figure 1.4). The typical I^{th} cross-section is characterized by the location of its centroid ${}_I d^*_0$ and by the two vectors $\{{}_I d^*_1, {}_I d^*_2\}$, which represent material line elements in this cross-section. Since $\{{}_I d^*_1, {}_I d^*_2\}$ are general vectors, the theory admits tangential shear deformation (i.e., the angle between the normal to the cross-section and the vector ${}_{I+1} d^*_0 - {}_I d^*_0$ can change), the cross-section admits normal extension (i.e., the lengths of ${}_I d^*_1$ and ${}_I d^*_2$ can change) and normal cross-sectional shear deformation (i.e., the angle between ${}_I d^*_1$ and ${}_I d^*_2$ can change).

Simo and Vu-Quoc (1986) developed a numerical formulation of a finite deformation rod theory proposed by Simo (1985), which is similar to that of Antman (1972) in that the cross-sections remain rigid. In this formulation, the orientations of the cross-sections are

specified by rotation tensors using Rodrigues' formula, and these authors have used special higher order shape functions to develop a Cosserat rod element based on a non-linear form of the theory of a Cosserat curve with rigid cross-sections and no shear deformation.

Cosserat rod theory has also been used by Pai (2002), who introduces Cosserat elasticity as a useful, accurate, physical model for simulating thin deformable objects. In the same work, he shows how the physical models can be discretized and solved efficiently for many applications in computer graphics. Later this combination of physical model and numerical solution (which is called as "STRAND") is shown to be a useful modelling tool for a wide variety of thin deformable objects in primitive computer graphics. Pai also briefly describes a specific application for simulating surgical sutures (Figure 1.5). Similar simulations are now used for DNA modelling.

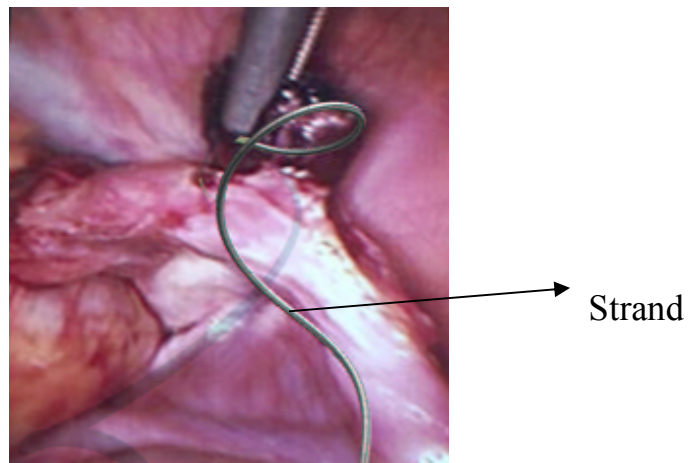


Figure 1.5: *A simulated strand of surgical suture that can twist and curl during manipulation of the needle during laparoscopic surgery, as discussed by Pai (2002).*

For a model of a power-generating tethered device of interest to the space industries, a detailed, geometrically exact bifurcation analysis was carried out by Valverde, Escalona, Dom'inguez, and Champneys (2006). The considered structure is a short electro-dynamic tether, which is comprised of a thin, long rod that is spun in a horizontal configuration from a satellite in low Earth orbit and has a massive electrically conducting disk at its free end. This system, which is located in a moving reference frame, is modelled by using a Cosserat formulation, with incorporation of effects including internal damping, intrinsic curvature due to the deployment method, and novel force and moment boundary conditions at the contactor. The problem of determining steady rotating solutions was formulated as a two-point boundary value problem. By using numerical continuation methods, a bifurcation analysis was carried out for different rotation speeds up to many times the critical resonance speed. Spatial finite differences were used to formulate the stability problem for each steady state.

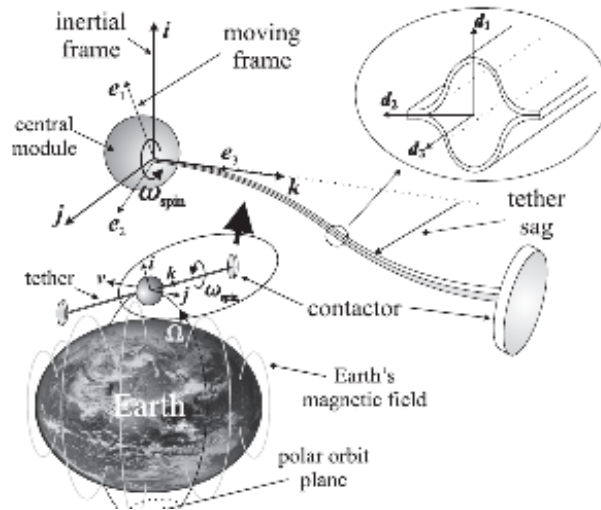


Figure 1.6: Orbit plane and orientation of a space tether, as discussed by Valverde et al. (2006).

In the present thesis work, the Cosserat rod element approach has been studied and used with constraints applied both to the system and to each rod element; the resulting rod element has the same 12 degrees of freedom as the element of Simo and Vu-Quoc (1986). However, these developments make use of standard techniques in finite elements and express the stiffness in terms of integrals over the element region of the position vector and the rotation tensor. For the purpose of this thesis, the author has used the often tried methods, and in addition, the constitutive equations developed by the direct approach are used and the quantities derived in the form of algebraic functions from a strain energy function are used; this requires no integration over the element region.

The governing equations of motion of rods are nonlinear partial differential equations, which are functions of one spatial variable and time. For static problems, the equations become ordinary differential equations, which can be solved by using standard techniques like the shooting method to satisfy the boundary conditions. By contrast, for dynamic problems, it is necessary to discretize the equations and use numerical procedures.

1.1.5 Cosserat Point

In rod theory, the constitutive equations necessarily require coupling of the geometry of the rod like structure and the material properties of the three-dimensional material from which the structure is made. For example, the typical coefficient $E \cdot I$ of the bending moment in a simple beam theory depends on the product of a material constant (young's modulus, E) and a geometric constant (the second moment of area of the cross section, I). In this regard, from a constitutive point of view the more general Cosserat theory with

two deformable directors becomes simpler than the theories in which the cross-section is rigid, since it is possible to develop restrictions on the constitutive equations for nonlinear elastic rods that use the three-dimensional strain energy function and ensure consistency between the solutions of the rod theory and those of the three-dimensional theory for all homogeneous deformations. Rubin(1995) and Simo, Rifai, and Fox (1990) also noted that the three-dimensional constitutive equations can be used in their numerical formulation of the Cosserat type shell theory when the director is deformable. Simo (1985) has discussed a convenient parameterization of the rod model developed by Antman (1972), and Simo and Vu-Quoc (1986) have considered the associated finite element formulation.

According to Rubin (1995), the theory of Cosserat point is a special continuum theory that models the deformation of a small structure that is essentially a point surrounded by some small but finite region. This theory has been used to determine numerical solutions of problems in continuum mechanics by Rubin (1995, 2004), and also by Green and Naghdi (1979) to model composite materials. Also, a unified treatment of constraints in the theory of Cosserat point has been considered by O'Reilly and Vardi (1998). This work generalized the notion of a Cosserat point to a collection of Cosserat points, which are connected by generalized constraints that can be explicit functions of time. Alternative theories of analyzing homogeneous deformations of zero dimensional bodies have been developed by Slawianowski (1982) and for pseudo-rigid bodies by Cohen and Muncaster (1984).

Rubin (2001) used a Cosserat point to model deformations of a Cosserat rod element that can experience both homogeneous and non-homogeneous deformations associated with bending and torsion, along with the initial rod curvature.

1.2 Microelectromechanical systems (MEMS) and applications

Microelectromechanical systems (MEMS) as the name suggests are electromechanical systems of the sizes ranging from few microns to a few millimeters. Any such system can comprise of one or more of the following: (a) a sensor that inputs information to the system, (b) an electronic circuit that conditions the sensor signal, and (c) an actuator that responds to the electrical signals generated within the circuit. A sensor or an actuator could be a MEMS device in its own right. A micro-system incorporating transducers and logic circuitry can be capable of sensing, signal processing, and actuation. Initial developments were driven by automotive and medical applications. However, since the mid-nineties there has been a growing interest in the use of MEMS for aeronautical applications. MEMS devices are widely used as actuators, gyroscopes, pressure sensors, filters, micro-mirrors, optical cross connects, and so on.

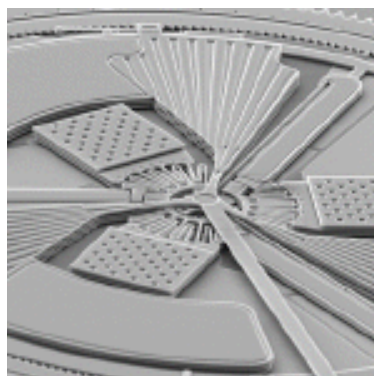


Figure 1.7: *A sophisticated MEMS Thermal Actuator, as discussed by Li (2006).*

The fabrication of MEMS devices can leverage the advances made in integrated circuit technology and enable integrated multiple functions, improved performance, batch fabrication, and reduced manufacturing cost and time. MEMS devices can be realized on a Si chip at a relatively low cost. However, to understand the device behavior, models that accurately capture the electromechanical behavior of these systems are needed. In this thesis, it is sought to use Cosserat mechanics for developing better mechanical models of MEMS structures.

1.2.1 Microresonators and Applications

As the demand for wireless communications technology continues to increase, so does the demand for effective and efficient band-pass filters, as these devices, which pass signals with frequency components inside a specific bandwidth while attenuating those outside of it, are often integral components of such technology. MEMS based mechanical resonators and filters are more desirable compared to their conventional counterparts, due to their promising characteristics (including high quality factor (Q) values) and good stability primarily due to their size, low power consumption, and ease of integration with electrical systems. MEMS filters have been shown to exhibit quality (Q) factors as high as 80,000.

Discrete filter components such as quartz and surface acoustic wave (SAW) resonators, filter components made from quartz and ceramic material currently make up the bulk of the volume and weight in receivers. Quartz resonators have the desirable characteristics of extreme frequency stability, temperature stability, and high quality factor values required for many clock operations. The typical frequency range covered by quartz

resonators is 1 kHz to 200 kHz. The typical range for ceramic SAW resonators is 50 MHz to 2 GHz. Ceramic resonators tend to have inferior Q values but they are cheaper and smaller, and they have replaced quartz resonators in many filter applications where frequency stability and high Q specifications have been relaxed. The fact that ceramic resonators are on the millimeter scale to the present day accentuates the need for new microelectromechanical systems radio frequency resonator technology. Micromachining and MEMS fabrication are technologies well suited for improving the performance, size, and cost of resonator systems.

The first demonstration of micromechanical polysilicon resonators was presented by Howe and Muller (1984). Since then, significant progress has been reported for resonators that utilize electrostatic transduction. For example, Nguyen, Wong, and Wang (2003) worked on micro-machined electromechanical filters. Roessig, Howe, and Pisano (1997) worked on MEMS accelerometers, Nguyen and Howe (1999) worked on micro-oscillators, and Lin, Howe and Pisano (1998), as well as Wang, Nguyen and Lee (2003, 2004) worked on coupled resonator filters.

There are also many other studies and applications, where the dynamics of a micro-machined structure is used to realize a mechanical transfer function between the drive and sense signals in the electrical domain. These devices have not replaced quartz and ceramic devices primarily because of the following issues: (i) the frequency range is not high enough; (ii) the need for vacuum conditions to attain a high Q ; and (iii) impedance values higher than those normally exhibited by macroscopic high- Q resonators as observed by Wang, Ren, and Nguyen (2003).

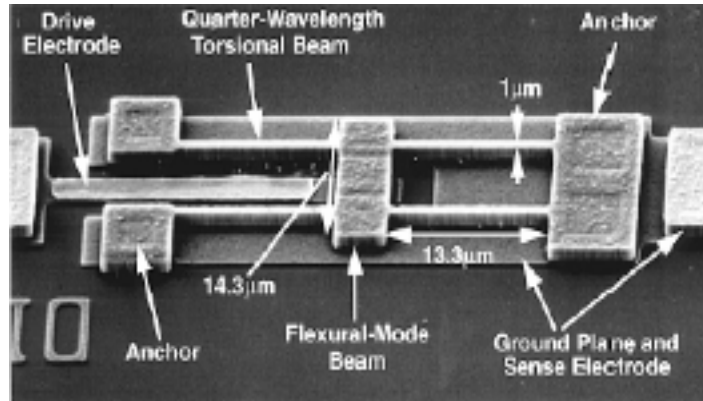


Figure 1.8: Scanning Electron Micrograph (SEM) of a 71.49-MHz free-free beam micromechanical resonator, as shown in the work of Wang et al. (2000).

By using concepts similar to those of the macro-scale resonant sensor patented by Weisbord (1969), Mullem, Blom, Fluitman, and Elwenspoek (1991), Fabula, Wagner, and Schmidt (1994), and Funk, Fabula, Flik and Larmer (1995) have reported work on bulk micro-machined piezoelectric resonators, where a clamped-clamped beam-like structure on the silicon substrate is electro-statically driven in its first resonance mode and sensed capacitively. Prak, Elwenspoek, and Fluitman (1992) developed a method to design the input/output electrodes for selectivity exciting or sensing modes. Abdalla, Reddy, Faris and Gürdal (2005) worked on the optimal design of the thickness and width for beams with different boundary conditions for maximum pull-in voltage. Turner, Miller, Hartwell, Macdonald, Strogartz, Adams and Zhang (1998, 2001) have investigated a parametrically driven torsion oscillator. Raskin, Brown, Khuri-Yakub and Rebeiz (2000) worked on parametric amplifier. DeVoe (1997) proposed a device that was an order of magnitude smaller than what was previously reported for bulk-micro-machined devices by using surface micro-machined piezoelectric filters in a process

compatible with backend CMOS processing. In this work, the center frequencies of the resonator reached up to 1.18 MHz.

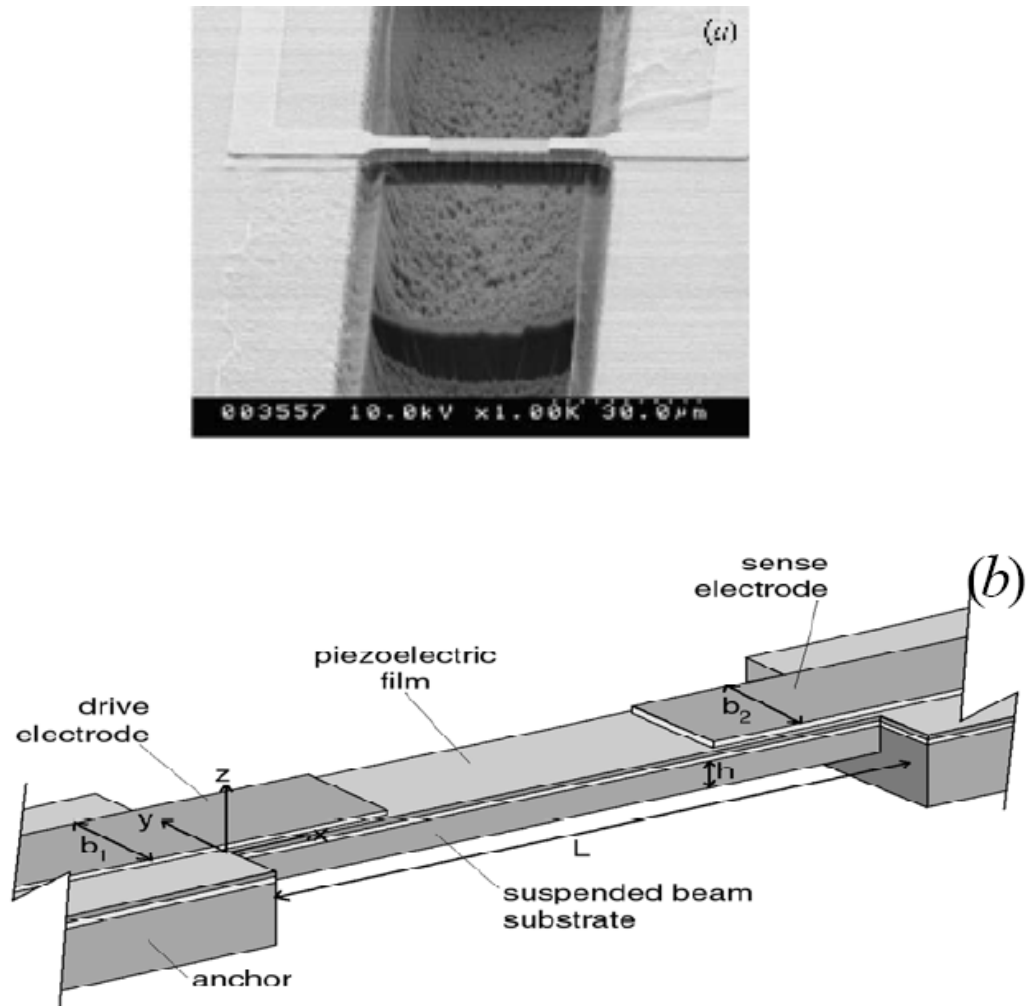


Figure 1.9: (a) SEM of a $50\ \mu\text{m}$ PZT micro-resonator, as shown in the work of Husain, Hone, Postma, Huang, Drake, Barbic, Scherer, and Roukes (2003) and (b) a schematic showing the details of the device structure, as shown in the work of Kumar, Li, Calhoun, Boudreaux, and DeVoe (2004), and DeVoe (2001).

Microresonators exhibit nonlinear behavior including jumps, buckling, and nonlinear resonance driven oscillations, as discussed in the work of Li and Balachandran (2003) and in the dissertation work of Li (2006). To understand this nonlinear behavior, it is important to consider models that will accurately capture the system behavior when it undergoes large deformations. In the present thesis work, Cosserat mechanics is used to address this point. Specifically, it is shown here, as to how one can better capture the stiffness characteristics of a system.

1.2.2 MEMS Gyroscopes and Applications

The simplest gyroscopes use a high speed, rotating inertial disk that is loosely coupled to the frame holding it. A rotation in the frame imparts a torque (rotation) to the spinning disk, which precesses (rotates) as a result (conservation of angular momentum). Practical uses usually limit the movement to measure rotation along only one axis (say, roll, pitch, or yaw axis). The induced torque is monitored by a meter that counteracts the torque with springs or a similar restoring mechanism.

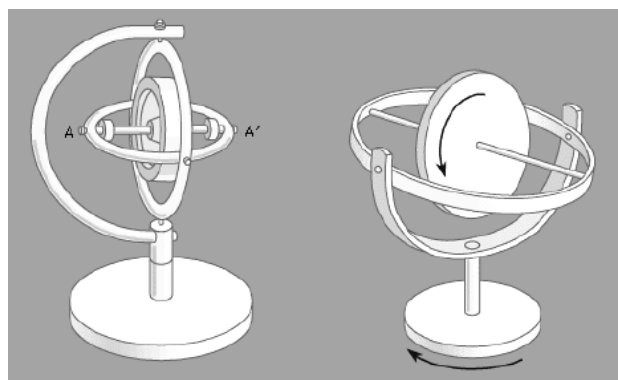


Figure 1.12: Classical gyroscope and Coriolis effect, as shown in the work of Goldstein (1952).

Microelectromechanical system (MEMS) gyroscopes are miniaturized versions of gyroscopes. A multitude of applications already have been developed for consumer and automotive markets for MEMS Gyroscopes. Examples of applications include vehicle stability control, rollover detection, navigation, load levelling/suspension control, event recording, collision avoidance; consumers, computer input devices, handheld computing devices, game controllers, virtual reality gear, sports equipment, camcorders, industrial robots, navigation of autonomous (robotic) guided vehicles, motion control of hydraulic equipment or robots, platform stabilization of heavy machinery, human transporters, yaw rate control of wind-power plants; aerospace/military; platform stabilization of avionics, stabilization of pointing systems for antennas, unmanned air vehicles, or land vehicles, inertial measurement units for inertial navigation, and many more.

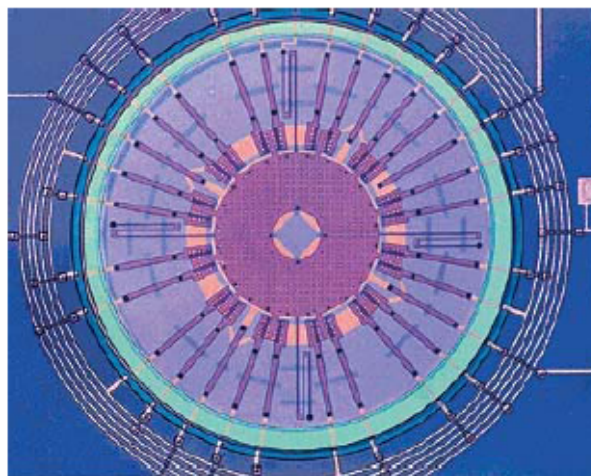


Figure 1.13: Polysilicon surface–micro machined vibrating wheel gyroscope designed at the Berkeley Sensors and Actuators Center, as discussed by Saratoga in “A Critical Review of MEMS Gyroscopes Technology and Commercialization Status”.

Almost all reported micro-machined gyroscopes use vibrating mechanical elements (proof-mass) to sense rotation. They have no rotating parts that require bearings, and hence they can be easily miniaturized and batch fabricated by using micro-machining techniques. All vibratory gyroscopes are based on the transfer of energy between two vibration modes of a structure caused by Coriolis acceleration. Coriolis acceleration, named after the French scientist and engineer G. G. de Coriolis (1792–1843), is an apparent acceleration that arises in a rotating reference frame and it is proportional to the rate of rotation.

1.3 Objectives of Thesis work

The overall objective is to explore the use of Cosserat mechanics to study micro-scale structures. Specific objectives include the following:

- (a) study the mechanics of Cosserat theory and its various formulations; their applicability to various systems
- (b) compare the results obtained by using a linear Cosserat model to those obtained by using a classical Euler–Bernoulli beam model for a cantilever structure
- (c) study different parameterization schemes of Cosserat theory for a generic microresonator model and verify the results obtained by Wang, Liu, and Cao (2004)
- (d) study the nonlinear stiffness characteristics of a gyroscope inclusive of the third order nonlinearities, explore two different parameterization schemes, and compare the results with those obtained by O’Reilly, Pisano, and Davis (2004)

1.4 Organization of Thesis

The thesis is organized as follows. The first chapter has been used to provide an introduction to Cosserat theory, a brief introduction to micro-systems, and outline the connection between the thesis work and micro-scale applications. In the second chapter, the author presents in detail, the various formulations of Cosserat theory. In Chapter 3, results obtained in the planar case with Cosserat analysis are compared with other results for two different micro-scale systems. In Chapter four, the work carried out with gyroscope tethers is reported, and subsequently, in Chapter five, results obtained on the dynamics of microresonators are discussed. Conclusions that can be drawn from this work are presented together with suggestions for future work in Chapter six.

CHAPTER 2: COSSERAT MECHANICS OF ROD

In this chapter, Cosserat continuum theory for rods, which forms the basis for this thesis research, is presented. The importance of rotation parameterization is examined, and the microresonator model developed using the Cosserat mechanics by Wang, Liu, and Cao (2004) is reviewed to illustrate the Cosserat rod mechanics based formulation. This formulation is used to study, linear model of a micro-scale structural system in Chapter 3.

2.1 Cosserat description of a curve in space

2.1.1 Convention and Nomenclature

The following conventions are used throughout this thesis. Vectors which are elements of Euclidean 3-space \mathbb{R}^3 , are denoted by lowercase, italicized symbols, for example, u, v and vector valued functions are denoted by lowercase, arrow above italicized symbols, for example, \vec{u}, \vec{v} ; Tensors and matrices are denoted by upper-case, uppercase, italic symbols, for example, I, J ; The three unit vectors $\{e_1, e_2, e_3\}$ are assumed to form a fixed right-handed orthogonal basis. The summation convention for repeated indices is used.

The symbols ∂_t and ∂_ξ denote differentiation with respect to time t and arc length parameter ξ , respectively. The symbols $(\dot{})$ and $(\overset{\circ}{})$ also denote differentiation with respect to time, “ t ” and length “ ξ ”, respectively.

2.1.2 Description

The Cosserat rod theory discussed here assumes that rods behave as shearable, extensible bodies. The motion of the rod is considered to be along the centroidal line along the rod, and this centroidal line is referred to as a “curve”.

There two ways, in which Cosserat mechanics is often formulated. Typically, for static applications, the formulation is based on displacement fields, and for dynamic applications, one goes beyond displacement fields and uses time dependent generalized coordinates in the formulation. For both formulations, the initial set up of the system’s (rod) configuration (Figure 2.1); that is, the parameterization of a curve in space, plays an essential role in the development of the governing equations. This parameterization remains the same for both static and dynamic applications.

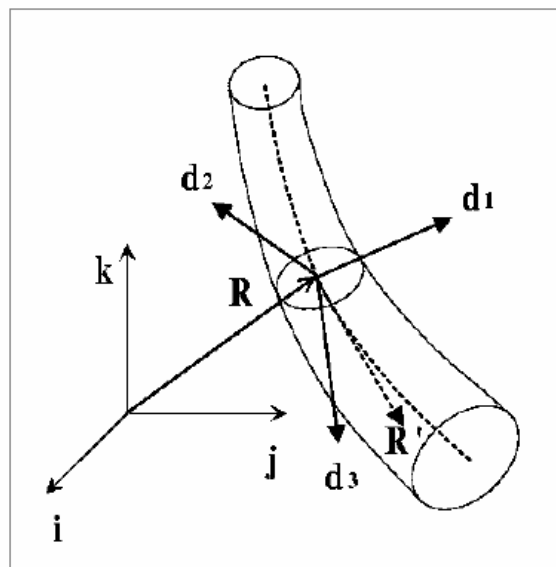


Figure 2.1: Illustration of Cosserat rod.

It is assumed that one has a regular curve in \mathbb{R}^3 (with no singular points), a parameterized curve \mathcal{C} , which is a map of “a” of an interval $P = [\xi_0, \xi_1] \in \mathbb{R}$ into \mathbb{R}^3 ; each point on Curve \mathcal{C} is a convected coordinate. According to the Euler-Bernoulli hypothesis, the plane cross-sections undergo only rigid rotations during a deformation and remain in the plane after the deformation and preserve their shape and area; in keeping with this, the area of cross-section ‘A’(not a matrix) is assumed to be a constant.

In the configuration shown in Figure 2.1, the Cosserat rod is defined by

- (a) A position vector, $\vec{r}_i = \vec{r}_i(\xi, t), i = (1, 2, 3)$ of the material points of \mathcal{C}
- (b) A local, orthonormal triad, $\vec{d}_i = \vec{d}_i(\xi, t), i = (1, 2, 3)$ moving along the cross-section of \mathcal{C}
- (c) A reference configuration, $\vec{D}_i = \vec{D}_i(\xi), i = (1, 2, 3)$

The reference configuration gives the flexibility of simulating the dynamic nature of system (rod), by simple parameterization either in terms of rotation matrices or in terms of linear or nonlinear extensions; in many ways, it can be said that this configuration helps defines the system. Placing restrictions on the reference configuration, and hence, the whole system allows for a simpler theory can be developed, called the “constrained Cosserat theory.”

2.2 Governing Equations of Motion

By using a free-body diagram of the system, assuming small strains and small displacements and linearizing, and carrying out a force balance and a moment balance, one obtains equations (2.1) and (2.2) to describe a Cosserat rod. In cases where the forces and moments acting at particular point are not straightforward and the direction of application is not known, the extended Hamilton's principle (Meirovitch, 2001) can be employed to arrive at the same.

$$\rho(\xi)A(\xi)\partial_{\eta}r = \partial_{\xi}n(\xi,t) + f(\xi,t) \quad (2.1)$$

$$\partial_{\xi}h(\xi,t) = \partial_{\xi}m(\xi,t) + v(\xi,t) \times n(\xi,t) + l(\xi,t) \quad (2.2)$$

In equations (2.1) and (2.2), $n(\xi,t) = n_i(\xi,t)d_i(\xi,t)$ and $m(\xi,t) = m_i(\xi,t)d_i(\xi,t)$ are respectively contact force and torque densities, while $h(\xi,t) = h_i(\xi,t)d_i(\xi,t)$ denotes the angular momentum densities. The quantities $f(\xi,t)$ and $l(\xi,t)$ denote the prescribed external force and torque densities, respectively. The axial stiffness, bending stiffness, and torsion stiffness are represented by the tensors K , J and I , respectively. Following the definition given by Antman (1972), one has

$$\begin{aligned} K(\xi,t) &= K_{ii}(\xi,t)(d_i(\xi,t) \otimes d_i(\xi,t)), \\ J(\xi,t) &= \sum_{i,j=1}^2 J_{ij}(\xi,t)(d_i(\xi,t) \otimes d_j(\xi,t)) + J_{33}(\xi,t)(d_3(\xi,t) \otimes d_3(\xi,t)), \\ I(\xi,t) &= \sum_{i,j=1}^2 I_{ij}(\xi,t)(d_i(\xi,t) \otimes d_j(\xi,t)) + I_{33}(\xi,t)(d_3(\xi,t) \otimes d_3(\xi,t)) \end{aligned} \quad (2.3)$$

The corresponding components are given by

$$\begin{aligned}
K_{11} &= K_{22} = GA(\xi) \\
K_{33} &= EA(\xi) \\
J_{11} &= \int_{A(\xi)} E\eta^2 dA \\
J_{22} &= \int_{A(\xi)} E\zeta^2 dA \\
J_{33} &= \int_{A(\xi)} E(\eta^2 + \zeta^2) dA \\
J_{12} &= -J_{21} = \int_{A(\xi)} E\zeta\eta dA \\
I_{11} &= \int_{A(\xi)} \rho(\xi)\eta^2 dA \\
I_{22} &= \int_{A(\xi)} \rho(\xi)\zeta^2 dA \\
I_{33} &= \int_{A(\xi)} \rho(\xi)(\eta^2 + \zeta^2) dA \\
I_{12} &= -I_{21} = \int_{A(\xi)} \rho(\xi)\eta\zeta dA
\end{aligned} \tag{2.4}$$

where E and G are the Young's modulus and shear modulus, respectively; ρ is material density; A is the area of cross-section; and ' ζ ' and ' η ' are variables used to define positions along the e_1 and e_2 directions, respectively. It is noted that in this formulation the strains are expressed in terms of displacements in the force and moment balance equations.

2.3 The Rotation Matrix – Parameterization

There are many ways to parameterize rotations. The choice of a particular parameterization (or *any* parameterization at all) depends on the application of interest.

The primary applications of rotations in mechanics are to encode orientations and describe and control the motion of rigid bodies and articulations in the transformation; the backbone of most mechanical systems, require not only free rotations, but also constrained one, two, and three degree-of-freedom (DOF) rotations whose angular range of motion is limited to more faithfully model the motions of examples such as ball and socket joints.

Parameterizing rotations for few applications is problematic mainly because rotations are non-Euclidean in nature (traveling infinitely far in any direction will bring one back to the starting point an infinite number of times). Any attempt to parameterize the entire set of three DOF rotations by an open subset of Euclidean space (as do Euler angles) will suffer from *gimbal lock*, the loss of rotational degrees of freedom, due to singularities in the parameter space. Intuitively, a singularity is a continuous subspace of the parameter space, all of whose elements correspond to the same rotation, thus movement within the subspace produces no change in rotation. Parameterizations that are themselves defined over non-Euclidean spaces (such as the set of unit quaternions embedded in \mathbb{R}^4) may remain singularity-free, and thus avoid gimbal lock. Employing such parameterizations is complicated. It is mentioned that most numerical tools often assume Euclidean parameterizations.

A number of geometrical approaches have been developed to deal with rotational motion. Approaches based on the exponential map of rotation, the Gibbs-Rodrigues parameters, the Wiener-Milencovic parameters (conformal rotation vector), and Eulerian angles and Euler-Rodrigues parameters (unit quaternions) and others have been used for

parameterization. To get a better understanding of this subject, next a presentation of rotation and rigid body motion parameterization is made.

2.4 Generic Parameterization (methods) preferred for Cosserat formulation

2.4.1 Direction Cosine Matrix (DCM): (Greenwood, 1988)

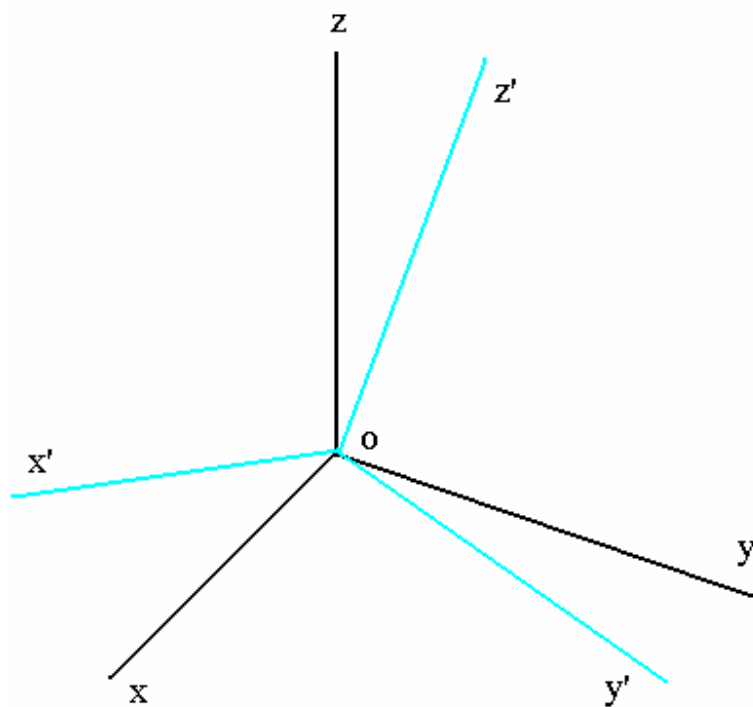


Figure 2.2: Two Cartesian coordinate systems with a common origin and an arbitrary orientation relative to each other.

Any two systems with the same origin but different orientation can be represented in a way that one system components are given by the cosines of the angles between the axes of the first and second systems.

$$\begin{bmatrix} x' \\ y' \\ z' \end{bmatrix} = \begin{bmatrix} C_{x'x} & C_{x'y} & C_{x'z} \\ C_{y'x} & C_{y'y} & C_{y'z} \\ C_{z'x} & C_{z'y} & C_{z'z} \end{bmatrix} \begin{bmatrix} x \\ y \\ z \end{bmatrix}$$

In the transformation taking one from the reference axes to the rotated axes, the coefficients C 's represent the direction cosines. The ease with which vectors can be rotated by using a DCM, as well as the ease of combining successive rotations, make the DCM a very useful and popular way to represent rotations, even though it is less concise than other representations.

2.4.2 Euler parameters -Baruh(1999)

The mathematics of Euler parameters was first introduced by Hamilton, in 1843. In order that the solutions be free from nonlinearities and avoid singularities, a preferable set of parameters used usually are the Euler Parameters. These parameters increase the number of variables one deals with from three to four, but they eliminate the nonlinearities and many of the numerical problems. Due to the increase in the number of variables, there will be redundancy with the use of Euler parameters. These parameters have been inspired from the Euler's theorem, which states that any rotation of the rigid body about a point can be accomplished by a single rotation by an angle ϕ , called the principal angle and direction cosines of the principal line.

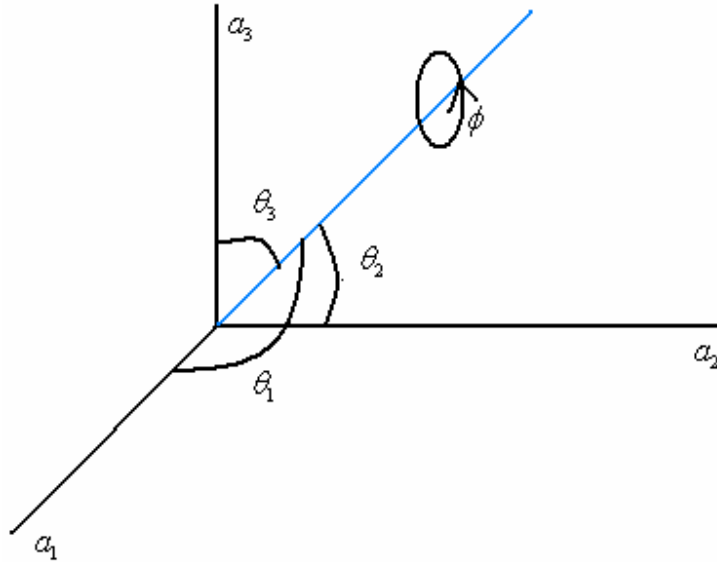


Figure 2.3: Illustration of principal line.

The direction cosines of the principal line are given by

$$c_1 = \cos \theta_1, c_2 = \cos \theta_2, c_3 = \cos \theta_3,$$

and the Euler parameters are defined as

$$e_0 = \cos \frac{\phi}{2}$$

$$e_1 = c_1 \sin \frac{\phi}{2}$$

$$e_2 = c_2 \sin \frac{\phi}{2}$$

$$e_3 = c_3 \sin \frac{\phi}{2}$$

2.4.3 Quaternion (as discussed by Hoffmann, 2002)

William Rowan Hamilton (1805-1865) had invented the quaternions. Quaternions are quadruples of real numbers, for which a special multiplication is defined.

$$Q = [q_1, q_2, q_3, q_4]^T$$

The rules for multiplication can be understood if one represents the quaternions by three complex base vectors i, j, k .

$$Q = q_1i + q_2j + q_3k + q_4$$

The first three components can be written as a vector or a column matrix “q”.

$$Q = q + q_4$$

This scheme is valid for the multiplication, for example, $j.k = i$

	i	j	k
i	-1	k	-j
j	-k	-1	i
k	j	-i	-1

A multiplication among two quaternions say Q and S, can now be executed as follows

$$\begin{aligned}
Q.S &= (q_1i + q_2j + q_3k + q_4) \cdot (s_1i + s_2j + s_3k + s_4) = \begin{bmatrix} q_4 & -q_3 & q_2 & q_1 \\ q_3 & q_4 & q_1 & q_2 \\ q_2 & q_1 & q_4 & q_3 \\ -q_1 & -q_2 & -q_3 & q_4 \end{bmatrix} \begin{bmatrix} s_1 \\ s_2 \\ s_3 \\ s_4 \end{bmatrix} \\
&= R(Q)S
\end{aligned}$$

Thus the result of multiplication is product of a quaternion matrix $R(Q)$, which is assigned to Q and the quaternion S , as column matrix. The norm of quaternion is one or is made to be one. For each quaternion Q , the components q_1, q_2, q_3, q_4 depend on the type and sequence of rotation angles which are called the Euler angles. The vector formulation of Euler parameters, which is used for quaternions was developed by Heaviside, O. Quaternions are often used for rotational transformations and angular velocity transformations.

Quaternions have been used to parameterize the rotation of DNA strings by Pai (2004) to reduce the Hamiltonian into a canonical Hamiltonian form and thus simplify the nature of the nonlinear equations.

2.4.4 Other Methods

Exponential parameterization (Kreizig, 2005)

Every non-zero vector in \mathbb{R}^3 has a direction and magnitude. One can associate a rotation with each vector by specifying the direction as an axis of rotation and the magnitude as the amount by which to rotate around the axis. If one augments this relationship by associating the zero vector with the identity rotation, the relationship is continuous, and

this is known as the exponential map. In short, the exponential map maps a vector in \mathbb{R}^3 describing the axis and magnitude of a three DOF rotation to the corresponding rotation. Unlike the quaternion parameterization, this parameterization is Euclidean, and so, it does contain singularities. There are many different formulations of the exponential map.

Rodrigues parameters (Baruh, 1999)

Rodrigues parameters are defined in terms of principal axis (Euler parameters) as

$$\rho_i = \frac{e_i}{e_0}; (i = 1, 2, 3)$$

and the Rodrigues vector is defined as

$$\rho = n \tan(\phi/2)$$

where n is the unit vector associated with principal line.

Cayley-Klein Parameters

The parameters α , β , γ and δ , like the three Euler angles, provide a way to uniquely characterize the orientation of a solid body. These parameters satisfy the identities

$$\begin{aligned} \alpha\bar{\alpha} + \gamma\bar{\gamma} &= 1 \\ \alpha\bar{\alpha} + \beta\bar{\beta} &= 1 \\ \beta\bar{\beta} + \delta\bar{\delta} &= 1 \\ \bar{\alpha}\beta + \bar{\gamma}\delta &= 0 \\ \alpha\delta - \beta\gamma &= 1 \\ \beta &= -\bar{\gamma} \\ \delta &= \bar{\alpha} \end{aligned}$$

2.5 Example: Rotation parameterization for a flexible beam (Rod)

In the work of Wang, Liu, and Cao (2004), the parameterization of rotation and its subsequent generalization to the case of general rigid motion, involving coupled translation and rotation are addressed. An ortho-normal basis $d_i(s,t);(i=1,2,3)$ is defined, at any chosen cross-section located at s , and these vectors are referred to as “basis or local directors”. These directors are such that d_1 and d_2 lie in the plane of the rotated cross-section and d_3 is normal to the rotated cross-section.

At any given time, \vec{r} , the position vector from the origin of the inertial frame to the point on the Cosserat curve describes the axis of the rod whose cross-section orientations are determined by $d_i; (i = 1,2,3)$ such that $\partial_s \vec{r} \cdot d_3 > 0$. This condition implies the following: (a) the local ratio of the deformed length to reference length of the axis cannot be reduced to zero since $|\partial_s \vec{r}| > 0$ and (b) a typical cross-section ($s = s_0$) cannot undergo a total shear in which the plane determined by d_1 and d_2 is tangent to the curve $r(s; t)$ at $r(s_0; t)$.

Thus, the position vector can be written in terms of the unit vectors fixed in the inertial frame as

$$\vec{r}(s,t) = r_i(s,t)e_i = x(s,t)e_1 + y(s,t)e_2 + z(s,t)e_3 \quad (2.5)$$

The motion involves both the velocity of the curve, $\partial_t r(s;t)$ and angular velocity of the cross-sections $w(s; t)$; that is,

$$\partial_t d_i(s, t) = w(s, t) \times d_i(s, t) \quad (2.6)$$

In a similar manner, the strains of the Cosserat rod are classified as follows:

“Linear strain” vector $v(s, t)$

$$v(s, t) = \partial_s r(s, t) \quad (2.7)$$

and

“Angular strain” vector $u(s, t)$

$$\partial_s d_i(s, t) = u(s, t) \times d_i(s, t) \quad (2.8)$$

Since the basis $\{d_1; d_2; d_3\}$ is convenient for the intrinsic description of deformation, the relevant vector valued functions are decomposed with respect to it as

$$\begin{aligned} v(s, t) &= v_i d_i(s, t) \\ u(s, t) &= u_i d_i(s, t) \\ w(s, t) &= w_i d_i(s, t) \end{aligned} \quad (2.9)$$

In order to parameterize, here, it is chosen to employ the rotational vector that is free both of singularities and constraints. Because of the orthogonality of the chosen unit vectors, the rotation matrix is a proper orthogonal matrix, its nine components can be expressed in terms of three independent parameters. Let S represent the spin matrix of a vector $a = a_i e_i$. This is given by

$$S(a) = \begin{pmatrix} 0 & -a_3 & a_2 \\ a_3 & 0 & -a_1 \\ -a_2 & a_1 & 0 \end{pmatrix} \quad (2.10)$$

Then, the rotation matrix R is determined by the expression

$$R(\phi) = I + \left(\frac{\sin \phi}{\phi}\right)S(\phi) + \left(\frac{1 - \cos \phi}{\phi^2}\right)S^2(\phi) \quad (2.11)$$

where $\phi = \phi_i e_i$ is the rotational vector, $S(\phi)$ is the spin matrix of ϕ defined by equation (2.10), and $\phi = (\phi_1^2 + \phi_2^2 + \phi_3^2)^{\frac{1}{2}}$ is the rotational norm or the length of the rotational vector. An expansion of trigonometric functions in equation (2.11) by using Taylor series yields

$$R = I + S + \frac{1}{2!}S^2 + \frac{1}{3!}S^3 + \dots + \frac{1}{n!}S^n + \dots = \exp(S) \quad (2.12)$$

Thus, the rotation matrix may alternatively be expressed by an exponential map, the exponentiation of the spin matrix associated with the rotational vector. Conversely, taking a given orthogonal matrix R as a rotation matrix, the associated rotation vector ϕ can be derived from equations (2.10) and (2.11). The rotational norm ϕ can be calculated from

$$\phi = \cos^{-1}\left(\frac{\text{Tr}(R) - 1}{2}\right) \quad (2.13)$$

By taking the matrix logarithm of R , one can obtain the skew-symmetric matrix S as follows.

$$S = \log(R) = \frac{\phi}{2 \sin \phi} (R - R^T) \quad (2.14)$$

Therefore, $\phi = \phi_i e_i$ with $\phi_1 = -S_{23}$, $\phi_2 = S_{13}$ and $\phi_3 = -S_{12}$.

For a typical beam component in used in a MEMS structure, the effect of shearing deformation can be negligible, and the cross-section of the rod can be assumed to be perpendicular to the tangent to the Cosserat curve; that is,

$$v(s, t) = \partial_s r(s, t) = |\partial_s r(s, t)| d_3(s, t) \quad (2.15)$$

where,

$$\begin{aligned} v_1(s, t) &= \frac{\partial_s x(s, t)}{|\partial_s r(s, t)|} \\ v_2(s, t) &= \frac{\partial_s y(s, t)}{|\partial_s r(s, t)|} \\ v_3(s, t) &= \frac{\partial_s z(s, t)}{|\partial_s r(s, t)|} \end{aligned} \quad (2.16)$$

It is assumed that the local directors $\{d_1, d_2, d_3\}$, can be obtained by going through the following steps:

Step 1: Rotate $\{e_1, e_2, e_3\}$, about e_3 , with an angle φ , and label the new directors as $\{\tilde{d}_1, \tilde{d}_2, e_3\}$. The rotation matrix, R_a associated with the rotation vector $\varphi_a = \varphi e_3$ is given by

$$R_a = \begin{pmatrix} \cos \varphi & -\sin \varphi & 0 \\ \sin \varphi & \cos \varphi & 0 \\ 0 & 0 & 1 \end{pmatrix} \quad (2.17)$$

Step 2: Rotate $\{\tilde{d}_1, \tilde{d}_2, e_3\}$ to $\{d_1, d_2, d_3\}$, assuming $d_3 \neq e_3$, The rotation vector and the rotation matrix are given by

$$\varphi_b = \frac{-\sin^{-1} \sqrt{v_1^2 + v_2^2}}{\sqrt{v_1^2 + v_2^2}} v_2 \tilde{d}_1 + \frac{-\sin^{-1} \sqrt{v_1^2 + v_2^2}}{\sqrt{v_1^2 + v_2^2}} v_1 \tilde{d}_2 \quad (2.18)$$

$$R_b = \begin{pmatrix} \frac{v_1^2 v_3 + v_2^2}{\sqrt{v_1^2 + v_2^2}} & \frac{v_1 v_2 (v_3 - 1)}{\sqrt{v_1^2 + v_2^2}} & v_1 \\ \frac{v_1 v_2 (v_3 - 1)}{\sqrt{v_1^2 + v_2^2}} & \frac{v_2^2 v_3 + v_1^2}{\sqrt{v_1^2 + v_2^2}} & v_2 \\ -v_1 & v_2 & v_3 \end{pmatrix}$$

From the above, the local moving directors $\{d_1, d_2, d_3\}$, can be derived to be

$$\begin{aligned} d_1 &= \left(\frac{v_1^2 v_3 + v_2^2}{v_1^2 + v_2^2} \cos \varphi + \frac{v_1 v_2 (v_3 - 1)}{v_1^2 + v_2^2} \sin \varphi \right) e_1 \\ &+ \left(\frac{v_2^2 v_3 + v_1^2}{v_1^2 + v_2^2} \sin \varphi + \frac{v_1 v_2 (v_3 - 1)}{v_1^2 + v_2^2} \cos \varphi \right) e_2 \\ &- (v_1 \cos \varphi + v_2 \sin \varphi) e_3 \end{aligned} \quad (2.19)$$

$$\begin{aligned}
d_2 = & \left(-\frac{v_1^2 v_3 + v_2^2}{v_1^2 + v_2^2} \sin \varphi + \frac{v_1 v_2 (v_3 - 1)}{v_1^2 + v_2^2} \cos \varphi \right) e_1 \\
& + \left(\frac{v_2^2 v_3 + v_1^2}{v_1^2 + v_2^2} \cos \varphi - \frac{v_1 v_2 (v_3 - 1)}{v_1^2 + v_2^2} \sin \varphi \right) e_2 \\
& - (v_1 \cos \varphi - v_2 \sin \varphi) e_3
\end{aligned} \tag{2.20}$$

$$d_3 = v_1 e_1 + v_2 e_2 + v_3 e_3 \tag{2.21}$$

Expanding the directors in terms of polynomials in φ and retaining the terms up to third order, one arrives at

$$\begin{aligned}
d_1(s, t) \approx & \left(1 - \frac{1}{2} \varphi^2(s, t) - \frac{1}{2} v_1^2(s, t) - \frac{1}{2} v_1(s, t) v_2(s, t) \varphi(s, t) \right) e_1 \\
& + \left(\varphi(s, t) - \frac{1}{2} v_1(s, t) - \frac{1}{2} v_2^2(s, t) \varphi(s, t) - \frac{1}{6} \varphi^3(s, t) \right) e_2 \\
& + \left(-v_1(s, t) - v_2(s, t) \varphi(s, t) + \frac{1}{2} v_1(s, t) \varphi^2(s, t) \right) e_3
\end{aligned} \tag{2.22}$$

$$\begin{aligned}
d_2(s, t) \approx & \left(-\varphi(s, t) - \frac{1}{2} v_1(s, t) v_2(s, t) + \frac{1}{2} v_1^2(s, t) \varphi(s, t) + \frac{1}{6} \varphi^3(s, t) \right) e_1 \\
& + \left(1 - \frac{1}{2} \varphi^2(s, t) - \frac{1}{2} v_2^2(s, t) - \frac{1}{2} v_1(s, t) v_2(s, t) \varphi(s, t) \right) e_2 \\
& + \left(-v_2(s, t) + v_1(s, t) \varphi(s, t) + \frac{1}{2} v_2(s, t) \varphi^2(s, t) \right) e_3
\end{aligned} \tag{2.23}$$

$$d_3(s, t) \approx v_1(s, t) e_1 + v_2(s, t) e_2 + \left(1 - \frac{1}{2} v_1^2(s, t) - \frac{1}{2} v_2^2(s, t) \right) e_3 \tag{2.24}$$

The rotational vector ϕ in the Inertial basis is given by

$$\phi = \phi_x(s, t) + \phi_y(s, t) + \phi_z(s, t) \quad (2.25)$$

Now using the already defined rotational matrices, R_a and R_b the spin matrix associated with respect to the rotational vector ϕ can be derived from

$$\phi = \cos^{-1} \left(\frac{\text{Tr}(R_a R_b) - 1}{2} \right) \quad (2.26)$$

and

$$S = \log(R_a R_b) = \frac{\phi}{2 \sin \phi} (R_a R_b - R_a^T R_b^T) \quad (2.27)$$

2.6 Energy Expressions and the Extended Hamilton Principle

As a representative example, it is mentioned that the displacement fields can be expanded as series expansions of the form

$$\begin{aligned} x(\xi, t) &= x_1(\xi) \cdot \phi(t) + x_2(\xi) \cdot (\phi(t))^2 + x_3(\xi) \cdot (\phi(t))^3 \\ y(\xi, t) &= y_1(\xi) \cdot \phi(t) + y_2(\xi) \cdot (\phi(t))^2 + y_3(\xi) \cdot (\phi(t))^3 \\ z(\xi, t) &= z_1(\xi) \cdot \phi(t) + z_2(\xi) \cdot (\phi(t))^2 + z_3(\xi) \cdot (\phi(t))^3 \\ \theta(\xi, t) &= \theta_1(\xi) \cdot \phi(t) + \theta_2(\xi) \cdot (\phi(t))^2 + \theta_3(\xi) \cdot (\phi(t))^3 \end{aligned} \quad (2.28)$$

This is further discussed in Chapter 4, where other parameterizations are also presented.

In order to determine the system equations, the extended Hamilton's principle is used.

This reads as

$$\int_{t_1}^{t_2} \delta(T - V)dt + \int_{t_1}^{t_2} \delta\bar{W}dt = 0 \quad (2.29)$$

where T is the total kinetic energy and V is the potential energy of the system, $\delta\bar{W}$ is the virtual work done and δ represents the variation. Here,

$$T = \frac{1}{2}(\rho A \partial_t r \cdot \partial_t r + I(w, w)) \quad (2.30)$$

$$V = \frac{1}{2}(J(u, u) + K_{33}(\bar{v}_3 - 1)^2) \quad (2.31)$$

where

u is the angular strain defined by $u = \frac{1}{2}d_i \times \partial_s d_i$

\bar{v}_3 is the linear stain per unit length, $\bar{v}_3 = |\partial_\xi r|$

and w is the angular velocity, $w = \frac{1}{2}d_i \times \partial_t d_i$.

CHAPTER 3: LINEAR ANALYSIS OF MICRO-SCALE STRUCTURES

In this chapter, Cosserat analysis of a micro-cantilever and a system consisting of four micro-scale beams attached to a mass in the middle are considered. Specifically, the linear equations of motion of these two systems are developed and predictions of the natural frequencies are made.

3.1 Motivation

Cosserat continuum theory is claimed to be a complete as compared to classical Euler-Bernoulli beam theory. Building on the material presented in Chapter 2, this is explored here in the context of the structures treated in the work of Wang, Liu, and Cao (2004). Also, the linear version of the constrained Cosserat mechanics used by Wang *et al.* (2004) is used in the treatment of this chapter.

3.2 Micro-scale structures of interest

In Figure 3.1, the micro-scale structure studied by Wang *et al.* (2004) is illustrated. This structure consists of four beam-like structures that are clamped at one end and attached to a common mass at the other end. This mass is treated as a rigid body. In Figure 3.2, the other micro-scale structure of interest is shown. This structure is a cantilever beam, which can undergo bending motions, as shown in Figure 3.3. In addition, this beam is also allowed to undergo twisting motions, as shown in Figure 3.4.

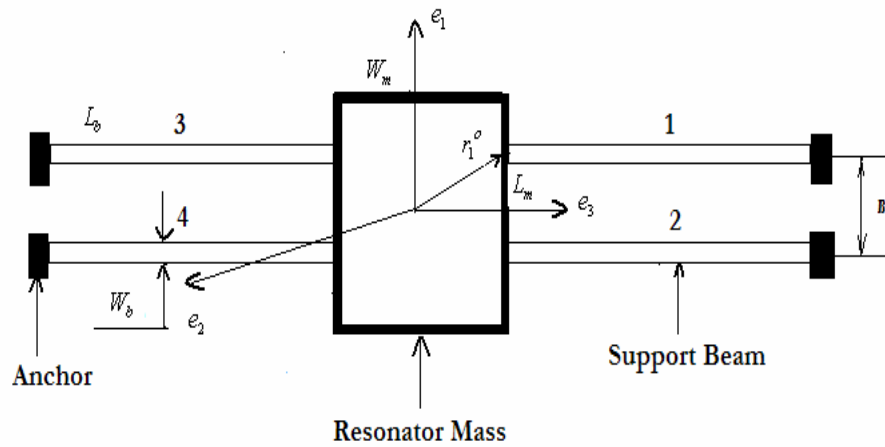


Figure 3.1: Schematic of micro-scale system studied by Wang et al. (2004).

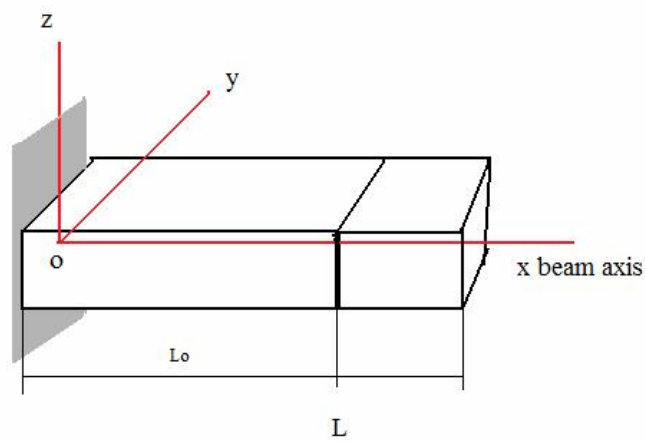


Figure 3.2: Illustration of a cantilever structure.

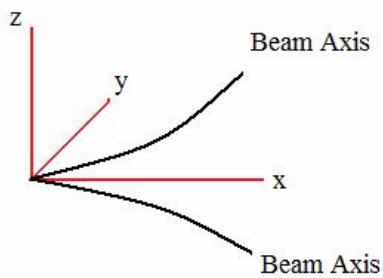


Figure 3.3: Cantilever beam bending.

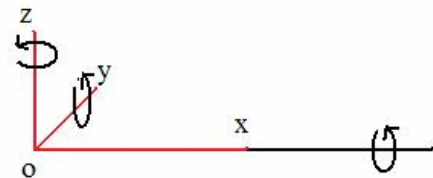


Figure 3.4: Cantilever beam undergoing twisting motions.

The inertia matrix for the central mass of Figure 3.1 is given by

$$M_R = \begin{pmatrix} mL & 0 & 0 \\ 0 & mL & 0 \\ 0 & 0 & I_{zz} \end{pmatrix};$$

where $m = \rho L W D$, $I_{zz} = \frac{\rho E}{12} (L^2 + D^2) L W D$, ρ is the mass density, L is the length of this body, E is the Young's modulus, W is the width of this body, and D is the thickness of this body. The four tethers shown in Figure 3.1 are treated as Cosserat rods. Following Wang et al. (2004), for illustrative purposes, the system parameters given next are chosen.

System parameters

Density of the central mass as well as the four tethers, $\rho = 2.33 \text{ g/cm}^3$

Length of beam, $L_b = 58.32 \text{ }\mu\text{m}$

Width of beam, $w_b = 2 \text{ }\mu\text{m}$

Thickness of beam, $t_b = 3 \text{ }\mu\text{m}$

Young's modulus, $E = 150 \text{ GPa}$

Poisson's parameter, $\gamma = 0.29$

Length of central mass, $L = 15.4 \text{ }\mu\text{m}$

Width of central mass, $W = 6 \text{ }\mu\text{m}$

Thickness of central mass, $D = 3 \text{ }\mu\text{m}$

3.3 Cosserat Cantilever Analysis

Following the development of Chapter 2, first, a position vector is defined as

$$(a) \quad \vec{r}_i = \vec{r}_i(\xi, t) \text{ where } i = (x, y) \text{ is a material point of the Cosserat curve } \mathbf{C}$$

Then, a local orthonormal triad is introduced according to

$$(b) \quad \vec{d}_i = \vec{d}_i(\xi, t), \quad i = (1, 2, 3)$$

to move along the cross-section of \mathbf{C} . Then, a reference configuration is defined as

$$(c) \quad \vec{D}_i = \vec{D}_i(\xi), \quad i = (1, 2, 3)$$

The reference configuration gives the flexibility of simulating the dynamic nature of system, as explained in Chapter 2. For the static case, the force and moment balance laws lead to

$$\frac{\partial n(\xi, t)}{\partial \xi} = 0$$

$$\frac{\partial m(\xi, t)}{\partial \xi} + v(\xi) \times n(\xi) = 0$$

The equations for the dynamic case, inclusive of the inertia terms, are given in Chapter 2 in the form of equations (2.1) and (2.2). Here,

$$n(\xi, t) = n_i(\xi, t) d_i(\xi, t)$$

and

$$m(\xi, t) = m_i(\xi, t) d_i(\xi, t)$$

are the contact force and torque densities, respectively. In expanded form, they are given as follows:

$$n_1 = K_{11}v_1, n_2 = K_{22}v_2$$

$$m_1 = j_{11}u_1, m_2 = j_{22}u_2$$

The motion of the cantilever beam involves both the velocity of the curve $\partial_t r(s, t)$ and the angular velocity of the cross-sections, $w(s; t)$; that is

$$\partial_t d_i(s, t) = w(s, t) \times d_i(s, t)$$

In a similar manner, as in Chapter 2, the strains of the Cosserat rod are classified as

“Linear strain” vector

$$v(s, t) = \partial_s r(s, t)$$

and the

“Angular strain” vector

$$\partial_s d_i(s, t) = u(s, t) \times d_i(s, t)$$

Since the basis $\{d_1, d_2, d_3\}$ is convenient for the intrinsic description of deformation, the relevant vector valued functions are decomposed with respect to it. This results in

$$v(s, t) = v_i d_i(s, t)$$

$$u(s, t) = u_i d_i(s, t)$$

$$w(s, t) = u_i d_i(s, t)$$

The parameterization of the rotation matrix follows the same scheme as that used by Wang *et al.* (2004), which is discussed in Chapter 2.

3.3.1 Shape functions

Following the treatment given by Wang *et al.* (2004), shape functions or interpolation functions are obtained so that each Cosserat element can be described by a reduced amount of information, which in this case, is six generalized coordinates. These coordinates correspond to the translational displacement amplitudes along the x and y

directions and the rotation amplitude about the z direction. Specifically, the generalized coordinates at the ends of a Cosserat element are represented as

$$q = \begin{pmatrix} q_a(t) \\ q_b(t) \end{pmatrix}, \text{ 3 generalized coordinates at each end.}$$

$$q_a = \begin{pmatrix} X_a(t) \\ Y_a(t) \\ \theta_a(t) \end{pmatrix} = \begin{pmatrix} 0 \\ 0 \\ 0 \end{pmatrix} \text{ at } s = 0$$

$$q_b = \begin{pmatrix} X_b(t) \\ Y_b(t) \\ \theta_b(t) \end{pmatrix} \text{ at } s = L$$

In addition, the nonlinear forms of the displacement fields are expanded in the following form

$$\begin{aligned} x(\xi, t) &= x_{11}(\xi)\phi(t) + x_{12}(\xi)(\phi(t))^2 + x_{13}(\xi)(\phi(t))^3 + O(\phi^4), \\ y(\xi, t) &= y_{21}(\xi)\phi(t) + y_{22}(\xi)(\phi(t))^2 + y_{23}(\xi)(\phi(t))^3 + O(\phi^4), \\ \theta_z(\xi, t) &= \theta_{31}(\xi)\phi(t) + \theta_{32}(\xi)(\phi(t))^2 + \theta_{33}(\xi)(\phi(t))^3 + O(\phi^4) \end{aligned}$$

where $\phi(t)$ is the rotation angle discussed in Chapter 2. Only two of the translational displacement fields and one rotational displacement field have been chosen, because of the planar case considered here. Making use of the boundary conditions, one can solve for the shape functions given above. Due to the algebra involved, they are not shown here.

3.3.2 System Energy

After determining the shape functions, the system energy expressions are determined for use in the Extended Hamilton's principle; that is,

$$\int_{t_1}^{t_2} \delta(T - V)dt + \int_{t_1}^{t_2} \delta W dt = 0$$

where the different terms are as explained in Chapter 2. Here,

$$T = \frac{1}{2} \{ \rho A \partial_t r \cdot \partial_t r + I(\dot{w}, \dot{w}) \}$$

$$V = \frac{1}{2} \{ J(u, u) + K_{33}(\bar{v}_3 - 1)^2 \}$$

Where,

K, J, and I are second-order tensors whose elements are defined as

$$K(s, t) = K_{ii}(s, t)(d_i(s, t) \otimes d_i(s, t)),$$

$$J(s, t) = \sum_{i,j=1}^2 J_{ij}(s, t)(d_i(s, t) \otimes d_j(s, t)) + J_{33}(s, t)(d_3(s, t) \otimes d_3(s, t))$$

$$I(s, t) = \sum_{i,j=1}^2 I_{ij}(s, t)(d_i(s, t) \otimes d_j(s, t)) + I_{33}(s, t)(d_3(s, t) \otimes d_3(s, t))$$

The tensor K represents a strain matrix. It takes the form

$$K = \begin{pmatrix} k_{11} = \text{shear strain}_x & & \\ & k_{22} = \text{shear strain}_y & \\ & & k_{33} = \text{axial strain}_z \end{pmatrix}$$

The inertia tensor J takes the form

$$J = \begin{pmatrix} j_{11} = 2^{\text{nd}} \text{ area} \\ \text{moment Inertia} & & \\ & j_{22} = 2^{\text{nd}} \text{ area} \\ & \text{moment Inertia} & \\ & & j_{33} = \text{Polar moment} \\ & & \text{of Inertia} \end{pmatrix}$$

where j_{11} and j_{22} resist volume bending, while j_{33} resists torsion. The remaining elements are zero because of the assumption that area is constant. Also in the present context, k_{33} , and j_{33} are inconsequential. The inertia matrix takes the form

$$I = \begin{pmatrix} I_{11} = \text{mass moment} \\ \text{of inertia} & & \\ & I_{22} = \text{mass moment} \\ & \text{of inertia} & \\ & & I_{33} = \text{mass moment} \\ & & \text{of inertia} \end{pmatrix}$$

In present case, only I_{33} comes into play.

Whose coefficients K_{ii} , J_{ii} , I_{ii} are given by:

$$K_{11} = K_{22} = GA(s)$$

$$K_{33} = EA(s)$$

$$J_{11} = \int_{A(s)} E\eta^2 dA$$

$$J_{22} = \int_{A(s)} E\xi^2 dA$$

$$J_{33} = \int_{A(s)} E(\eta^2 + \xi^2) dA$$

$$J_{12} = -J_{21} = \int_{A(s)} E\xi\eta dA$$

$$I_{11} = \int_{A(s)} \rho(s)\eta^2 dA$$

$$I_{22} = \int_{A(s)} \rho(s)\xi^2 dA$$

$$I_{33} = \int_{A(s)} \rho(s)(\eta^2 + \xi^2) dA$$

$$I_{12} = -I_{21} = \int_{A(s)} \rho(s)\xi\eta dA$$

and

u is the angular strain defined by $u = \frac{1}{2}d_i \times \partial_s d_i$

\bar{v}_3 is the linear strain per unit length, $\bar{v}_3 = |\partial_\xi r|$

and w is the angular velocity, $w = \frac{1}{2}d_i \times \partial_t d_i$.

3.3.4 Cosserat beam solution

For the system parameter values given previously, the first natural frequencies of a cantilevered tether is determined along the x and y directions. The corresponding mass and stiffness matrices (which have been normalized) read as

$$\text{Massmatrix}, M_c = \begin{pmatrix} 0.4154 \times 10^{-17} & 0 \\ 0 & 0.4154 \times 10^{-17} \end{pmatrix} \text{Kg};$$

$$\text{StiffnessMatrix}, K_c = \begin{pmatrix} 0.15 \times 10^{-2} & 0 \\ 0 & 0.65187 \times 10^{-3} \end{pmatrix} \text{N/m}$$

from which one can determine the natural frequencies as

$$\omega_1 = 1.8790\text{e}+007 \text{ rad/s}$$

$$\omega_2 = 1.2527\text{e}+007 \text{ rad/s}$$

Considering the system of Figure 3.1, as a whole, the reduced set of linear equations of motion take the form

$$\ddot{x} + \omega_{x0}^2 x = 0$$

$$\ddot{y} + \omega_{y0}^2 y = 0$$

$$\ddot{\theta} + \omega_{\phi z0}^2 \theta = 0$$

The mass matrix of the central mass in this given by

$$\text{Massofmembrane}, M_m = \begin{pmatrix} 0.4907 \times 10^{-3} & 0 & 0 \\ 0 & 0.4907 \times 10^{-3} & 0 \\ 0 & 0 & 2.0931 \times 10^{-2} \end{pmatrix} \text{Kg}$$

The mass matrix for the whole system is given by $4 \times M_c + M_m$, and the stiffness matrix for the whole system is given by $4 \times K_c$. Then, the system's natural frequencies are given by

$$\omega_{x_0} = 1.3340$$

$$\omega_{y_0} = 0.8893 \text{ rad/s}$$

$$\omega_{\phi_{z_0}} = 0.2767$$

The ratio of the first two frequencies is in agreement with those presented by Wang *et al.* (2004). However, the same is not true for the other ratios.

3.4 Comparisons with Euler Bernoulli Theory and Remarks

Treating the tether as a Euler-Bernoulli beam since the length to thickness ratio is more than ten, the following expression (Meirovitch, 2001) is used to determine the first natural frequency of bending along the x and y directions:

$$\omega = 2\pi f = \frac{3.5160}{L^2} \sqrt{\left(\frac{EI}{m}\right)}$$

The use of this relation leads to the following results:

$$\omega_1 = 1.8097e+007 \text{ rad/s}$$

$$\omega_2 = 2.7146e+007 \text{ rad/s}$$

While there is good agreement between the first natural frequency between the Cosserat analysis and the Euler-Bernoulli analysis along the x direction, the same is not true along the y direction. The first natural frequency determined along the y direction is

determined to be lower in the case of Cosserat analysis. This may be reasonable, as the Cosserat analysis imposes lesser kinematic constraints than the Euler-Bernoulli beam analysis.

If each of the tethers of the system shown in Figure 3.1 is modeled as an Euler-Bernoulli beam, then the obtained system natural frequencies are given by

$$\omega_{x_0} = 1.4$$

$$\omega_{y_0} = 1 \quad \text{rad/s}$$

$$\omega_{\phi_{z_0}} = 0.4$$

These frequencies are not far from those determined previously by using the Cosserat analysis. Although the stiffnesses of the individual tethers are influenced when one uses Cosserat analysis as opposed to the Euler-Bernoulli beam analysis, not much difference is seen in the system natural frequencies because of the large central mass.

A comparison of Cosserat Beam frequencies to those of Euler-Bernoulli Beam frequencies at different Aspect Ratios is shown in the following table.

Aspect Ratio (L/W)	Cosserat Frequencies (rad/s)	Euler-Bernoulli Frequencies (rad/s)
20	$\omega_x = 1.8790 \times 10^7$ $\omega_y = 1.2527 \times 10^7$	$\omega_x = 1.8090 \times 10^7$ $\omega_y = 2.7146 \times 10^7$
25	$\omega_x = 6.760 \times 10^6$ $\omega_y = 4.5146 \times 10^6$	$\omega_x = 6.5150 \times 10^6$ $\omega_y = 9.7725 \times 10^6$
50	$\omega_x = 1.6911 \times 10^6$ $\omega_y = 1.1274 \times 10^6$	$\omega_x = 1.6288 \times 10^6$ $\omega_y = 2.4431 \times 10^6$

Table 3.1: Cosserat & Euler-Bernoulli frequencies at various aspect ratios

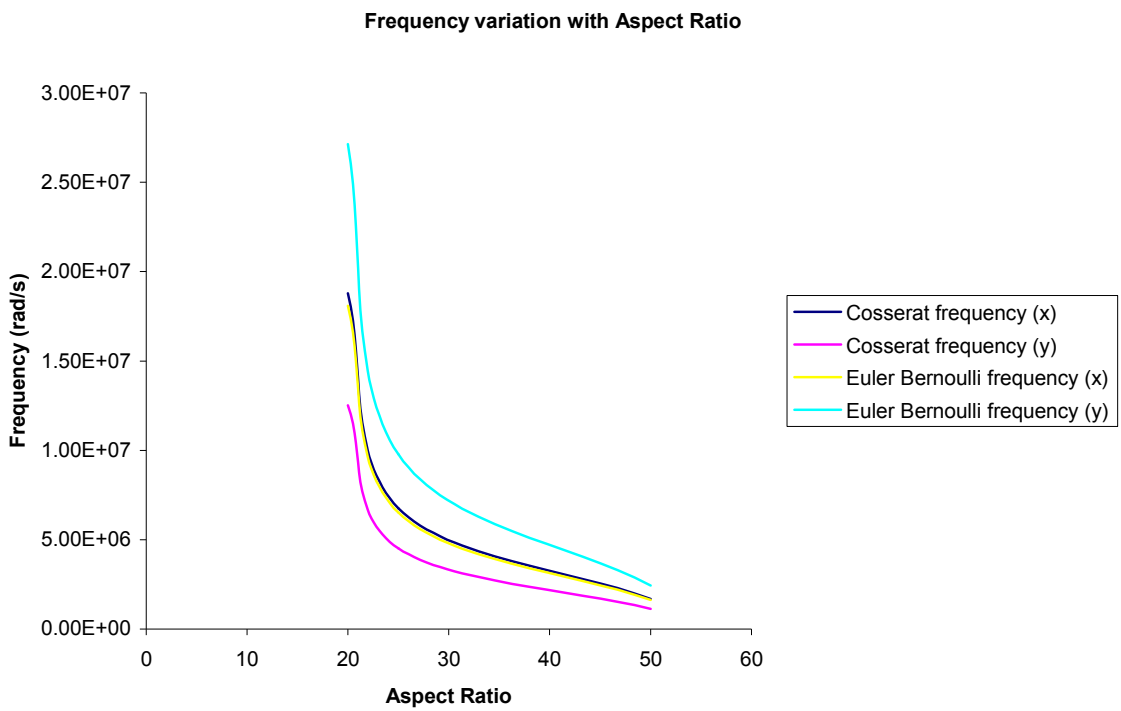


Fig 3.5: frequency variation with increase in aspect ratio of the beam

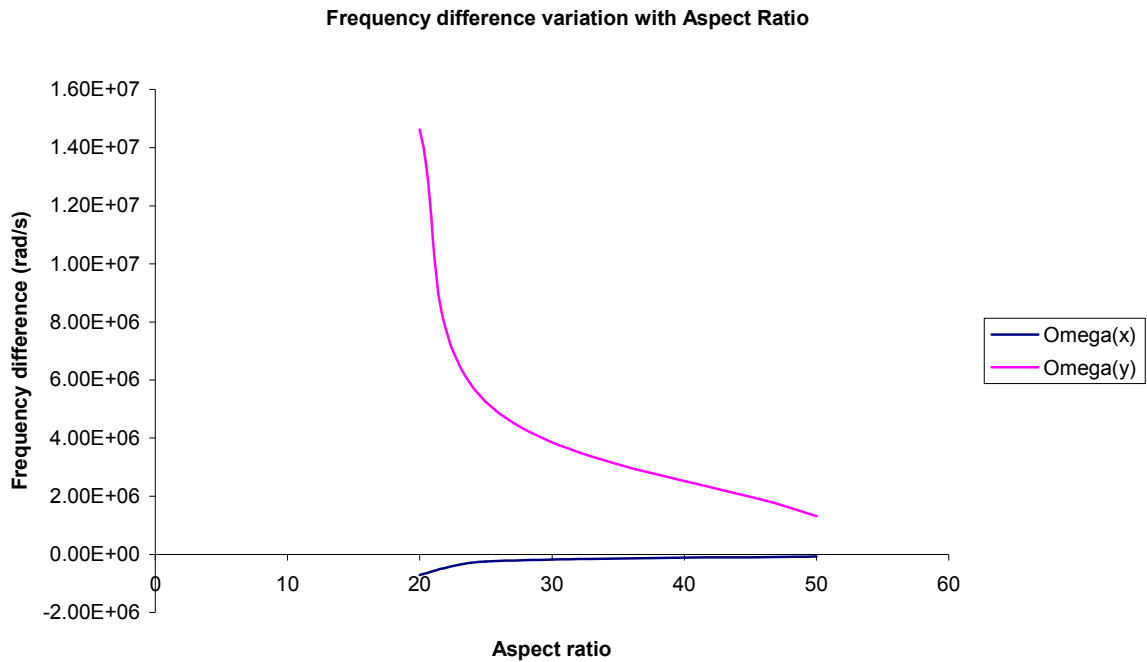


Fig 3.6: *Cosserat and Euler frequency difference plotted against aspect ratio*

The results of this section point out that one needs to be careful in using Euler-Bernoulli beam analysis and that Cosserat analysis may be more relevant in some instances. In general, as the displacements get larger, Cosserat analysis with nonlinear shape functions would be appropriate. Although there is no coupling in the linear case, there is coupling in the nonlinear case. It is recalled that Cosserat theory is a continuum based theory that accounts for strains in all the directions at each of the material points along the curve of consideration as explained earlier in this chapter. Cosserat analysis may also be more relevant for systems with nonlinear boundary conditions (e.g., Tucker and Wang, 2003). Although micro-scale structures are considered here, this type of analysis is applicable to other flexible structures at other scales such as drill strings used for oil well exploration applications.

CHAPTER 4:

TETHER SUSPENDED MICROMACHINED GYROSCOPE

In this chapter, Cosserat modeling of tethers used in a micro-scale gyroscope are studied. The treatment follows the development presented in Chapter 2. Two different parameterizations are determining the displacement fields and the results obtained by using both of these parameterizations are compared with those published in the literature.

4.1 Motivation

Micromachining technology has made it possible to fabricate microelectromechanical systems (MEMS) in high volumes at low individual cost. A key component of inertial measurement systems based on MEMS is the angular rate sensor, or a gyroscope (see Chapter 1). Several designs for micromachined gyroscopes have been reported in recent times, and one class of micromachined gyroscopes is based on the vibrations of a proof-mass which is suspended above a substrate by elastic beams or tethers. These gyroscopes often exhibit a host of undesirable characteristics, including mechanical nonlinearity, quadrature error, and cross-axis sensitivity, which are commonly assumed to depend on manufacturing defects. As discussed by Pratt, Jonson, Howe (1991), Gui, Legtaben, Tilman, and Fluitman (1998), Fujita, Hatsano, Maenaka, Mizuno, Matsuoko, Kojima, Oshima, and Maeda (1999) very little analysis has been done in order to predict the behavior both prior to and after fabrication.

In this chapter, Cosserat nonlinear theory of rods is brought to bear upon tether modeling and determination of the nonlinear stiffness characteristics of the tether. The results obtained here are compared to those published by O'Reilly et al. (2004).

4.2 Gyroscope Model

In Figures 4.1 and 4.2, illustration of a micromachined gyroscope is shown along with models of its tether supports.

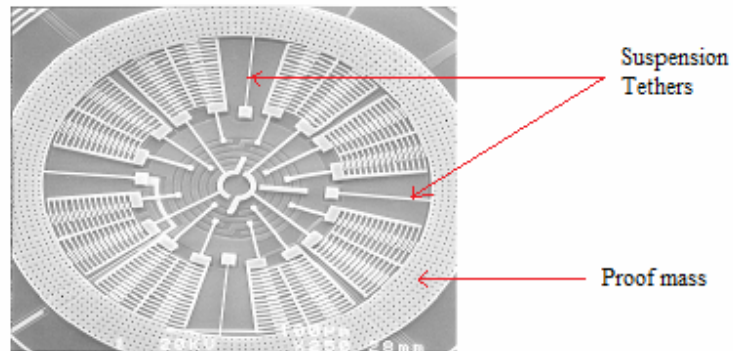
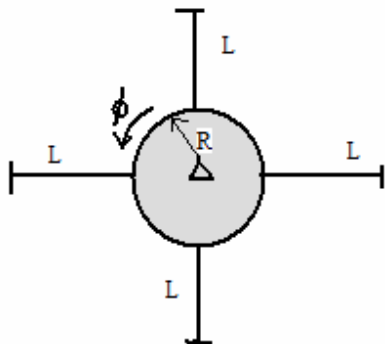


Figure 4.1: Scanning electron micrograph of a rotation-based micromachined gyroscope .

(a)



(b)

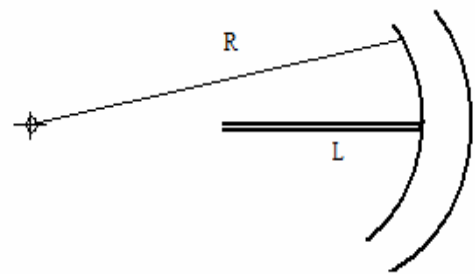


Figure 4.2: Two geometries of tether suspensions of interest: (a) inside suspended ring and (b) outside suspended ring.

4.2.1 Nonlinear Tether modeling

As explained in Chapter 2, Cosserat continuum theory can be described as follows. To every material point of a Cosserat curve, a set of deformable vectors, known as directors, is attached. It is assumed that the two directors d_1 and d_2 , which are oriented along the local axes, exist. The directors and the position vector \bar{r} to points on the material curve are vector-valued functions of ζ and t , where ζ is a convected coordinate locating material points along the curve, and t is time. The vectors in a fixed reference configuration B are denoted by $D_1(\zeta)$, $D_2(\zeta)$, and $R(\zeta)$ respectively. The mechanics of the beam can be described by the mapping of $D_1(\zeta)$, $D_2(\zeta)$, and $R(\zeta)$ from the reference configuration B to the vectors $d_1(\zeta, t)$, $d_2(\zeta, t)$, and $r(\zeta, t)$ on the Cosserat curve (the configuration, B^*), as illustrated in Figure 4.3.

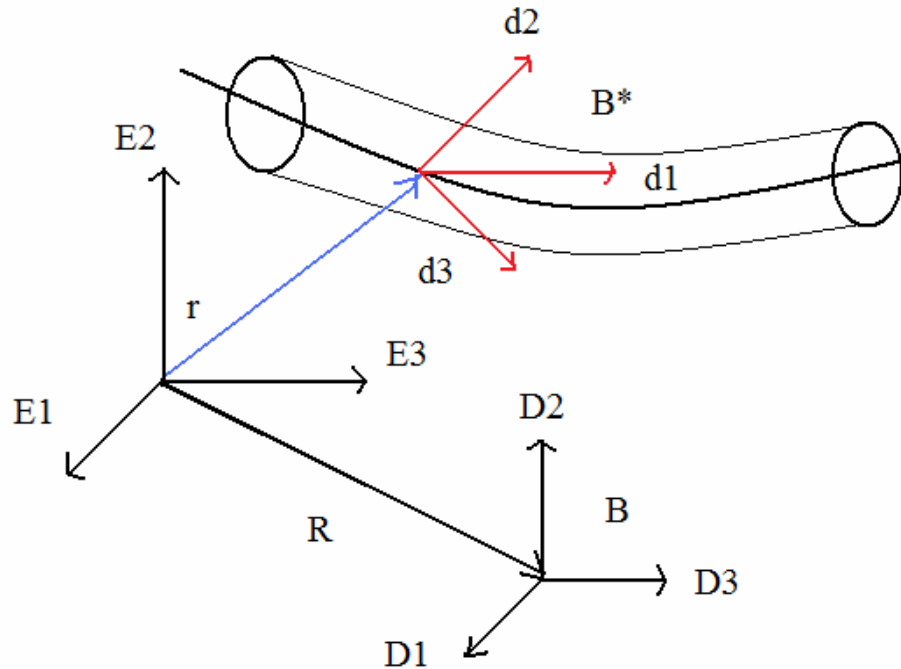


Figure 4.3: Reference configuration (B) and present configuration (B^*) of a Cosserat curve.

For simplicity, a single suspension tether is analyzed, and the same analysis can be applied to any number of tethers connected to the rigid mass shown in Figure 4.1. Again, in terms of notation, let $\bar{r} = \bar{r}(\xi, t)$ be the position vector, the two director fields be $\bar{d}_1 = \bar{d}_1(\xi, t)$ and $\bar{d}_2 = \bar{d}_2(\xi, t)$. As stated before, the reference configuration is defined by $R = R(\xi)$, $D_1 = D_1(\xi)$ and $D_2 = D_2(\xi, t)$. Here, attention is restricted to a constrained Cosserat rod theory for the purpose of modeling the tether, which is subjected to the constraints $\bar{d}_3 = \bar{r}'$ and $D_3 = R'$.

Let $\{e_1, e_2, e_3\}$ to be a right-handed Cartesian basis for the Euclidean three space. For present purposes, the directors are subject to the constraints

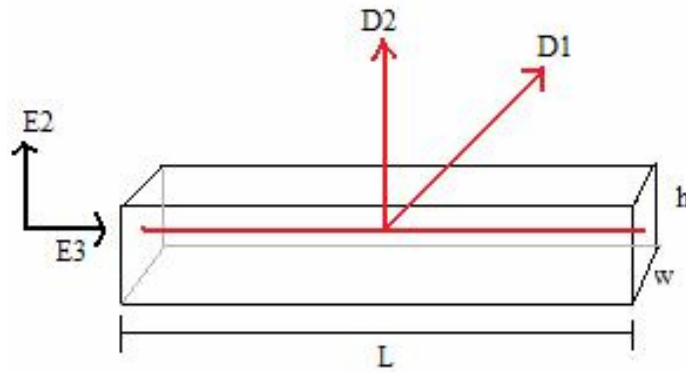


Figure 4.4: The tether geometry and the reference configuration for the Cosserat rod. The axial centerline of the rod coincides with the reference configuration of the material curve C of the Cosserat rod and $D_3 = e_3$.

$$R = \xi e_3,$$

$$D_1 = e_1,$$

$$D_2 = e_2, \text{ and}$$

$$d_2 = D_2$$

Assuming there is no shear deformation, one has

$$d_1 \cdot d_1 = 1,$$

$$d_2 \cdot d_2 = 1$$

$$d_1 \cdot d_2 = 0$$

Next, in the analysis, rotation parameterization and the balance equations are considered.

The position vector describing the motion of the body in terms of the displacements u_1 and u_3 is given by

$$\bar{r} = u_1 D_1 + (\xi + u_3) D_3$$

Parameterizing the basis vector d_1 using the angle of rotation θ , one can write

$$d_1 = \cos(\theta) D_1 - \sin(\theta) D_3$$

Assuming there is no external force acting on the tether, the force (per unit length, ξ)

balance equation reads as

$$\frac{\partial n}{\partial \xi} = 0,$$

where n is the contact force. The moment balance (per unit length, ξ) equation takes the form

$$\frac{\partial M}{\partial \xi} + d_3 \times n = 0,$$

where M is the moment.

Calculating the strains, following the convention used by Antman (1972), the nontrivial strains are as determined as

$$\gamma_{13} = d_1 \cdot d_3 - D_1 \cdot D_3 = u_1' \cos(\theta) - (1 + u_3') \sin(\theta),$$

$$\gamma_{33} = d_3 \cdot d_3 - D_3 \cdot D_3 = (u_1')^2 + 2u_3' + (u_3')^2,$$

$$k_{13} = d_1' \cdot d_3 - D_1' \cdot D_3 = -\theta'(u_1' \sin(\theta) + (1 + u_3') \cos(\theta))$$

O' Reilly *et al.* (2004) pointed that, if one were to linearize the strains given above under the assumptions of small strains and displacements, then the resulting forms closely resemble the expressions for shear strain, extension, and curvature obtained respectively from linear rod theory; that is,

$$\gamma_{13} \approx u_1' - \theta,$$

$$\gamma_{33} \approx 2u_3',$$

$$k_{13} \approx -\theta'$$

Incorporating the strains in the balance equations, leads to

$$n = GAk\gamma_{13}d_1 + \frac{EA}{2}\gamma_{33}d_3 + EI_2k_{13}d_1',$$

$$M = EI_2k_{13}d_1 \times d_3$$

where G is the shear modulus, A is the area of cross-section, and I_2 is the area moment of inertia, and k is the shear coefficient.

4.3 Perturbation analysis using the rotation angle as a gauge parameter

In this section, as in the work of O'Reilly et al. (2004), the angle of the spin of the gyroscope ϕ , which is shown in Figure 4.4, is used as a gauge parameter in expanding the displacement fields. After using the boundary conditions, the different terms in the expansion are determined, and finally, the coefficients in the nonlinear torsion stiffness relationship are determined. In Section 4.5, it is shown that one can carry out the same analysis by using an arbitrary book-keeping parameter as the gauge function and obtain the same results (Appendix II).

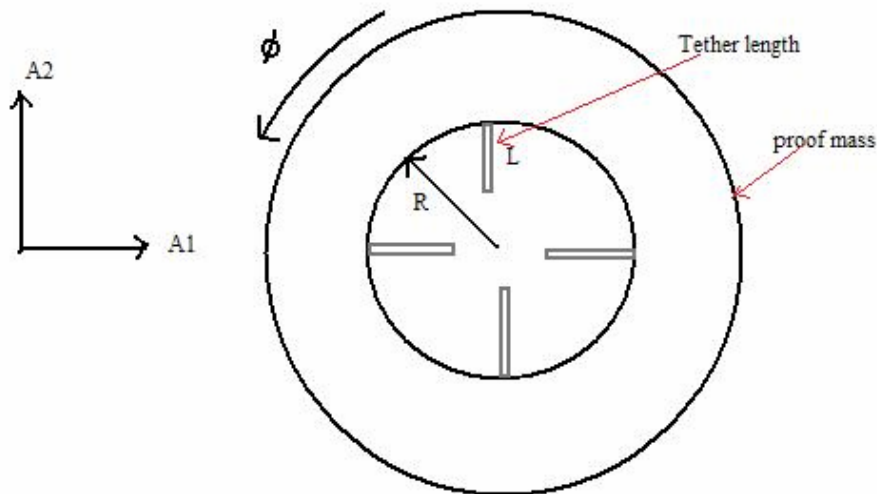


Figure 4.5: Schematic of a proof mass (rotor) suspended by four identical tethers of length L .

The displacement fields are expanded as

$$\begin{aligned} u_1(\xi) &= u_{11}(\xi)\phi + u_{12}(\xi)(\phi)^2 + u_{13}(\xi)(\phi)^3 + O(\phi^4), \\ u_2(\xi) &= u_{21}(\xi)\phi + u_{22}(\xi)(\phi)^2 + u_{23}(\xi)(\phi)^3 + O(\phi^4), \\ u_3(\xi) &= u_{31}(\xi)\phi + u_{32}(\xi)(\phi)^2 + u_{33}(\xi)(\phi)^3 + O(\phi^4) \end{aligned}$$

After substituting the series expansions into the balance laws and retaining terms upto third order, the following boundary-value problems are constructed at the different levels of hierarchy.

First order equations, $O(\phi)$:

$$\begin{aligned} GAk(u_{11}'' - \theta_1') &= 0 \\ EI_2\theta_1'' + GAk(u_{11}' - \theta_1) &= 0 \\ EAu_{31}'' &= 0 \end{aligned}$$

Second order equations, $O(\phi^2)$:

$$\begin{aligned} GAk(u_{12}'' - \theta_2') &= 0 \\ EI_2\theta_2'' + GAk(u_{12}' - \theta_2) &= 0 \\ EAu_{32}'' + 3EI_2\theta_1'\theta_1' + EAu_{11}'u_{11}'' &= 0 \end{aligned}$$

Third order equations, $O(\phi^3)$:

$$\begin{aligned} GAk(u_{13}'' - \theta_3') &= -EI_2((\theta_1')^3 + 3\theta_1\theta_1'\theta_1'') - \frac{3}{2}EA(u_{11}')^2u_{11}'' - EA(u_{11}'u_{32}')' \\ &+ GAK(\theta_1\theta_1'u_{11}' + (\theta_1u_{32}')') \\ EI_2\theta_3'' + GAk(u_{13}' - \theta_3) &= -\frac{2}{3}GAk\theta_1^3 - EI_2(\theta_1')^2u_{11}' - GAk(u_{11}'u_{32}') - 2EI_2u_{32}'\theta_1'' \\ &+ (2GAku_{11}' + EI_2\theta_1'')\theta_1^2 - 2EI_2\theta_1(u_{11}'\theta_1')' + EI_2\theta_1(\theta_1')^2 - GAk\theta_1((u_{11}')^2 - 2u_{32}') - 2EI_2\theta_1'u_{32}'' \\ EAu_{33}'' &= 0 \end{aligned}$$

The boundary conditions are given by

$$\begin{aligned} u_1(0) &= 0, \\ u_2(0) &= 0, \\ u_3(0) &= 0, \\ \theta(0) &= 0. \end{aligned} \quad \text{at } \zeta = 0$$

where

$$u_{11}(0) = \theta_1(0) = u_{31}(0) = 0,$$

$$u_{12}(0) = \theta_2(0) = u_{32}(0) = 0,$$

$$u_{13}(0) = u_{33}(0) = \theta_3(0) = 0$$

and

$$\begin{aligned} u_1(l) &= R \sin(\phi) \\ u_2(l) &= 0 \\ u_3(l) &= R(\cos(\phi) - 1) \\ \theta(l) &= \phi \end{aligned} \quad \text{at } \zeta = l$$

where

$$u_{31}(l) = 0$$

$$\theta_1(l) = 1,$$

$$u_{11}(l) = R$$

$$u_{12}(l) = 0$$

$$\theta_2(l) = 0,$$

$$u_{32}(l) = -\frac{R}{2}$$

and

$$u_{33}(l) = 0$$

$$\theta_3(l) = 0$$

$$u_{13}(l) = -\frac{R}{6}$$

In this thesis work, the boundary value problems are solved by using Maple programs(Appendix I) to determine the shape functions for displacement fields u_1 , u_3 and θ , up to third order.

4.4 Free Body Diagrams and Torque

As shown in Figures 4.2(a) and 4.2(b), there is a proof mass rotor suspended by four, identical, symmetrically aligned tethers of length L . The proof mass is rigidly rotated through the angle ϕ , and through that a torque is generated. Next, different scenarios are considered.

Case 1:

Consider the free-body diagram of an inside suspended ring, as shown in Figure 4.5;

The torque acting on the rigid body from each of the tether is derived as

$$\vec{\tau} = (-R \cos(\phi)e_3 + R \sin(\phi)e_1) \times (n_1e_1 + n_3e_3) + M_2e_2$$

where

$$e_2 \times e_3 = -e_1$$

and the magnitude of the torque is

$$\tau = Rn_3(L) \sin(\phi) - Rn_1(L) \cos(\phi) - M_2(L)$$

for a beam of length L . Hence, the total torque on the proof mass due to the four tethers is given by

$$\tau = 4 \times (Rn_3(L) \sin(\phi) - Rn_1(L) \cos(\phi) - M_2(L))$$

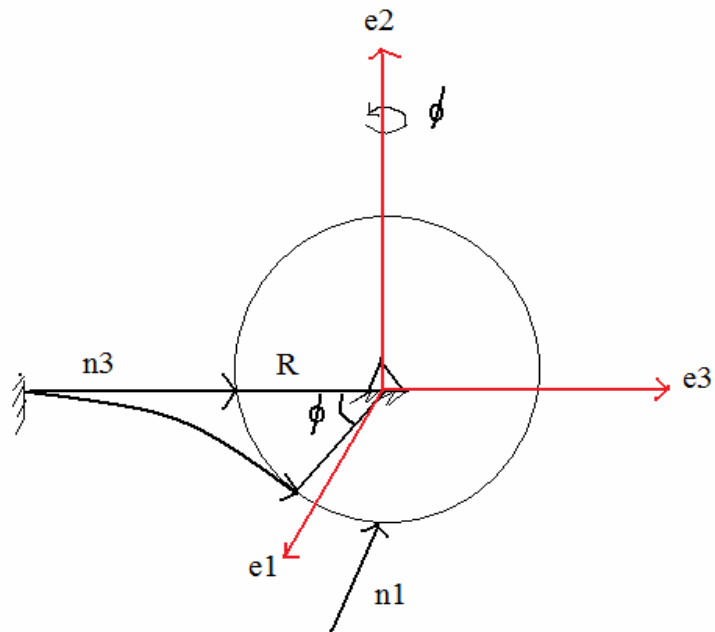


Figure 4.6: Free-body diagram of an inside suspended ring.

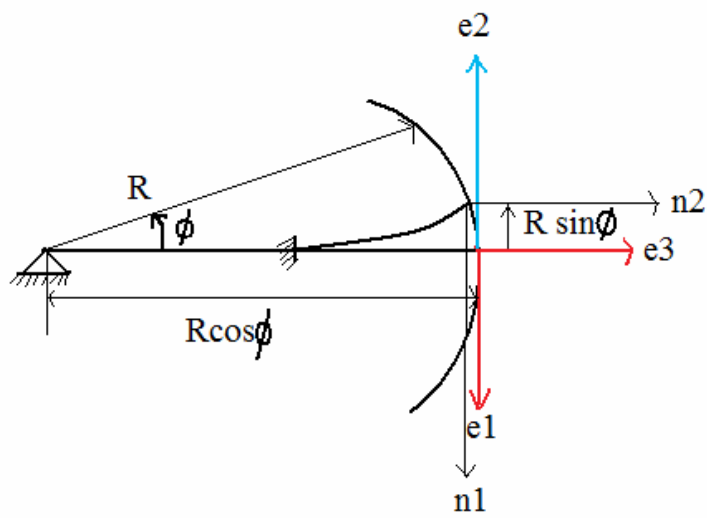


Figure 4.7: Free-body diagram of an outside suspended ring.

Case 2:

Now consider the free-body diagram of an outside suspended ring as shown in Figure 4.6,

The torque in this case is derived to be

$$\begin{aligned}\tau &= (R \cos(\phi)e_3 - R \sin(\phi)e_1) \times (n_1e_1 + n_3e_3) - M_2e_2 \\ &= R(L) \sin(\phi) - R \cos(L)(\phi) - M_2(L), \text{ for beam of length } L.\end{aligned}$$

and hence, the total torque is given by

$$\tau = 4 \times (R(L) \sin(\phi) - R \cos(L)(\phi) - M_2(L))$$

In both of the cases mentioned above,

$$\begin{aligned}n_1 &= n \cdot D_1 = GAk(u'_1 \cos(\theta) - (1 + u'_3) \sin(\theta)) \cos(\theta) \\ &+ \frac{EA}{2}((u'_1)^2 + 2u'_3 + (u'_3)^2)u'_1 + EI_2(\theta')^2(u'_1 \sin(\theta) + (1 + u'_3) \cos(\theta)) \sin(\theta) \\ n_2 &= n \cdot D_2 = GAk(u'_1 \cos(\theta) - (1 + u'_3) \sin(\theta)) \sin(\theta) \\ &+ \frac{EA}{2}((u'_1)^2 + 2u'_3 + (u'_3)^2)(1 + u'_3) + EI_2(\theta')^2(u'_1 \sin(\theta) + (1 + u'_3) \cos(\theta)) \cos(\theta) \\ M_2 &= M \cdot D_2 = EI_2(\theta')(u'_1 \sin(\theta) + (1 + u'_3) \cos(\theta))^2\end{aligned}$$

Here, u_1, u_2, u_3, θ are nonlinear functions determined by solving the boundary-value problem using Maple codes written by the author of this thesis.

The restoring torque can also be viewed as having a nonlinear relationship with the rotation angle; that is,

$$\tau = -K_1\phi - K_2\phi^2 - K_3\phi^3 + O(\phi^4).$$

Then, for Case 1, the stiffness coefficients turn out to be

$$K_1 = \frac{16EI_2(GAk(L^2 - 3LR + 3R^2) + 3EI_2)}{GAkL^3 + 12EI_2L}$$

$$K_2 = 0$$

$$K_3 = \frac{\beta L}{1575EA(GAkL^3 + 12EI_2)^4}$$

For Case 2, the nonlinear stiffness coefficients turn out to be

$$K_1 = \frac{16EI_2(GAk(L^2 + 3LR + 3R^2) + 3EI_2)}{GAkL^3 + 12EI_2L}$$

$$K_2 = 0$$

$$K_3 = \frac{\alpha L}{1575EA(GAkL^3 + 12EI_2)^4}$$

where the details of α and β can be found in the appendix . These results agree with those provided by O'Reilly *et al.* (2004).

4.5 Perturbation analysis using an arbitrary book keeping parameter as a gauge parameter

This section's development complements that given in Section 4.3. Here, a bookkeeping parameter ε is used to order the different terms in the expansion of the displacement fields as opposed to the rotation angle ϕ used previously; that is, the displacement fields are expanded as

$$\begin{aligned}
u_1(\xi) &= u_{11}(\xi)\varepsilon + u_{12}(\xi)\varepsilon^2 + u_{13}(\xi)\varepsilon^3 + O(\varepsilon^4), \\
u_2(\xi) &= u_{21}(\xi)\varepsilon + u_{22}(\xi)\varepsilon^2 + u_{23}(\xi)\varepsilon^3 + O(\varepsilon^4), \\
u_3(\xi) &= u_{31}(\xi)\varepsilon + u_{32}(\xi)\varepsilon^2 + u_{33}(\xi)\varepsilon^3 + O(\varepsilon^4)
\end{aligned}$$

The above equations are substituted into the balance laws and the boundary-value problems are solved at different levels of hierarchy, and the linear and nonlinear stiffness coefficients are determined. The results are shown below for the two cases discussed in Section 4.4.

For Case 1:

$$\begin{aligned}
K_1 &= \frac{16EI_2(GAk(L^2 - 3LR + 3R^2) + 3EI_2)}{GAkL^3 + 12EI_2L} \\
K_2 &= 0 \\
K_3 &= \frac{\beta L}{1575EA(GAkL^3 + 12EI_2)^4}
\end{aligned}$$

For Case 2:

$$\begin{aligned}
K_1 &= \frac{16EI_2(GAk(L^2 + 3LR + 3R^2) + 3EI_2)}{GAkL^3 + 12EI_2L} \\
K_2 &= 0 \\
K_3 &= \frac{\alpha L}{1575EA(GAkL^3 + 12EI_2)^4}
\end{aligned}$$

As expected, the results are the same as that obtained in Section 4.3. This shows that in other applications, when a physical quantity is not readily available for use as a gauge function, one can use an arbitrary bookkeeping parameter to carry out the ordering.

CHAPTER 5: MICRORESONATOR

In this chapter a representative microresonator which was examined in Chapter 3 is again studied. Here a nonlinear analysis is carried out to build on the development of chapter 3.

5.1 Motivation

As explained in chapter 1, microresonators are currently being developed as key components in various resonator-based micro-systems, such as resonant accelerometers and microvibromotors. Yet many of the present computations and systems analyses do not incorporate the geometrical complexity and physical conditions of the system, although the ability to effectively simulate and predict the linear and nonlinear behavior of these systems is critical in estimating system performance.

5.2 Model of a Typical Micro Resonator

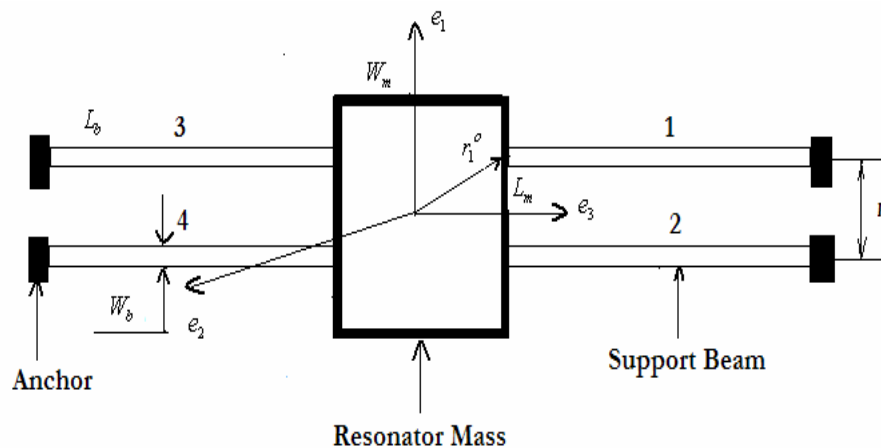


Figure 5.1: Model of a representative microresonator

In Figures 5.1, an illustration of a micro-resonator studied by Wang *et al.* (2004) is shown. This structure consists of four beam-like structures that are clamped at one end and attached to a common mass membrane at the other end. This membrane in the centre is treated as a rigid body. The micro resonator in consideration, is discussed for a linear case simulation in Chapter 3, and in the present chapter, the author discusses the nonlinear analysis.

Each of the four beams is considered to be a Cosserat rod for the purpose of analysis. One end is fixed to a rigid contact, so is considered a cantilever beam. A similar approach as discussed in Chapter 4, is followed in order to derive the nonlinear shape functions for each cantilever beam, But with a changed boundary problem.

The inertia matrix for the central mass of Figure 5.1 is given by

$$M_R = \begin{pmatrix} mL & 0 & 0 \\ 0 & mL & 0 \\ 0 & 0 & I_{zz} \end{pmatrix};$$

where $m = \rho LWD$, $I_{zz} = \frac{\rho E}{12}(L^2 + D^2)LWD$, ρ is the mass density, L is the length of this body, E is the Young's modulus, W is the width of this body, and D is the thickness of this body. For illustrative purposes, the system parameters given next are chosen.

System parameters

Density of the central mass as well as the four tethers, $\rho = 2.33 \text{ g/cm}^3$

Length of beam, $L_b = 58.32 \text{ }\mu\text{m}$

Width of beam, $w_b = 2 \mu m$

Thickness of beam, $t_b = 3 \mu m$

Young's modulus, $E = 150 \text{ GPa}$

Poisson's parameter, $\gamma = 0.29$

Length of central mass, $L = 15.4 \mu m$

Width of central mass, $W = 6 \mu m$

Thickness of central mass, $D = 3 \mu m$

5.2.1 Nonlinear Beam modeling

As shown in Figure 5.2, let $\bar{r} = \bar{r}(\xi, t)$ be the position vector, and $\{e_1, e_2, e_3\}$ be a right-handed Cartesian basis for the Euclidean three space. The local two director fields are $\bar{d}_1 = \bar{d}_1(\xi, t)$ and $\bar{d}_2 = \bar{d}_2(\xi, t)$. The reference configuration is defined by $R = R(\xi)$, $D_1 = D_1(\xi)$ and $D_2 = D_2(\xi)$. As in Chapter 4, similar constraints are placed for the purpose of modeling beam; that is,

$$\bar{d}_3 = \bar{r}' \text{ and } D_3 = R';$$

$$R = \xi e_3,$$

$$D_1 = e_1,$$

$$D_2 = e_2, \text{ and}$$

$$d_2 = D_2$$

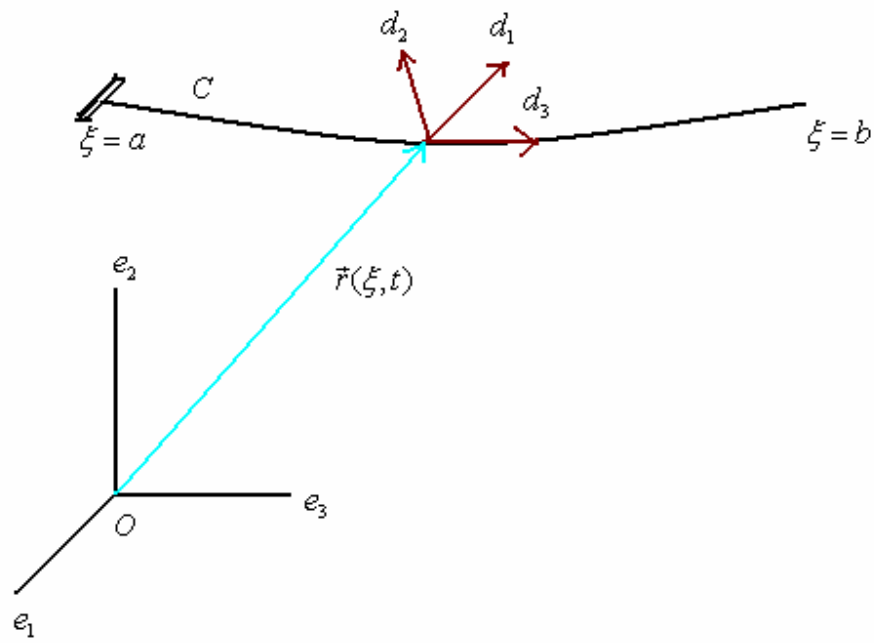


Figure 5.2: Position vector along the cosserat curve C of the beam.

and assuming no shear,

$$d_1 \cdot d_1 = 1,$$

$$d_2 \cdot d_2 = 1$$

$$d_1 \cdot d_2 = 0$$

The position vector in terms of displacements and reference configuration as a base is,

$$\bar{r} = u_1 D_1 + (\xi + u_3) D_3$$

Parameterizing the local directors with of the reference frame as a base

$$d_1 = \cos(\theta) D_1 - \sin(\theta) D_3$$

In zero external force condition, the balance laws which govern the beam are

$$\frac{\partial n}{\partial \xi} = 0,$$

$$\frac{\partial M}{\partial \xi} + d_3 \times n = 0;$$

In the above equations, n is the contact force and M , the moment.

Calculating the strains, following the convention used by Antman (1972), the nontrivial strains are as determined as

$$\gamma_{13} = d_1 \cdot d_3 - D_1 \cdot D_3 = u_1' \cos(\theta) - (1 + u_3') \sin(\theta),$$

$$\gamma_{33} = d_3 \cdot d_3 - D_3 \cdot D_3 = (u_1')^2 + 2u_3' + (u_3')^2,$$

$$k_{13} = d_1' \cdot d_3 - D_1' \cdot D_3 = -\theta'(u_1' \sin(\theta) + (1 + u_3') \cos(\theta))$$

Substituting the strains in the balance equations

$$n = GAk\gamma_{13}d_1 + \frac{EA}{2}\gamma_{33}d_3 + EI_2k_{13}d_1',$$

$$M = EI_2k_{13}d_1 \times d_3$$

where G is the shear modulus, A is the area of cross-section, and I_2 is the area moment of inertia, and k is the shear coefficient.

For the case of nonlinear analysis, displacement fields are expanded as

$$u_1(\xi) = u_{11}(\xi)\phi + u_{12}(\xi)(\phi)^2 + u_{13}(\xi)(\phi)^3 + O(\phi^4),$$

$$u_2(\xi) = u_{21}(\xi)\phi + u_{22}(\xi)(\phi)^2 + u_{23}(\xi)(\phi)^3 + O(\phi^4),$$

$$u_3(\xi) = u_{31}(\xi)\phi + u_{32}(\xi)(\phi)^2 + u_{33}(\xi)(\phi)^3 + O(\phi^4)$$

After substituting the series expansions into the balance laws and retaining terms up to third order, the following boundary-value problems are constructed at the different levels of hierarchy.

The first order equations, $O(\phi)$:

$$\begin{aligned} GAK(u_{11}'' - \theta_1') &= 0 \\ EI_2\theta_1'' + GAK(u_{11}' - \theta_1) &= 0 \\ EAu_{31}'' &= 0 \end{aligned}$$

The second order equations, $O(\phi^2)$:

$$\begin{aligned} GAK(u_{12}'' - \theta_2') &= 0 \\ EI_2\theta_2'' + GAK(u_{12}' - \theta_2) &= 0 \\ EAu_{32}'' + 3EI_2\theta_1'\theta_1' + EAu_{11}'u_{11}'' &= 0 \end{aligned}$$

The third order equations, $O(\phi^3)$:

$$\begin{aligned} GAK(u_{13}'' - \theta_3') &= -EI_2((\theta_1')^3 + 3\theta_1\theta_1'\theta_1'') - \frac{3}{2}EA(u_{11}')^2u_1'' - EA(u_{11}'u_{32}')' \\ &+ GAK(\theta_1\theta_1'u_{11}' + (\theta_1u_{32}')') \\ EI_2\theta_3'' + GAK(u_{13}' - \theta_3) &= -\frac{2}{3}GAK\theta_1^3 - EI_2(\theta_1')^2u_{11}' - GAK(u_{11}'u_{32}') - 2EI_2u_{32}'\theta_1'' \\ &+ (2GAKu_{11}' + EI_2\theta_1'')\theta_1^2 - 2EI_2\theta_1(u_{11}'\theta_1')' + EI_2\theta_1(\theta_1')^2 - GAK\theta_1((u_{11}')^2 - 2u_{32}') - 2EI_2\theta_1'u_{32}'' \\ EAu_{33}'' &= 0 \end{aligned}$$

and the boundary conditions are

$$\begin{aligned} u_1(0) &= 0, \\ u_2(0) &= 0, \\ u_3(0) &= 0, \\ \theta(0) &= 0. \end{aligned} \quad \text{at } L=0;$$

where,

$$u_{11}(0) = \theta_1(0) = u_{31}(0) = 0,$$

$$u_{12}(0) = \theta_2(0) = u_{32}(0) = 0,$$

$$u_{13}(0) = u_{33}(0) = \theta_3(0) = 0$$

and

$$\begin{aligned}
u_1(L_o) &= X_b \\
u_2(L_o) &= Y_b \\
u_3(L_o) &= Z_b \\
\theta(L_o) &= \theta_y
\end{aligned}$$

where,

$$\begin{aligned}
u_{11}(L_0) &= X_b \\
u_{31}(L_0) &= Z_b \\
\theta_1(L_0) &= \theta_y
\end{aligned}$$

Here, X_b, Z_b, θ_b are all generalized coordinates at the free end of the beam and all the higher order boundary terms are zero.

The boundary-value problems can be solved using a Maple program for shape functions up to the third order, associated with the displacement fields u_1, u_3 and θ_y .

5.2.2 System Energy

After determining the shape functions, the system energy expressions are determined for use in the Extended Hamilton's principle; that is,

$$\int_{t_1}^{t_2} \delta(T - V)dt + \int_{t_1}^{t_2} \delta W dt = 0$$

where the different terms are as explained in Chapter 2. Here,

$$T = \frac{1}{2} \{ \rho A \partial_t r \cdot \partial_t r + I(\omega, \omega) \}$$

$$V = \frac{1}{2} \{ J(u, u) + K_{33} (\bar{v}_3 - 1)^2 \}$$

and

$$u \text{ is the angular strain defined by } u = \frac{1}{2} d_i \times \partial_s d_i$$

$$\bar{v}_3 \text{ is the linear strain per unit length, } \bar{v}_3 = |\partial_\xi r|$$

$$\text{and } w \text{ is the angular velocity, } w = \frac{1}{2} d_i \times \partial_t d_i.$$

5.2.3 Cosserat beam solution

. The corresponding mass and stiffness matrices of the beam, taking in to consideration until the second order nonlinearities, (which have been normalized) read as

$$\text{Massmatrix, } M = \begin{pmatrix} \frac{47.5 \cdot L^2 \cdot EI}{EA} & 0 & 0 \\ 0 & \frac{119.74 \cdot L^2 \cdot (EI)}{EA(L^2 + 19 \frac{EI}{L})} & 0 \\ 0 & 0 & \frac{9I_{33}}{GAk(L^2 + 0.5 \cdot L)} \end{pmatrix} \text{ Kg;}$$

$$\text{StiffnessMatrix, } K = \begin{pmatrix} EA \cdot L^3 \cdot j22 & 0 & 0 \\ 0 & \frac{k33}{96 \cdot L^6} & 0 \\ 0 & 0 & j33 \cdot \beta \end{pmatrix}; \beta = \text{constant; N/m}$$

CHAPTER 6:

SUMMARY AND SUGGESTIONS FOR FUTURE WORK

In this chapter, a brief summary of the thesis work is provided along with conclusions that one can draw from this work. In addition, suggestions for future work are also provided.

6.1 Thesis Summary

In this thesis, the author has presented constrained Cosserat continuum theory with the viewpoint of applying to the study of micro-scale structural systems. A background to Cosserat theory is provided along with brief discussions of formulations that can be used for shells, rods, and points. In this context, material issues and parameterization constraints are also examined. The mechanics of the Cosserat rod theory is studied and applied to different micro-scale structural systems. Comparisons between results obtained on the basis of Euler-Bernoulli beam mechanics and Cosserat rod mechanics are made and discussed. Also, it is shown as to how Cosserat mechanics can be used to determine nonlinear stiffness properties of tether structures in micro-scale devices, in particular, micro-scale gyroscopes. In this context, it is also shown that an arbitrary bookkeeping parameter can be used to carry out the straightforward perturbation analysis when a physical parameter may not be readily available as a bookkeeping parameter. Modeling and results in the context of PZT microresonators are also presented and discussed.

6.2 Conclusions

- Cosserat mechanics is much more comprehensive as compared to classical mechanics such as Euler-Bernoulli beam mechanics, because of the way the kinematics and strain fields are defined and it is important to consider this mechanics for structures that undergo large deformations as shown in this thesis.
- Constrained rod theory can be a convenient formulation to use to model different micro-scale structures including micro-cantilevers, micro-scale gyroscope tethers, and clamped-clamped microresonators.
- Determination of nonlinear stiffness and inertia characteristics of micro-scale structures can benefit from Cosserat analysis, as shown in this thesis.

6.3 Recommendation for future work

It is recommended that other more comprehensive formulations of Cosserat mechanics be applied for systems with more complex boundary conditions that may not necessarily arise in the context of micro-scale systems. Also, the question of how to take the internal damping into account needs some consideration. Last, but not least, the algebraic computations involved in solving for the shape functions needs some attention so as to enable efficient computations.

APPENDIX – I

Defining Displacements

$$\begin{aligned} > x := xI(\xi, t); \\ & \qquad \qquad \qquad x := xI(\xi, t) \end{aligned} \tag{3}$$

$$\begin{aligned} > y := yI(\xi, t); \\ & \qquad \qquad \qquad y := yI(\xi, t) \end{aligned} \tag{4}$$

$$\begin{aligned} > z := zI(\xi, t); \\ & \qquad \qquad \qquad z := zI(\xi, t) \end{aligned} \tag{5}$$

$$\begin{aligned} > \theta := \theta I(\xi, t); \\ & \qquad \qquad \qquad \theta := \theta I(\xi, t) \end{aligned} \tag{6}$$

Expanding θ

$$\begin{aligned} > \cos\theta := 1 - \frac{\theta^2}{2}; \\ & \qquad \qquad \qquad \cos\theta := 1 - \frac{1}{2} \theta^2 \end{aligned} \tag{1}$$

$$\begin{aligned} > \sin\theta := \theta - \frac{\theta^3}{6}; \\ & \qquad \qquad \qquad \sin\theta := \theta - \frac{1}{6} \theta^3 \end{aligned} \tag{2}$$

Defining Axes and Position Vector

$$\begin{aligned} > \text{with}(\text{VectorCalculus}) : \\ > \\ > r := \langle x, 0, (\xi + z) \rangle; \\ & \qquad \qquad \qquad r := (xI(\xi, t))e_x + (\xi + zI(\xi, t))e_z \end{aligned} \tag{7}$$

$$\begin{aligned} > D1 := \langle 1, 0, 0 \rangle; \\ & \qquad \qquad \qquad D1 := e_x \end{aligned} \tag{8}$$

$$\begin{aligned} > D2 := \langle 0, 1, 0 \rangle; \\ & \qquad \qquad \qquad D2 := e_y \end{aligned} \tag{9}$$

$$\begin{aligned} > D3 := \langle 0, 0, 1 \rangle; \\ & \qquad \qquad \qquad D3 := e_z \end{aligned} \tag{10}$$

$$\begin{aligned} > d1 := \langle \cos\theta, 0, -\sin\theta \rangle; \\ & \qquad \qquad \qquad d1 := \left(1 - \frac{1}{2} \theta I(\xi, t)^2\right)e_x + \left(-\theta I(\xi, t) + \frac{1}{6} \theta I(\xi, t)^3\right)e_z \end{aligned} \tag{11}$$

$$\begin{aligned} > d2 := \langle 0, 1, 0 \rangle; \\ & \qquad \qquad \qquad d2 := e_y \end{aligned} \tag{12}$$

$$\begin{aligned} > d3 := \text{diff}(r, \xi); \\ & \qquad \qquad \qquad d3 := \left(\frac{\partial}{\partial \xi} xI(\xi, t)\right)e_x + \left(1 + \frac{\partial}{\partial \xi} zI(\xi, t)\right)e_z \end{aligned} \tag{13}$$

Strains

$$\begin{aligned} &> \gamma_3 := (d1 \cdot d3) - (D1 \cdot D3); \\ \gamma_3 &:= \left(1 - \frac{1}{2} \theta l(\xi, t)^2\right) \left(\frac{\partial}{\partial \xi} x l(\xi, t)\right) + \left(-\theta l(\xi, t) + \frac{1}{6} \theta l(\xi, t)^3\right) \left(1 + \frac{\partial}{\partial \xi} z l(\xi, t)\right) \end{aligned} \quad (14)$$

$$\begin{aligned} &> \beta_3 := (d3 \cdot d3) - (D3 \cdot D3); \\ \beta_3 &:= \left(\frac{\partial}{\partial \xi} x l(\xi, t)\right)^2 + \left(1 + \frac{\partial}{\partial \xi} z l(\xi, t)\right)^2 - 1 \end{aligned} \quad (15)$$

$$\begin{aligned} &> k13 := (\text{diff}(d1, \xi) \cdot d3) - (\text{diff}(D1, \xi) \cdot D3); \\ k13 &:= -\theta l(\xi, t) \left(\frac{\partial}{\partial \xi} \theta l(\xi, t)\right) \left(\frac{\partial}{\partial \xi} x l(\xi, t)\right) + \left(-\left(\frac{\partial}{\partial \xi} \theta l(\xi, t)\right) + \frac{1}{2} \theta l(\xi, t)^2 \left(\frac{\partial}{\partial \xi} \theta l(\xi, t)\right)\right) \left(1 + \frac{\partial}{\partial \xi} z l(\xi, t)\right) \end{aligned} \quad (16)$$

Balance Equations

$$\begin{aligned} &> \text{constants} := EA, GA, k, \\ & \qquad \qquad \qquad \text{constants} := EA, GA, k \end{aligned} \quad (17)$$

$$\begin{aligned} &> n := GA \cdot k \cdot \gamma_3 \cdot d1 + \frac{EA \cdot \beta_3 \cdot d3}{2} + EI \cdot k13 \cdot \text{diff}(d1, \xi); \\ n &:= \left(GA k \left(\left(1 - \frac{1}{2} \theta l(\xi, t)^2\right) \left(\frac{\partial}{\partial \xi} x l(\xi, t)\right) + \left(-\theta l(\xi, t) + \frac{1}{6} \theta l(\xi, t)^3\right) \left(1 + \frac{\partial}{\partial \xi} z l(\xi, t)\right) \right) \right. \\ & \quad \left. + \frac{\partial}{\partial \xi} z l(\xi, t) \right) \left(1 - \frac{1}{2} \theta l(\xi, t)^2\right) + \frac{1}{2} EA \left(\left(\frac{\partial}{\partial \xi} x l(\xi, t)\right)^2 + \left(1 + \frac{\partial}{\partial \xi} z l(\xi, t)\right)^2 \right. \\ & \quad \left. - 1 \right) \left(\frac{\partial}{\partial \xi} x l(\xi, t)\right) - EI \left(-\theta l(\xi, t) \left(\frac{\partial}{\partial \xi} \theta l(\xi, t)\right) \left(\frac{\partial}{\partial \xi} x l(\xi, t)\right) + \left(-\left(\frac{\partial}{\partial \xi} \theta l(\xi, t)\right) \right. \right. \\ & \quad \left. \left. + \frac{1}{2} \theta l(\xi, t)^2 \left(\frac{\partial}{\partial \xi} \theta l(\xi, t)\right)\right) \left(1 + \frac{\partial}{\partial \xi} z l(\xi, t)\right) \right) \theta l(\xi, t) \left(\frac{\partial}{\partial \xi} \theta l(\xi, t)\right) \Bigg) e_x \\ & \quad + \left(GA k \left(\left(1 - \frac{1}{2} \theta l(\xi, t)^2\right) \left(\frac{\partial}{\partial \xi} x l(\xi, t)\right) + \left(-\theta l(\xi, t) + \frac{1}{6} \theta l(\xi, t)^3\right) \left(1 + \frac{\partial}{\partial \xi} z l(\xi, t)\right) \right) \right. \\ & \quad \left. + \frac{\partial}{\partial \xi} z l(\xi, t) \right) \left(-\theta l(\xi, t) + \frac{1}{6} \theta l(\xi, t)^3\right) + \frac{1}{2} EA \left(\left(\frac{\partial}{\partial \xi} x l(\xi, t)\right)^2 + \left(1 + \frac{\partial}{\partial \xi} z l(\xi, t)\right)^2 \right. \\ & \quad \left. - 1 \right) \left(1 + \frac{\partial}{\partial \xi} z l(\xi, t)\right) + EI \left(-\theta l(\xi, t) \left(\frac{\partial}{\partial \xi} \theta l(\xi, t)\right) \left(\frac{\partial}{\partial \xi} x l(\xi, t)\right) + \left(-\left(\frac{\partial}{\partial \xi} \theta l(\xi, t)\right) \right. \right. \\ & \quad \left. \left. + \frac{1}{2} \theta l(\xi, t)^2 \left(\frac{\partial}{\partial \xi} \theta l(\xi, t)\right)\right) \left(1 + \frac{\partial}{\partial \xi} z l(\xi, t)\right) \right) \left(-\left(\frac{\partial}{\partial \xi} \theta l(\xi, t)\right) + \frac{1}{2} \theta l(\xi, t)^2 \left(\frac{\partial}{\partial \xi} \theta l(\xi, t)\right) \right) \Bigg) e_z \end{aligned} \quad (18)$$

$$\begin{aligned}
&> m := EI \cdot k13 \cdot (d1 \times d3); \\
m &:= \left(EI \left(-\theta l(\xi, t) \left(\frac{\partial}{\partial \xi} \theta l(\xi, t) \right) \left(\frac{\partial}{\partial \xi} x l(\xi, t) \right) + \left(-\left(\frac{\partial}{\partial \xi} \theta l(\xi, t) \right) + \frac{1}{2} \theta l(\xi, t) \right)^2 \left(\frac{\partial}{\partial \xi} \theta l(\xi, t) \right) \right) \left(1 + \frac{\partial}{\partial \xi} z l(\xi, t) \right) \left(\left(-\theta l(\xi, t) + \frac{1}{6} \theta l(\xi, t)^3 \right) \left(\frac{\partial}{\partial \xi} x l(\xi, t) \right) - \left(1 - \frac{1}{2} \theta l(\xi, t)^2 \right) \left(1 + \frac{\partial}{\partial \xi} z l(\xi, t) \right) \right) \right) e_y
\end{aligned} \tag{19}$$

>

ϕ As book keeping parameter for expanding series

$$\begin{aligned}
&> x l(\xi, t) := u11(\xi) \cdot \phi(t) + u12(\xi) \cdot \phi^2(t) + u13(\xi) \cdot \phi^3(t); \\
x l &:= (\xi, t) \rightarrow u11(\xi) \phi(t) + u12(\xi) \phi(t)^2 + u13(\xi) \phi(t)^3
\end{aligned} \tag{23}$$

$$\begin{aligned}
&> y l(\xi, t) := u21(\xi) \cdot \phi(t) + u22(\xi) \cdot \phi^2(t) + u23(\xi) \cdot \phi^3(t); \\
y l &:= (\xi, t) \rightarrow u21(\xi) \phi(t) + u22(\xi) \phi(t)^2 + u23(\xi) \phi(t)^3
\end{aligned} \tag{24}$$

$$\begin{aligned}
&> z l(\xi, t) := u31(\xi) \cdot \phi(t) + u32(\xi) \cdot \phi^2(t) + u33(\xi) \cdot \phi^3(t); \\
z l &:= (\xi, t) \rightarrow u31(\xi) \phi(t) + u32(\xi) \phi(t)^2 + u33(\xi) \phi(t)^3
\end{aligned} \tag{25}$$

$$\begin{aligned}
&> \theta l(\xi, t) := \alpha l(\xi) \cdot \phi(t) + \alpha 2(\xi) \cdot \phi^2(t) + \alpha 3(\xi) \cdot \phi^3(t); \\
\theta l &:= (\xi, t) \rightarrow \alpha l(\xi) \phi(t) + \alpha 2(\xi) \phi(t)^2 + \alpha 3(\xi) \phi(t)^3
\end{aligned} \tag{26}$$

Boundary Value Problem

$$\begin{aligned}
&> BV11 := \text{coeff}(n1d, \phi(t), 1); \\
BV11 &:= GAk \left(\frac{d^2}{d\xi^2} u11(\xi) - \left(\frac{d}{d\xi} \alpha l(\xi) \right) \right)
\end{aligned} \tag{30}$$

$$\begin{aligned}
&> BV12 := \text{coeff}(n3d, \phi(t), 1); \\
BV12 &:= EA \left(\frac{d^2}{d\xi^2} u31(\xi) \right)
\end{aligned} \tag{31}$$

$$\begin{aligned}
&> BV13 := \text{coeff}(m2d, \phi(t), 1); \\
BV13 &:= EI \left(\frac{d^2}{d\xi^2} \alpha l(\xi) \right) + GAk \left(\frac{d}{d\xi} u11(\xi) - \alpha l(\xi) \right)
\end{aligned} \tag{32}$$

$$\begin{aligned}
&> BV21 := \text{coeff}(n1d, \phi(t), 2); \\
BV21 &:= GAk \left(-\left(\frac{d}{d\xi} \alpha l(\xi) \right) \left(\frac{d}{d\xi} u31(\xi) \right) - \left(\frac{d}{d\xi} \alpha 2(\xi) \right) - \alpha l(\xi) \left(\frac{d^2}{d\xi^2} u31(\xi) \right) \right. \\
&\quad \left. + \frac{d^2}{d\xi^2} u12(\xi) \right) + EA \left(\frac{d^2}{d\xi^2} u31(\xi) \right) \left(\frac{d}{d\xi} u11(\xi) \right)
\end{aligned} \tag{33}$$

$$+ EA \left(\frac{d}{d\xi} u_{31}(\xi) \right) \left(\frac{d^2}{d\xi^2} u_{11}(\xi) \right)$$

> $BV22 := \text{coeff}(n3d, \phi(t), 2)$;

$$\begin{aligned} BV22 := & -GAK \left(\frac{d^2}{d\xi^2} u_{11}(\xi) - \left(\frac{d}{d\xi} \alpha l(\xi) \right) \right) \alpha l(\xi) - GAK \left(\frac{d}{d\xi} u_{11}(\xi) \right. \\ & \left. - \alpha l(\xi) \right) \left(\frac{d}{d\xi} \alpha l(\xi) \right) + 2EA \left(\frac{d^2}{d\xi^2} u_{31}(\xi) \right) \left(\frac{d}{d\xi} u_{31}(\xi) \right) \\ & + \frac{1}{2} EA \left(2 \left(\frac{d^2}{d\xi^2} u_{32}(\xi) \right) + 2 \left(\frac{d}{d\xi} u_{31}(\xi) \right) \left(\frac{d^2}{d\xi^2} u_{31}(\xi) \right) \right) \\ & + 2 \left(\frac{d}{d\xi} u_{11}(\xi) \right) \left(\frac{d^2}{d\xi^2} u_{11}(\xi) \right) + 2EI \left(\frac{d^2}{d\xi^2} \alpha l(\xi) \right) \left(\frac{d}{d\xi} \alpha l(\xi) \right) \end{aligned} \quad (34)$$

> $BV31 := \text{coeff}(n1d, \phi(t), 3)$;

$$\begin{aligned} BV31 := & -\frac{1}{2} GAK \left(\frac{d^2}{d\xi^2} u_{11}(\xi) - \left(\frac{d}{d\xi} \alpha l(\xi) \right) \right) \alpha l(\xi)^2 + GAK \left(\right. \\ & \left. - \left(\frac{d}{d\xi} \alpha l(\xi) \right) \left(\frac{d}{d\xi} u_{32}(\xi) \right) - \left(\frac{d}{d\xi} \alpha l(\xi) \right) \left(\frac{d}{d\xi} u_{31}(\xi) \right) - \left(\frac{d}{d\xi} \alpha l(\xi) \right) \right) \\ & + \frac{1}{2} \alpha l(\xi)^2 \left(\frac{d}{d\xi} \alpha l(\xi) \right) - \alpha l(\xi) \left(\frac{d^2}{d\xi^2} u_{32}(\xi) \right) - \alpha l(\xi) \left(\frac{d^2}{d\xi^2} u_{31}(\xi) \right) \\ & + \frac{d^2}{d\xi^2} u_{13}(\xi) - \frac{1}{2} \alpha l(\xi)^2 \left(\frac{d^2}{d\xi^2} u_{11}(\xi) \right) - \alpha l(\xi) \left(\frac{d}{d\xi} \alpha l(\xi) \right) \left(\frac{d}{d\xi} u_{11}(\xi) \right) \\ & - GAK \left(\frac{d}{d\xi} u_{11}(\xi) - \alpha l(\xi) \right) \alpha l(\xi) \left(\frac{d}{d\xi} \alpha l(\xi) \right) \\ & + EA \left(\frac{d^2}{d\xi^2} u_{31}(\xi) \right) \left(\frac{d}{d\xi} u_{12}(\xi) \right) + \frac{1}{2} EA \left(2 \left(\frac{d^2}{d\xi^2} u_{32}(\xi) \right) \right) \\ & + 2 \left(\frac{d}{d\xi} u_{31}(\xi) \right) \left(\frac{d^2}{d\xi^2} u_{31}(\xi) \right) + 2 \left(\frac{d}{d\xi} u_{11}(\xi) \right) \left(\frac{d^2}{d\xi^2} u_{11}(\xi) \right) \end{aligned} \quad (36)$$

> $BV32 := \text{coeff}(n3d, \phi(t), 3);$

$$\begin{aligned}
BV32 := & -GAk \left(\frac{d^2}{d\xi^2} u11(\xi) - \left(\frac{d}{d\xi} \alpha l(\xi) \right) \right) \alpha l(\xi) - GAk \left(\right. \\
& - \left(\frac{d}{d\xi} \alpha l(\xi) \right) \left(\frac{d}{d\xi} u31(\xi) \right) - \left(\frac{d}{d\xi} \alpha l(\xi) \right) - \alpha l(\xi) \left(\frac{d^2}{d\xi^2} u31(\xi) \right) \\
& \left. + \frac{d^2}{d\xi^2} u12(\xi) \right) \alpha l(\xi) - GAk \left(\frac{d}{d\xi} u11(\xi) - \alpha l(\xi) \right) \left(\frac{d}{d\xi} \alpha l(\xi) \right) - GAk \left(\right. \\
& - \alpha l(\xi) \left(\frac{d}{d\xi} u31(\xi) \right) - \alpha l(\xi) + \frac{d}{d\xi} u12(\xi) \left. \right) \left(\frac{d}{d\xi} \alpha l(\xi) \right) \\
& + EA \left(\frac{d^2}{d\xi^2} u31(\xi) \right) \left(\frac{d}{d\xi} u32(\xi) \right) + \frac{1}{2} EA \left(2 \left(\frac{d^2}{d\xi^2} u32(\xi) \right) \right. \\
& \left. + 2 \left(\frac{d}{d\xi} u31(\xi) \right) \left(\frac{d^2}{d\xi^2} u31(\xi) \right) + 2 \left(\frac{d}{d\xi} u11(\xi) \right) \left(\frac{d^2}{d\xi^2} u11(\xi) \right) \right) \\
& \left(\frac{d}{d\xi} u31(\xi) \right) + \frac{1}{2} EA \left(2 \left(\frac{d^2}{d\xi^2} u33(\xi) \right) + 2 \left(\frac{d}{d\xi} u31(\xi) \right) \left(\frac{d^2}{d\xi^2} u32(\xi) \right) \right. \\
& \left. + 2 \left(\frac{d}{d\xi} u32(\xi) \right) \left(\frac{d^2}{d\xi^2} u31(\xi) \right) + 2 \left(\frac{d}{d\xi} u11(\xi) \right) \left(\frac{d^2}{d\xi^2} u12(\xi) \right) \right. \\
& \left. + 2 \left(\frac{d}{d\xi} u12(\xi) \right) \left(\frac{d^2}{d\xi^2} u11(\xi) \right) \right) + EA \left(\frac{d}{d\xi} u31(\xi) \right) \left(\frac{d^2}{d\xi^2} u32(\xi) \right) \\
& + \frac{1}{2} EA \left(\left(\frac{d}{d\xi} u11(\xi) \right)^2 + 2 \left(\frac{d}{d\xi} u32(\xi) \right) + \left(\frac{d}{d\xi} u31(\xi) \right)^2 \right) \left(\frac{d^2}{d\xi^2} u31(\xi) \right) \\
& + EI \left(\frac{d^2}{d\xi^2} \alpha l(\xi) \right) \left(\frac{d}{d\xi} \alpha l(\xi) \right) - EI \left(- \left(\frac{d^2}{d\xi^2} \alpha l(\xi) \right) \left(\frac{d}{d\xi} u31(\xi) \right) \right. \\
& \left. - \left(\frac{d^2}{d\xi^2} \alpha l(\xi) \right) - \left(\frac{d}{d\xi} \alpha l(\xi) \right) \left(\frac{d^2}{d\xi^2} u31(\xi) \right) \right) \left(\frac{d}{d\xi} \alpha l(\xi) \right) \\
& + EI \left(\frac{d}{d\xi} \alpha l(\xi) \right) \left(\frac{d^2}{d\xi^2} \alpha l(\xi) \right) - EI \left(- \left(\frac{d}{d\xi} \alpha l(\xi) \right) \left(\frac{d}{d\xi} u31(\xi) \right) \right)
\end{aligned}$$

$$\begin{aligned}
&> BV33 := \text{coeff}(m2d, \phi(t), 3); \\
BV33 := & -EI \left(\frac{d^2}{d\xi^2} \alpha l(\xi) \right) \left(-\alpha l(\xi) \left(\frac{d}{d\xi} u11(\xi) \right) - \left(\frac{d}{d\xi} u32(\xi) \right) + \frac{1}{2} \alpha l(\xi)^2 \right) \\
& -EI \left(- \left(\frac{d^2}{d\xi^2} \alpha l(\xi) \right) \left(\frac{d}{d\xi} u31(\xi) \right) - \left(\frac{d^2}{d\xi^2} \alpha \omega(\xi) \right) \right. \\
& - \left. \left(\frac{d}{d\xi} \alpha l(\xi) \right) \left(\frac{d^2}{d\xi^2} u31(\xi) \right) \right) \left(\frac{d}{d\xi} u31(\xi) \right) -EI \left(\right. \\
& - \left. \left(\frac{d}{d\xi} \alpha l(\xi) \right)^2 \left(\frac{d}{d\xi} u11(\xi) \right) - \alpha l(\xi) \left(\frac{d^2}{d\xi^2} \alpha l(\xi) \right) \left(\frac{d}{d\xi} u11(\xi) \right) \right. \\
& - \alpha l(\xi) \left(\frac{d}{d\xi} \alpha l(\xi) \right) \left(\frac{d^2}{d\xi^2} u11(\xi) \right) - \left(\frac{d^2}{d\xi^2} \alpha l(\xi) \right) \left(\frac{d}{d\xi} u32(\xi) \right) \\
& - \left(\frac{d^2}{d\xi^2} \alpha \omega(\xi) \right) \left(\frac{d}{d\xi} u31(\xi) \right) - \left(\frac{d^2}{d\xi^2} \alpha \beta(\xi) \right) + \alpha l(\xi) \left(\frac{d}{d\xi} \alpha l(\xi) \right)^2 \\
& + \frac{1}{2} \alpha l(\xi)^2 \left(\frac{d^2}{d\xi^2} \alpha l(\xi) \right) - \left(\frac{d}{d\xi} \alpha l(\xi) \right) \left(\frac{d^2}{d\xi^2} u32(\xi) \right) \\
& - \left(\frac{d}{d\xi} \alpha \omega(\xi) \right) \left(\frac{d^2}{d\xi^2} u31(\xi) \right) \left. \right) -EI \left(\frac{d}{d\xi} \alpha l(\xi) \right) \left(- \left(\frac{d}{d\xi} \alpha l(\xi) \right) \left(\frac{d}{d\xi} u11(\xi) \right) \right. \\
& - \alpha l(\xi) \left(\frac{d^2}{d\xi^2} u11(\xi) \right) - \left(\frac{d^2}{d\xi^2} u32(\xi) \right) + \alpha l(\xi) \left(\frac{d}{d\xi} \alpha l(\xi) \right) \left. \right) -EI \left(\right. \\
& - \left. \left(\frac{d}{d\xi} \alpha l(\xi) \right) \left(\frac{d}{d\xi} u31(\xi) \right) - \left(\frac{d}{d\xi} \alpha \omega(\xi) \right) \right) \left(\frac{d^2}{d\xi^2} u31(\xi) \right) \\
& + \left(\frac{d}{d\xi} u31(\xi) \right) \left(GAk \left(-\alpha l(\xi) \left(\frac{d}{d\xi} u31(\xi) \right) - \alpha \omega(\xi) + \frac{d}{d\xi} u12(\xi) \right) \right. \\
& + EA \left(\frac{d}{d\xi} u31(\xi) \right) \left(\frac{d}{d\xi} u11(\xi) \right) \left. \right) + \frac{1}{2} EA \left(\left(\frac{d}{d\xi} u11(\xi) \right)^2 + 2 \left(\frac{d}{d\xi} u32(\xi) \right) \right. \\
& + \left. \left(\frac{d}{d\xi} u31(\xi) \right)^2 \right) \left(\frac{d}{d\xi} u11(\xi) \right) - \frac{1}{2} GAk \left(\frac{d}{d\xi} u11(\xi) - \alpha l(\xi) \right) \alpha l(\xi)^2 \\
& + GAk \left(-\alpha l(\xi) \left(\frac{d}{d\xi} u32(\xi) \right) - \alpha \omega(\xi) \left(\frac{d}{d\xi} u31(\xi) \right) - \alpha \beta(\xi) + \frac{1}{6} \alpha l(\xi)^3 \right. \\
& + \left. \frac{d}{d\xi} u13(\xi) - \frac{1}{2} \alpha l(\xi)^2 \left(\frac{d}{d\xi} u11(\xi) \right) \right) + EI \left(\frac{d}{d\xi} \alpha l(\xi) \right)^2 \alpha l(\xi) \\
& + \left(\frac{d}{d\xi} u32(\xi) \right) GAk \left(\frac{d}{d\xi} u11(\xi) - \alpha l(\xi) \right) - \left(\frac{d}{d\xi} u11(\xi) \right) \left(-GAk \left(\frac{d}{d\xi} u11(\xi) \right) \right.
\end{aligned}$$

Complete expressions and Boundary value Problem Solving have not been included in the code above and can be provided upon request.

APPENDIX – II

Defining Displacements

$$\begin{aligned}u1 &:= \epsilon \cdot u11(\xi, t) + \epsilon^2 \cdot u12(\xi, t) + \epsilon^3 \cdot u13(\xi, t); \\ &\quad u1 := \epsilon u11(\xi, t) + \epsilon^2 u12(\xi, t) + \epsilon^3 u13(\xi, t) \\ u2 &:= \epsilon \cdot u21(\xi, t) + \epsilon^2 \cdot u22(\xi, t) + \epsilon^3 \cdot u23(\xi, t); \\ &\quad u2 := \epsilon u21(\xi, t) + \epsilon^2 u22(\xi, t) + \epsilon^3 u23(\xi, t) \\ u3 &:= \epsilon \cdot u31(\xi, t) + \epsilon^2 \cdot u32(\xi, t) + \epsilon^3 \cdot u33(\xi, t); \\ &\quad u3 := \epsilon u31(\xi, t) + \epsilon^2 u32(\xi, t) + \epsilon^3 u33(\xi, t) \\ \theta &:= \epsilon \cdot \theta1(\xi, t) + \epsilon^2 \cdot \theta2(\xi, t) + \epsilon^3 \cdot \theta3(\xi, t); \\ &\quad \theta := \epsilon \theta1(\xi, t) + \epsilon^2 \theta2(\xi, t) + \epsilon^3 \theta3(\xi, t)\end{aligned}$$

Defining Axes and Position Vector

$$\begin{aligned}e1 &:= \langle 1, 0, 0 \rangle; & e1 &:= e_x \\ e3 &:= \langle 0, 0, 1 \rangle; & e3 &:= e_z \\ e2 &:= \langle 0, 1, 0 \rangle; & e2 &:= e_y \\ r &:= \langle u1, 0, \xi + u3 \rangle; \\ &= (\epsilon u11(\xi, t) + \epsilon^2 u12(\xi, t) + \epsilon^3 u13(\xi, t))e_x + (\xi + \epsilon u31(\xi, t) + \epsilon^2 u32(\xi, t) \\ &\quad + \epsilon^3 u33(\xi, t))e_z \\ rs &:= \text{diff}(r, \xi); \\ &:= \left(\epsilon \left(\frac{\partial}{\partial \xi} u11(\xi, t) \right) + \epsilon^2 \left(\frac{\partial}{\partial \xi} u12(\xi, t) \right) + \epsilon^3 \left(\frac{\partial}{\partial \xi} u13(\xi, t) \right) \right) e_x + \left(1 \right. \\ &\quad \left. + \epsilon \left(\frac{\partial}{\partial \xi} u31(\xi, t) \right) + \epsilon^2 \left(\frac{\partial}{\partial \xi} u32(\xi, t) \right) + \epsilon^3 \left(\frac{\partial}{\partial \xi} u33(\xi, t) \right) \right) e_z \\ dl &:= \langle \cos\theta, 0, -\sin\theta \rangle; & dl &:= (\cos\theta)e_x - \sin\theta e_z\end{aligned}$$

Strains

> $r13 := \text{DotProduct}(d1, d3);$

$$Y13 := \cos\theta \left(\epsilon \left(\frac{\partial}{\partial \xi} u11(\xi, t) \right) + \epsilon^2 \left(\frac{\partial}{\partial \xi} u12(\xi, t) \right) + \epsilon^3 \left(\frac{\partial}{\partial \xi} u13(\xi, t) \right) \right) - \sin\theta \left(1 + \epsilon \left(\frac{\partial}{\partial \xi} u31(\xi, t) \right) + \epsilon^2 \left(\frac{\partial}{\partial \xi} u32(\xi, t) \right) + \epsilon^3 \left(\frac{\partial}{\partial \xi} u33(\xi, t) \right) \right)$$

> $r33 := \text{DotProduct}(d3, d3) - \text{DotProduct}(e3, e3);$

$$Y33 := \left(\epsilon \left(\frac{\partial}{\partial \xi} u11(\xi, t) \right) + \epsilon^2 \left(\frac{\partial}{\partial \xi} u12(\xi, t) \right) + \epsilon^3 \left(\frac{\partial}{\partial \xi} u13(\xi, t) \right) \right)^2 + \left(1 + \epsilon \left(\frac{\partial}{\partial \xi} u31(\xi, t) \right) + \epsilon^2 \left(\frac{\partial}{\partial \xi} u32(\xi, t) \right) + \epsilon^3 \left(\frac{\partial}{\partial \xi} u33(\xi, t) \right) \right)^2 - 1$$

> $k[13] := \text{DotProduct}(\text{diff}(d1, \xi), d3);$

$$k_{13} := -(\epsilon \theta 1(\xi, t) + \epsilon^2 \theta 2(\xi, t) + \epsilon^3 \theta 3(\xi, t)) \left(\epsilon \left(\frac{\partial}{\partial \xi} \theta 1(\xi, t) \right) + \epsilon^2 \left(\frac{\partial}{\partial \xi} \theta 2(\xi, t) \right) + \epsilon^3 \left(\frac{\partial}{\partial \xi} \theta 3(\xi, t) \right) \right) \left(\epsilon \left(\frac{\partial}{\partial \xi} u11(\xi, t) \right) + \epsilon^2 \left(\frac{\partial}{\partial \xi} u12(\xi, t) \right) + \epsilon^3 \left(\frac{\partial}{\partial \xi} u13(\xi, t) \right) \right) + \left(-\epsilon \left(\frac{\partial}{\partial \xi} \theta 1(\xi, t) \right) - \epsilon^2 \left(\frac{\partial}{\partial \xi} \theta 2(\xi, t) \right) - \epsilon^3 \left(\frac{\partial}{\partial \xi} \theta 3(\xi, t) \right) + \frac{1}{2} (\epsilon \theta 1(\xi, t) + \epsilon^2 \theta 2(\xi, t) + \epsilon^3 \theta 3(\xi, t))^2 \right) \left(\epsilon \left(\frac{\partial}{\partial \xi} \theta 1(\xi, t) \right) + \epsilon^2 \left(\frac{\partial}{\partial \xi} \theta 2(\xi, t) \right) + \epsilon^3 \left(\frac{\partial}{\partial \xi} \theta 3(\xi, t) \right) \right) \left(1 + \epsilon \left(\frac{\partial}{\partial \xi} u31(\xi, t) \right) + \epsilon^2 \left(\frac{\partial}{\partial \xi} u32(\xi, t) \right) + \epsilon^3 \left(\frac{\partial}{\partial \xi} u33(\xi, t) \right) \right)$$

Balance Equations

> $n1 := \text{coeff}(n, \epsilon, 1);$

$$n1 := \left(G A k \left(\frac{\partial}{\partial \xi} u11(\xi, t) - \theta 1(\xi, t) \right) \right) e_x + \left(E A \left(\frac{\partial}{\partial \xi} u31(\xi, t) \right) \right) e_z$$

> $n2 := \text{coeff}(n, \epsilon, 2);$

$$n2 := \left(G A k \left(\frac{\partial}{\partial \xi} u12(\xi, t) - \theta 1(\xi, t) \left(\frac{\partial}{\partial \xi} u31(\xi, t) \right) - \theta 2(\xi, t) \right) + E A \left(\frac{\partial}{\partial \xi} u31(\xi, t) \right) \right) \left(\frac{\partial}{\partial \xi} u11(\xi, t) \right) e_x + \left(-G A k \left(\frac{\partial}{\partial \xi} u11(\xi, t) - \theta 1(\xi, t) \right) \theta 1(\xi, t) + E A \left(\frac{\partial}{\partial \xi} u31(\xi, t) \right)^2 + \frac{1}{2} E A \left(\left(\frac{\partial}{\partial \xi} u11(\xi, t) \right)^2 + 2 \left(\frac{\partial}{\partial \xi} u32(\xi, t) \right) + \left(\frac{\partial}{\partial \xi} u31(\xi, t) \right)^2 \right) + E I m_2 \left(\frac{\partial}{\partial \xi} \theta 1(\xi, t) \right)^2 \right) e_z$$

$$\cdot m1 := \text{coeff}(m, \epsilon, 1);$$

$$m1 := \left(E I m_2 \left(\frac{\partial}{\partial \xi} \theta l(\xi, t) \right) \right) e_y$$

ϵ As book keeping parameter for expanding series

$$u1 := \epsilon \cdot u11(\xi, t) + \epsilon^2 \cdot u12(\xi, t) + \epsilon^3 \cdot u13(\xi, t);$$

$$u1 := \epsilon u11(\xi, t) + \epsilon^2 u12(\xi, t) + \epsilon^3 u13(\xi, t)$$

$$u2 := \epsilon \cdot u21(\xi, t) + \epsilon^2 \cdot u22(\xi, t) + \epsilon^3 \cdot u23(\xi, t);$$

$$u2 := \epsilon u21(\xi, t) + \epsilon^2 u22(\xi, t) + \epsilon^3 u23(\xi, t)$$

$$u3 := \epsilon \cdot u31(\xi, t) + \epsilon^2 \cdot u32(\xi, t) + \epsilon^3 \cdot u33(\xi, t);$$

$$u3 := \epsilon u31(\xi, t) + \epsilon^2 u32(\xi, t) + \epsilon^3 u33(\xi, t)$$

$$\theta := \epsilon \cdot \theta1(\xi, t) + \epsilon^2 \cdot \theta2(\xi, t) + \epsilon^3 \cdot \theta3(\xi, t);$$

$$\theta := \epsilon \theta1(\xi, t) + \epsilon^2 \theta2(\xi, t) + \epsilon^3 \theta3(\xi, t)$$

Boundary Value Problem

$$> BV11 := \text{coeff}(n1d, \phi(t), 1);$$

$$BV11 := G A k \left(\frac{d^2}{d\xi^2} u11(\xi) - \left(\frac{d}{d\xi} \alpha l(\xi) \right) \right) \quad (30)$$

$$> BV12 := \text{coeff}(n3d, \phi(t), 1);$$

$$BV12 := E A \left(\frac{d^2}{d\xi^2} u31(\xi) \right) \quad (31)$$

$$> BV13 := \text{coeff}(m2d, \phi(t), 1);$$

$$BV13 := E I \left(\frac{d^2}{d\xi^2} \alpha l(\xi) \right) + G A k \left(\frac{d}{d\xi} u11(\xi) - \alpha l(\xi) \right) \quad (32)$$

$$> BV21 := \text{coeff}(n1d, \phi(t), 2);$$

$$BV21 := G A k \left(- \left(\frac{d}{d\xi} \alpha l(\xi) \right) \left(\frac{d}{d\xi} u31(\xi) \right) - \left(\frac{d}{d\xi} \alpha l(\xi) \right) - \alpha l(\xi) \left(\frac{d^2}{d\xi^2} u31(\xi) \right) \right. \\ \left. + \frac{d^2}{d\xi^2} u12(\xi) \right) + E A \left(\frac{d^2}{d\xi^2} u31(\xi) \right) \left(\frac{d}{d\xi} u11(\xi) \right) \quad (33)$$

$$+ EA \left(\frac{d}{d\xi} u_{31}(\xi) \right) \left(\frac{d^2}{d\xi^2} u_{11}(\xi) \right)$$

> $BV22 := \text{coeff}(n3d, \phi(t), 2);$

$$\begin{aligned} BV22 := & -GAK \left(\frac{d^2}{d\xi^2} u_{11}(\xi) - \left(\frac{d}{d\xi} \alpha l(\xi) \right) \right) \alpha l(\xi) - GAK \left(\frac{d}{d\xi} u_{11}(\xi) \right. \\ & \left. - \alpha l(\xi) \right) \left(\frac{d}{d\xi} \alpha l(\xi) \right) + 2EA \left(\frac{d^2}{d\xi^2} u_{31}(\xi) \right) \left(\frac{d}{d\xi} u_{31}(\xi) \right) \\ & + \frac{1}{2} EA \left(2 \left(\frac{d^2}{d\xi^2} u_{32}(\xi) \right) + 2 \left(\frac{d}{d\xi} u_{31}(\xi) \right) \left(\frac{d^2}{d\xi^2} u_{31}(\xi) \right) \right) \\ & + 2 \left(\frac{d}{d\xi} u_{11}(\xi) \right) \left(\frac{d^2}{d\xi^2} u_{11}(\xi) \right) + 2EI \left(\frac{d^2}{d\xi^2} \alpha l(\xi) \right) \left(\frac{d}{d\xi} \alpha l(\xi) \right) \end{aligned} \quad (34)$$

> $BV31 := \text{coeff}(n1d, \phi(t), 3);$

$$\begin{aligned} BV31 := & -\frac{1}{2} GAK \left(\frac{d^2}{d\xi^2} u_{11}(\xi) - \left(\frac{d}{d\xi} \alpha l(\xi) \right) \right) \alpha l(\xi)^2 + GAK \left(\right. \\ & \left. - \left(\frac{d}{d\xi} \alpha l(\xi) \right) \left(\frac{d}{d\xi} u_{32}(\xi) \right) - \left(\frac{d}{d\xi} \alpha l(\xi) \right) \left(\frac{d}{d\xi} u_{31}(\xi) \right) - \left(\frac{d}{d\xi} \alpha s(\xi) \right) \right. \\ & \left. + \frac{1}{2} \alpha l(\xi)^2 \left(\frac{d}{d\xi} \alpha l(\xi) \right) - \alpha l(\xi) \left(\frac{d^2}{d\xi^2} u_{32}(\xi) \right) - \alpha l(\xi) \left(\frac{d^2}{d\xi^2} u_{31}(\xi) \right) \right) \\ & + \frac{d^2}{d\xi^2} u_{13}(\xi) - \frac{1}{2} \alpha l(\xi)^2 \left(\frac{d^2}{d\xi^2} u_{11}(\xi) \right) - \alpha l(\xi) \left(\frac{d}{d\xi} \alpha l(\xi) \right) \left(\frac{d}{d\xi} u_{11}(\xi) \right) \\ & - GAK \left(\frac{d}{d\xi} u_{11}(\xi) - \alpha l(\xi) \right) \alpha l(\xi) \left(\frac{d}{d\xi} \alpha l(\xi) \right) \\ & + EA \left(\frac{d^2}{d\xi^2} u_{31}(\xi) \right) \left(\frac{d}{d\xi} u_{12}(\xi) \right) + \frac{1}{2} EA \left(2 \left(\frac{d^2}{d\xi^2} u_{32}(\xi) \right) \right. \\ & \left. + 2 \left(\frac{d}{d\xi} u_{31}(\xi) \right) \left(\frac{d^2}{d\xi^2} u_{31}(\xi) \right) + 2 \left(\frac{d}{d\xi} u_{11}(\xi) \right) \left(\frac{d^2}{d\xi^2} u_{11}(\xi) \right) \right) \end{aligned} \quad (36)$$

> $BV32 := \text{coeff}(n3d, \phi(t), 3);$

$$\begin{aligned}
BV32 := & -GAk \left(\frac{d^2}{d\xi^2} u11(\xi) - \left(\frac{d}{d\xi} \alpha l(\xi) \right) \right) \alpha l(\xi) - GAk \left(\right. \\
& - \left(\frac{d}{d\xi} \alpha l(\xi) \right) \left(\frac{d}{d\xi} u31(\xi) \right) - \left(\frac{d}{d\xi} \alpha l(\xi) \right) - \alpha l(\xi) \left(\frac{d^2}{d\xi^2} u31(\xi) \right) \\
& \left. + \frac{d^2}{d\xi^2} u12(\xi) \right) \alpha l(\xi) - GAk \left(\frac{d}{d\xi} u11(\xi) - \alpha l(\xi) \right) \left(\frac{d}{d\xi} \alpha l(\xi) \right) - GAk \left(\right. \\
& - \alpha l(\xi) \left(\frac{d}{d\xi} u31(\xi) \right) - \alpha l(\xi) + \frac{d}{d\xi} u12(\xi) \left. \right) \left(\frac{d}{d\xi} \alpha l(\xi) \right) \\
& + EA \left(\frac{d^2}{d\xi^2} u31(\xi) \right) \left(\frac{d}{d\xi} u32(\xi) \right) + \frac{1}{2} EA \left(2 \left(\frac{d^2}{d\xi^2} u32(\xi) \right) \right. \\
& \left. + 2 \left(\frac{d}{d\xi} u31(\xi) \right) \left(\frac{d^2}{d\xi^2} u31(\xi) \right) + 2 \left(\frac{d}{d\xi} u11(\xi) \right) \left(\frac{d^2}{d\xi^2} u11(\xi) \right) \right) \\
& \left(\frac{d}{d\xi} u31(\xi) \right) + \frac{1}{2} EA \left(2 \left(\frac{d^2}{d\xi^2} u33(\xi) \right) + 2 \left(\frac{d}{d\xi} u31(\xi) \right) \left(\frac{d^2}{d\xi^2} u32(\xi) \right) \right. \\
& \left. + 2 \left(\frac{d}{d\xi} u32(\xi) \right) \left(\frac{d^2}{d\xi^2} u31(\xi) \right) + 2 \left(\frac{d}{d\xi} u11(\xi) \right) \left(\frac{d^2}{d\xi^2} u12(\xi) \right) \right. \\
& \left. + 2 \left(\frac{d}{d\xi} u12(\xi) \right) \left(\frac{d^2}{d\xi^2} u11(\xi) \right) \right) + EA \left(\frac{d}{d\xi} u31(\xi) \right) \left(\frac{d^2}{d\xi^2} u32(\xi) \right) \\
& + \frac{1}{2} EA \left(\left(\frac{d}{d\xi} u11(\xi) \right)^2 + 2 \left(\frac{d}{d\xi} u32(\xi) \right) + \left(\frac{d}{d\xi} u31(\xi) \right)^2 \right) \left(\frac{d^2}{d\xi^2} u31(\xi) \right) \\
& + EI \left(\frac{d^2}{d\xi^2} \alpha l(\xi) \right) \left(\frac{d}{d\xi} \alpha l(\xi) \right) - EI \left(- \left(\frac{d^2}{d\xi^2} \alpha l(\xi) \right) \left(\frac{d}{d\xi} u31(\xi) \right) \right. \\
& \left. - \left(\frac{d^2}{d\xi^2} \alpha l(\xi) \right) - \left(\frac{d}{d\xi} \alpha l(\xi) \right) \left(\frac{d^2}{d\xi^2} u31(\xi) \right) \right) \left(\frac{d}{d\xi} \alpha l(\xi) \right) \\
& + EI \left(\frac{d}{d\xi} \alpha l(\xi) \right) \left(\frac{d^2}{d\xi^2} \alpha l(\xi) \right) - EI \left(- \left(\frac{d}{d\xi} \alpha l(\xi) \right) \left(\frac{d}{d\xi} u31(\xi) \right) \right)
\end{aligned}$$

> BV33 := coeff(m2d, phi(t), 3);

$$\begin{aligned}
BV33 := & -EI \left(\frac{d^2}{d\xi^2} \alpha l(\xi) \right) \left(-\alpha l(\xi) \left(\frac{d}{d\xi} u11(\xi) \right) - \left(\frac{d}{d\xi} u32(\xi) \right) + \frac{1}{2} \alpha l(\xi)^2 \right) \\
& -EI \left(- \left(\frac{d^2}{d\xi^2} \alpha l(\xi) \right) \left(\frac{d}{d\xi} u31(\xi) \right) - \left(\frac{d^2}{d\xi^2} \alpha \omega(\xi) \right) \right. \\
& \left. - \left(\frac{d}{d\xi} \alpha l(\xi) \right) \left(\frac{d^2}{d\xi^2} u31(\xi) \right) \right) \left(\frac{d}{d\xi} u31(\xi) \right) -EI \left(\right. \\
& \left. - \left(\frac{d}{d\xi} \alpha l(\xi) \right)^2 \left(\frac{d}{d\xi} u11(\xi) \right) - \alpha l(\xi) \left(\frac{d^2}{d\xi^2} \alpha l(\xi) \right) \left(\frac{d}{d\xi} u11(\xi) \right) \right. \\
& \left. - \alpha l(\xi) \left(\frac{d}{d\xi} \alpha l(\xi) \right) \left(\frac{d^2}{d\xi^2} u11(\xi) \right) - \left(\frac{d^2}{d\xi^2} \alpha l(\xi) \right) \left(\frac{d}{d\xi} u32(\xi) \right) \right. \\
& \left. - \left(\frac{d^2}{d\xi^2} \alpha \omega(\xi) \right) \left(\frac{d}{d\xi} u31(\xi) \right) - \left(\frac{d^2}{d\xi^2} \alpha \beta(\xi) \right) + \alpha l(\xi) \left(\frac{d}{d\xi} \alpha l(\xi) \right)^2 \right. \\
& \left. + \frac{1}{2} \alpha l(\xi)^2 \left(\frac{d^2}{d\xi^2} \alpha l(\xi) \right) - \left(\frac{d}{d\xi} \alpha l(\xi) \right) \left(\frac{d^2}{d\xi^2} u32(\xi) \right) \right. \\
& \left. - \left(\frac{d}{d\xi} \alpha \omega(\xi) \right) \left(\frac{d^2}{d\xi^2} u31(\xi) \right) \right) -EI \left(\frac{d}{d\xi} \alpha l(\xi) \right) \left(- \left(\frac{d}{d\xi} \alpha l(\xi) \right) \left(\frac{d}{d\xi} u11(\xi) \right) \right. \\
& \left. - \alpha l(\xi) \left(\frac{d^2}{d\xi^2} u11(\xi) \right) - \left(\frac{d^2}{d\xi^2} u32(\xi) \right) + \alpha l(\xi) \left(\frac{d}{d\xi} \alpha l(\xi) \right) \right) -EI \left(\right. \\
& \left. - \left(\frac{d}{d\xi} \alpha l(\xi) \right) \left(\frac{d}{d\xi} u31(\xi) \right) - \left(\frac{d}{d\xi} \alpha \omega(\xi) \right) \right) \left(\frac{d^2}{d\xi^2} u31(\xi) \right) \\
& + \left(\frac{d}{d\xi} u31(\xi) \right) \left(GAk \left(-\alpha l(\xi) \left(\frac{d}{d\xi} u31(\xi) \right) - \alpha \omega(\xi) + \frac{d}{d\xi} u12(\xi) \right) \right. \\
& \left. + EA \left(\frac{d}{d\xi} u31(\xi) \right) \left(\frac{d}{d\xi} u11(\xi) \right) \right) + \frac{1}{2} EA \left(\left(\frac{d}{d\xi} u11(\xi) \right)^2 + 2 \left(\frac{d}{d\xi} u32(\xi) \right) \right. \\
& \left. + \left(\frac{d}{d\xi} u31(\xi) \right)^2 \right) \left(\frac{d}{d\xi} u11(\xi) \right) - \frac{1}{2} GAk \left(\frac{d}{d\xi} u11(\xi) - \alpha l(\xi) \right) \alpha l(\xi)^2 \\
& + GAk \left(-\alpha l(\xi) \left(\frac{d}{d\xi} u32(\xi) \right) - \alpha \omega(\xi) \left(\frac{d}{d\xi} u31(\xi) \right) - \alpha \beta(\xi) + \frac{1}{6} \alpha l(\xi)^3 \right. \\
& \left. + \frac{d}{d\xi} u13(\xi) - \frac{1}{2} \alpha l(\xi)^2 \left(\frac{d}{d\xi} u11(\xi) \right) \right) + EI \left(\frac{d}{d\xi} \alpha l(\xi) \right)^2 \alpha l(\xi) \\
& + \left(\frac{d}{d\xi} u32(\xi) \right) GAk \left(\frac{d}{d\xi} u11(\xi) - \alpha l(\xi) \right) - \left(\frac{d}{d\xi} u11(\xi) \right) \left(-GAk \left(\frac{d}{d\xi} u11(\xi) \right) \right.
\end{aligned}$$

Complete expressions and Boundary value Problem Solving have not been included in the code above and can be provided upon request.

Defining Displacements

$$\begin{aligned} > x := x1(\xi, t); \\ & \qquad \qquad \qquad x := x1(\xi, t) \end{aligned} \tag{3}$$

$$\begin{aligned} > y := y1(\xi, t); \\ & \qquad \qquad \qquad y := y1(\xi, t) \end{aligned} \tag{4}$$

$$\begin{aligned} > z := z1(\xi, t); \\ & \qquad \qquad \qquad z := z1(\xi, t) \end{aligned} \tag{5}$$

$$\begin{aligned} > \theta := \theta1(\xi, t); \\ & \qquad \qquad \qquad \theta := \theta1(\xi, t) \end{aligned} \tag{6}$$

Expanding θ

$$\begin{aligned} > \cos\theta := 1 - \frac{\theta^2}{2}; \\ & \qquad \qquad \qquad \cos\theta := 1 - \frac{1}{2} \theta^2 \end{aligned} \tag{1}$$

$$\begin{aligned} > \sin\theta := \theta - \frac{\theta^3}{6}; \\ & \qquad \qquad \qquad \sin\theta := \theta - \frac{1}{6} \theta^3 \end{aligned} \tag{2}$$

Defining Axes and Position Vector

$$\begin{aligned} > \text{with}(\text{VectorCalculus}) : \\ > r := \langle x, 0, (\xi + z) \rangle; \\ & \qquad \qquad \qquad r := (x1(\xi, t))e_x + (\xi + z1(\xi, t))e_z \end{aligned} \tag{7}$$

$$\begin{aligned} > D1 := \langle 1, 0, 0 \rangle; \\ & \qquad \qquad \qquad D1 := e_x \end{aligned} \tag{8}$$

$$\begin{aligned} > D2 := \langle 0, 1, 0 \rangle; \\ & \qquad \qquad \qquad D2 := e_y \end{aligned} \tag{9}$$

$$\begin{aligned} > D3 := \langle 0, 0, 1 \rangle; \\ & \qquad \qquad \qquad D3 := e_z \end{aligned} \tag{10}$$

$$\begin{aligned} > d1 := \langle \cos\theta, 0, -\sin\theta \rangle; \\ & \qquad \qquad \qquad d1 := \left(1 - \frac{1}{2} \theta1(\xi, t)^2\right)e_x + \left(-\theta1(\xi, t) + \frac{1}{6} \theta1(\xi, t)^3\right)e_z \end{aligned} \tag{11}$$

$$\begin{aligned} > d2 := \langle 0, 1, 0 \rangle; \\ & \qquad \qquad \qquad d2 := e_y \end{aligned} \tag{12}$$

$$\begin{aligned} > d3 := \text{diff}(r, \xi); \\ & \qquad \qquad \qquad d3 := \left(\frac{\partial}{\partial \xi} x1(\xi, t)\right)e_x + \left(1 + \frac{\partial}{\partial \xi} z1(\xi, t)\right)e_z \end{aligned} \tag{13}$$

Strains

$$\begin{aligned} &> \gamma 3 := (d1 \cdot d3) - (D1 \cdot D3); \\ \gamma 3 &:= \left(1 - \frac{1}{2} \theta l(\xi, t)^2\right) \left(\frac{\partial}{\partial \xi} x l(\xi, t)\right) + \left(-\theta l(\xi, t) + \frac{1}{6} \theta l(\xi, t)^3\right) \left(1 + \frac{\partial}{\partial \xi} z l(\xi, t)\right) \end{aligned} \quad (14)$$

$$\begin{aligned} &> \beta 3 := (d3 \cdot d3) - (D3 \cdot D3); \\ \beta 3 &:= \left(\frac{\partial}{\partial \xi} x l(\xi, t)\right)^2 + \left(1 + \frac{\partial}{\partial \xi} z l(\xi, t)\right)^2 - 1 \end{aligned} \quad (15)$$

$$\begin{aligned} &> k13 := (\text{diff}(d1, \xi) \cdot d3) - (\text{diff}(D1, \xi) \cdot D3); \\ k13 &:= -\theta l(\xi, t) \left(\frac{\partial}{\partial \xi} \theta l(\xi, t)\right) \left(\frac{\partial}{\partial \xi} x l(\xi, t)\right) + \left(-\left(\frac{\partial}{\partial \xi} \theta l(\xi, t)\right) + \frac{1}{2} \theta l(\xi, t)^2 \left(\frac{\partial}{\partial \xi} \theta l(\xi, t)\right)\right) \left(1 + \frac{\partial}{\partial \xi} z l(\xi, t)\right) \end{aligned} \quad (16)$$

Balance Equations

$$\begin{aligned} &> \text{constants} := EA, GA, k, \\ & \qquad \qquad \qquad \text{constants} := EA, GA, k \end{aligned} \quad (17)$$

$$\begin{aligned} &> n := GA \cdot k \cdot \gamma 3 \cdot d1 + \frac{EA \cdot \beta 3 \cdot d3}{2} + EI \cdot k13 \cdot \text{diff}(d1, \xi); \\ n &:= \left(GA k \left(\left(1 - \frac{1}{2} \theta l(\xi, t)^2\right) \left(\frac{\partial}{\partial \xi} x l(\xi, t)\right) + \left(-\theta l(\xi, t) + \frac{1}{6} \theta l(\xi, t)^3\right) \left(1 + \frac{\partial}{\partial \xi} z l(\xi, t)\right) \right) \right. \\ & \quad \left. + \frac{\partial}{\partial \xi} z l(\xi, t) \right) \left(1 - \frac{1}{2} \theta l(\xi, t)^2\right) + \frac{1}{2} EA \left(\left(\frac{\partial}{\partial \xi} x l(\xi, t)\right)^2 + \left(1 + \frac{\partial}{\partial \xi} z l(\xi, t)\right)^2 \right. \\ & \quad \left. - 1 \right) \left(\frac{\partial}{\partial \xi} x l(\xi, t)\right) - EI \left(-\theta l(\xi, t) \left(\frac{\partial}{\partial \xi} \theta l(\xi, t)\right) \left(\frac{\partial}{\partial \xi} x l(\xi, t)\right) + \left(-\left(\frac{\partial}{\partial \xi} \theta l(\xi, t)\right) \right. \right. \\ & \quad \left. \left. + \frac{1}{2} \theta l(\xi, t)^2 \left(\frac{\partial}{\partial \xi} \theta l(\xi, t)\right)\right) \left(1 + \frac{\partial}{\partial \xi} z l(\xi, t)\right) \right) \theta l(\xi, t) \left(\frac{\partial}{\partial \xi} \theta l(\xi, t)\right) \Big|_{e_x} \\ & \quad + \left(GA k \left(\left(1 - \frac{1}{2} \theta l(\xi, t)^2\right) \left(\frac{\partial}{\partial \xi} x l(\xi, t)\right) + \left(-\theta l(\xi, t) + \frac{1}{6} \theta l(\xi, t)^3\right) \left(1 + \frac{\partial}{\partial \xi} z l(\xi, t)\right) \right) \right. \\ & \quad \left. + \frac{\partial}{\partial \xi} z l(\xi, t) \right) \left(-\theta l(\xi, t) + \frac{1}{6} \theta l(\xi, t)^3\right) + \frac{1}{2} EA \left(\left(\frac{\partial}{\partial \xi} x l(\xi, t)\right)^2 + \left(1 + \frac{\partial}{\partial \xi} z l(\xi, t)\right)^2 \right. \\ & \quad \left. - 1 \right) \left(1 + \frac{\partial}{\partial \xi} z l(\xi, t)\right) + EI \left(-\theta l(\xi, t) \left(\frac{\partial}{\partial \xi} \theta l(\xi, t)\right) \left(\frac{\partial}{\partial \xi} x l(\xi, t)\right) + \left(-\left(\frac{\partial}{\partial \xi} \theta l(\xi, t)\right) \right. \right. \\ & \quad \left. \left. + \frac{1}{2} \theta l(\xi, t)^2 \left(\frac{\partial}{\partial \xi} \theta l(\xi, t)\right)\right) \left(1 + \frac{\partial}{\partial \xi} z l(\xi, t)\right) \right) \left(-\left(\frac{\partial}{\partial \xi} \theta l(\xi, t)\right) + \frac{1}{2} \theta l(\xi, t)^2 \left(\frac{\partial}{\partial \xi} \theta l(\xi, t)\right) \right) \Big|_{e_z} \end{aligned} \quad (18)$$

$$\begin{aligned}
&> m := EI \cdot k13 \cdot (d1 \times d3); \\
m &:= \left(EI \left(-\theta I(\xi, t) \left(\frac{\partial}{\partial \xi} \theta I(\xi, t) \right) \left(\frac{\partial}{\partial \xi} xI(\xi, t) \right) + \left(- \left(\frac{\partial}{\partial \xi} \theta I(\xi, t) \right) + \frac{1}{2} \theta I(\xi, t) \right)^2 \left(\frac{\partial}{\partial \xi} \theta I(\xi, t) \right) \right) \left(1 + \frac{\partial}{\partial \xi} zI(\xi, t) \right) \left(\left(-\theta I(\xi, t) + \frac{1}{6} \theta I(\xi, t)^3 \right) \left(\frac{\partial}{\partial \xi} xI(\xi, t) \right) - \left(1 - \frac{1}{2} \theta I(\xi, t)^2 \right) \left(1 + \frac{\partial}{\partial \xi} zI(\xi, t) \right) \right) \right) e_y
\end{aligned} \tag{19}$$

>

ϕ As book keeping parameter for expanding series

$$\begin{aligned}
&> xI(\xi, t) := u11(\xi) \cdot \phi(t) + u12(\xi) \cdot \phi^2(t) + u13(\xi) \cdot \phi^3(t); \\
xI &:= (\xi, t) \rightarrow u11(\xi) \phi(t) + u12(\xi) \phi(t)^2 + u13(\xi) \phi(t)^3
\end{aligned} \tag{23}$$

$$\begin{aligned}
&> yI(\xi, t) := u21(\xi) \cdot \phi(t) + u22(\xi) \cdot \phi^2(t) + u23(\xi) \cdot \phi^3(t); \\
yI &:= (\xi, t) \rightarrow u21(\xi) \phi(t) + u22(\xi) \phi(t)^2 + u23(\xi) \phi(t)^3
\end{aligned} \tag{24}$$

$$\begin{aligned}
&> zI(\xi, t) := u31(\xi) \cdot \phi(t) + u32(\xi) \cdot \phi^2(t) + u33(\xi) \cdot \phi^3(t); \\
zI &:= (\xi, t) \rightarrow u31(\xi) \phi(t) + u32(\xi) \phi(t)^2 + u33(\xi) \phi(t)^3
\end{aligned} \tag{25}$$

$$\begin{aligned}
&> \theta I(\xi, t) := \alpha I(\xi) \cdot \phi(t) + \alpha 2(\xi) \cdot \phi^2(t) + \alpha 3(\xi) \cdot \phi^3(t); \\
\theta I &:= (\xi, t) \rightarrow \alpha I(\xi) \phi(t) + \alpha 2(\xi) \phi(t)^2 + \alpha 3(\xi) \phi(t)^3
\end{aligned} \tag{26}$$

Boundary Value Problem

$$\begin{aligned}
&> BV11 := \text{coeff}(n1d, \phi(t), 1); \\
BV11 &:= GAk \left(\frac{d^2}{d\xi^2} u11(\xi) - \left(\frac{d}{d\xi} \alpha I(\xi) \right) \right)
\end{aligned} \tag{30}$$

$$\begin{aligned}
&> BV12 := \text{coeff}(n3d, \phi(t), 1); \\
BV12 &:= EA \left(\frac{d^2}{d\xi^2} u31(\xi) \right)
\end{aligned} \tag{31}$$

$$\begin{aligned}
&> BV13 := \text{coeff}(m2d, \phi(t), 1); \\
BV13 &:= EI \left(\frac{d^2}{d\xi^2} \alpha I(\xi) \right) + GAk \left(\frac{d}{d\xi} u11(\xi) - \alpha I(\xi) \right)
\end{aligned} \tag{32}$$

$$\begin{aligned}
&> BV21 := \text{coeff}(n1d, \phi(t), 2); \\
BV21 &:= GAk \left(- \left(\frac{d}{d\xi} \alpha I(\xi) \right) \left(\frac{d}{d\xi} u31(\xi) \right) - \left(\frac{d}{d\xi} \alpha 2(\xi) \right) - \alpha I(\xi) \left(\frac{d^2}{d\xi^2} u31(\xi) \right) \right. \\
&\quad \left. + \frac{d^2}{d\xi^2} u12(\xi) \right) + EA \left(\frac{d^2}{d\xi^2} u31(\xi) \right) \left(\frac{d}{d\xi} u11(\xi) \right)
\end{aligned} \tag{33}$$

$$+ EA \left(\frac{d}{d\xi} u_{31}(\xi) \right) \left(\frac{d^2}{d\xi^2} u_{11}(\xi) \right)$$

> $BV22 := \text{coeff}(n3d, \phi(t), 2);$

$$\begin{aligned} BV22 := & -GAK \left(\frac{d^2}{d\xi^2} u_{11}(\xi) - \left(\frac{d}{d\xi} \alpha l(\xi) \right) \right) \alpha l(\xi) - GAK \left(\frac{d}{d\xi} u_{11}(\xi) \right. \\ & \left. - \alpha l(\xi) \right) \left(\frac{d}{d\xi} \alpha l(\xi) \right) + 2EA \left(\frac{d^2}{d\xi^2} u_{31}(\xi) \right) \left(\frac{d}{d\xi} u_{31}(\xi) \right) \\ & + \frac{1}{2} EA \left(2 \left(\frac{d^2}{d\xi^2} u_{32}(\xi) \right) + 2 \left(\frac{d}{d\xi} u_{31}(\xi) \right) \left(\frac{d^2}{d\xi^2} u_{31}(\xi) \right) \right) \\ & + 2 \left(\frac{d}{d\xi} u_{11}(\xi) \right) \left(\frac{d^2}{d\xi^2} u_{11}(\xi) \right) + 2EI \left(\frac{d^2}{d\xi^2} \alpha l(\xi) \right) \left(\frac{d}{d\xi} \alpha l(\xi) \right) \end{aligned} \quad (34)$$

> $BV31 := \text{coeff}(n1d, \phi(t), 3);$

$$\begin{aligned} BV31 := & -\frac{1}{2} GAK \left(\frac{d^2}{d\xi^2} u_{11}(\xi) - \left(\frac{d}{d\xi} \alpha l(\xi) \right) \right) \alpha l(\xi)^2 + GAK \left(\right. \\ & \left. - \left(\frac{d}{d\xi} \alpha l(\xi) \right) \left(\frac{d}{d\xi} u_{32}(\xi) \right) - \left(\frac{d}{d\xi} \alpha l(\xi) \right) \left(\frac{d}{d\xi} u_{31}(\xi) \right) - \left(\frac{d}{d\xi} \alpha s(\xi) \right) \right. \\ & \left. + \frac{1}{2} \alpha l(\xi)^2 \left(\frac{d}{d\xi} \alpha l(\xi) \right) - \alpha l(\xi) \left(\frac{d^2}{d\xi^2} u_{32}(\xi) \right) - \alpha l(\xi) \left(\frac{d^2}{d\xi^2} u_{31}(\xi) \right) \right) \\ & + \frac{d^2}{d\xi^2} u_{13}(\xi) - \frac{1}{2} \alpha l(\xi)^2 \left(\frac{d^2}{d\xi^2} u_{11}(\xi) \right) - \alpha l(\xi) \left(\frac{d}{d\xi} \alpha l(\xi) \right) \left(\frac{d}{d\xi} u_{11}(\xi) \right) \\ & - GAK \left(\frac{d}{d\xi} u_{11}(\xi) - \alpha l(\xi) \right) \alpha l(\xi) \left(\frac{d}{d\xi} \alpha l(\xi) \right) \\ & + EA \left(\frac{d^2}{d\xi^2} u_{31}(\xi) \right) \left(\frac{d}{d\xi} u_{12}(\xi) \right) + \frac{1}{2} EA \left(2 \left(\frac{d^2}{d\xi^2} u_{32}(\xi) \right) \right. \\ & \left. + 2 \left(\frac{d}{d\xi} u_{31}(\xi) \right) \left(\frac{d^2}{d\xi^2} u_{31}(\xi) \right) + 2 \left(\frac{d}{d\xi} u_{11}(\xi) \right) \left(\frac{d^2}{d\xi^2} u_{11}(\xi) \right) \right) \end{aligned} \quad (36)$$

> $BV32 := \text{coeff}(n3d, \phi(t), 3);$

$$\begin{aligned}
BV32 := & -GAk \left(\frac{d^2}{d\xi^2} u11(\xi) - \left(\frac{d}{d\xi} \alpha l(\xi) \right) \right) \alpha l(\xi) - GAk \left(\right. \\
& - \left(\frac{d}{d\xi} \alpha l(\xi) \right) \left(\frac{d}{d\xi} u31(\xi) \right) - \left(\frac{d}{d\xi} \alpha l(\xi) \right) - \alpha l(\xi) \left(\frac{d^2}{d\xi^2} u31(\xi) \right) \\
& \left. + \frac{d^2}{d\xi^2} u12(\xi) \right) \alpha l(\xi) - GAk \left(\frac{d}{d\xi} u11(\xi) - \alpha l(\xi) \right) \left(\frac{d}{d\xi} \alpha l(\xi) \right) - GAk \left(\right. \\
& - \alpha l(\xi) \left(\frac{d}{d\xi} u31(\xi) \right) - \alpha l(\xi) + \frac{d}{d\xi} u12(\xi) \left. \right) \left(\frac{d}{d\xi} \alpha l(\xi) \right) \\
& + EA \left(\frac{d^2}{d\xi^2} u31(\xi) \right) \left(\frac{d}{d\xi} u32(\xi) \right) + \frac{1}{2} EA \left(2 \left(\frac{d^2}{d\xi^2} u32(\xi) \right) \right. \\
& \left. + 2 \left(\frac{d}{d\xi} u31(\xi) \right) \left(\frac{d^2}{d\xi^2} u31(\xi) \right) + 2 \left(\frac{d}{d\xi} u11(\xi) \right) \left(\frac{d^2}{d\xi^2} u11(\xi) \right) \right) \\
& \left(\frac{d}{d\xi} u31(\xi) \right) + \frac{1}{2} EA \left(2 \left(\frac{d^2}{d\xi^2} u33(\xi) \right) + 2 \left(\frac{d}{d\xi} u31(\xi) \right) \left(\frac{d^2}{d\xi^2} u32(\xi) \right) \right. \\
& \left. + 2 \left(\frac{d}{d\xi} u32(\xi) \right) \left(\frac{d^2}{d\xi^2} u31(\xi) \right) + 2 \left(\frac{d}{d\xi} u11(\xi) \right) \left(\frac{d^2}{d\xi^2} u12(\xi) \right) \right. \\
& \left. + 2 \left(\frac{d}{d\xi} u12(\xi) \right) \left(\frac{d^2}{d\xi^2} u11(\xi) \right) \right) + EA \left(\frac{d}{d\xi} u31(\xi) \right) \left(\frac{d^2}{d\xi^2} u32(\xi) \right) \\
& + \frac{1}{2} EA \left(\left(\frac{d}{d\xi} u11(\xi) \right)^2 + 2 \left(\frac{d}{d\xi} u32(\xi) \right) + \left(\frac{d}{d\xi} u31(\xi) \right)^2 \right) \left(\frac{d^2}{d\xi^2} u31(\xi) \right) \\
& + EI \left(\frac{d^2}{d\xi^2} \alpha l(\xi) \right) \left(\frac{d}{d\xi} \alpha l(\xi) \right) - EI \left(- \left(\frac{d^2}{d\xi^2} \alpha l(\xi) \right) \left(\frac{d}{d\xi} u31(\xi) \right) \right. \\
& \left. - \left(\frac{d^2}{d\xi^2} \alpha l(\xi) \right) - \left(\frac{d}{d\xi} \alpha l(\xi) \right) \left(\frac{d^2}{d\xi^2} u31(\xi) \right) \right) \left(\frac{d}{d\xi} \alpha l(\xi) \right) \\
& + EI \left(\frac{d}{d\xi} \alpha l(\xi) \right) \left(\frac{d^2}{d\xi^2} \alpha l(\xi) \right) - EI \left(- \left(\frac{d}{d\xi} \alpha l(\xi) \right) \left(\frac{d}{d\xi} u31(\xi) \right) \right)
\end{aligned}$$

$$\begin{aligned}
&> BV33 := \text{coeff}(m2d, \phi(t), 3); \\
BV33 := & -EI \left(\frac{d^2}{d\xi^2} \alpha l(\xi) \right) \left(-\alpha l(\xi) \left(\frac{d}{d\xi} u11(\xi) \right) - \left(\frac{d}{d\xi} u32(\xi) \right) + \frac{1}{2} \alpha l(\xi)^2 \right) \\
& - EI \left(- \left(\frac{d^2}{d\xi^2} \alpha l(\xi) \right) \left(\frac{d}{d\xi} u31(\xi) \right) - \left(\frac{d^2}{d\xi^2} \alpha \omega(\xi) \right) \right. \\
& - \left. \left(\frac{d}{d\xi} \alpha l(\xi) \right) \left(\frac{d^2}{d\xi^2} u31(\xi) \right) \right) \left(\frac{d}{d\xi} u31(\xi) \right) - EI \left(\right. \\
& - \left. \left(\frac{d}{d\xi} \alpha l(\xi) \right)^2 \left(\frac{d}{d\xi} u11(\xi) \right) - \alpha l(\xi) \left(\frac{d^2}{d\xi^2} \alpha l(\xi) \right) \left(\frac{d}{d\xi} u11(\xi) \right) \right. \\
& - \alpha l(\xi) \left(\frac{d}{d\xi} \alpha l(\xi) \right) \left(\frac{d^2}{d\xi^2} u11(\xi) \right) - \left(\frac{d^2}{d\xi^2} \alpha l(\xi) \right) \left(\frac{d}{d\xi} u32(\xi) \right) \\
& - \left(\frac{d^2}{d\xi^2} \alpha \omega(\xi) \right) \left(\frac{d}{d\xi} u31(\xi) \right) - \left(\frac{d^2}{d\xi^2} \alpha \omega(\xi) \right) + \alpha l(\xi) \left(\frac{d}{d\xi} \alpha l(\xi) \right)^2 \\
& + \frac{1}{2} \alpha l(\xi)^2 \left(\frac{d^2}{d\xi^2} \alpha l(\xi) \right) - \left(\frac{d}{d\xi} \alpha l(\xi) \right) \left(\frac{d^2}{d\xi^2} u32(\xi) \right) \\
& - \left(\frac{d}{d\xi} \alpha \omega(\xi) \right) \left(\frac{d^2}{d\xi^2} u31(\xi) \right) \left. \right) - EI \left(\frac{d}{d\xi} \alpha l(\xi) \right) \left(- \left(\frac{d}{d\xi} \alpha l(\xi) \right) \left(\frac{d}{d\xi} u11(\xi) \right) \right. \\
& - \alpha l(\xi) \left(\frac{d^2}{d\xi^2} u11(\xi) \right) - \left(\frac{d^2}{d\xi^2} u32(\xi) \right) + \alpha l(\xi) \left(\frac{d}{d\xi} \alpha l(\xi) \right) \left. \right) - EI \left(\right. \\
& - \left. \left(\frac{d}{d\xi} \alpha l(\xi) \right) \left(\frac{d}{d\xi} u31(\xi) \right) - \left(\frac{d}{d\xi} \alpha \omega(\xi) \right) \right) \left(\frac{d^2}{d\xi^2} u31(\xi) \right) \\
& + \left(\frac{d}{d\xi} u31(\xi) \right) \left(GAk \left(-\alpha l(\xi) \left(\frac{d}{d\xi} u31(\xi) \right) - \alpha \omega(\xi) + \frac{d}{d\xi} u12(\xi) \right) \right. \\
& + EA \left(\frac{d}{d\xi} u31(\xi) \right) \left(\frac{d}{d\xi} u11(\xi) \right) \left. \right) + \frac{1}{2} EA \left(\left(\frac{d}{d\xi} u11(\xi) \right)^2 + 2 \left(\frac{d}{d\xi} u32(\xi) \right) \right. \\
& + \left. \left(\frac{d}{d\xi} u31(\xi) \right)^2 \right) \left(\frac{d}{d\xi} u11(\xi) \right) - \frac{1}{2} GAk \left(\frac{d}{d\xi} u11(\xi) - \alpha l(\xi) \right) \alpha l(\xi)^2 \\
& + GAk \left(-\alpha l(\xi) \left(\frac{d}{d\xi} u32(\xi) \right) - \alpha \omega(\xi) \left(\frac{d}{d\xi} u31(\xi) \right) - \alpha \omega(\xi) + \frac{1}{6} \alpha l(\xi)^3 \right. \\
& + \left. \frac{d}{d\xi} u13(\xi) - \frac{1}{2} \alpha l(\xi)^2 \left(\frac{d}{d\xi} u11(\xi) \right) \right) + EI \left(\frac{d}{d\xi} \alpha l(\xi) \right)^2 \alpha l(\xi) \\
& + \left(\frac{d}{d\xi} u32(\xi) \right) GAk \left(\frac{d}{d\xi} u11(\xi) - \alpha l(\xi) \right) - \left(\frac{d}{d\xi} u11(\xi) \right) \left(-GAk \left(\frac{d}{d\xi} u11(\xi) \right) \right.
\end{aligned}$$

Complete expressions and Boundary value Problem Solving have not been included in the code above and can be provided upon request.

BIBLIOGRAPHY

- ❖ Abdalla, M. M., Reddy, C. K., Faris, W. F., and Gürdal, Z., “Optimal Design of an Electrostatically Actuated Microbeam for Maximum Pull-in Voltage,” *Computers and Structures*, Vol. 83, pp. 1320-1329, 2005.
- ❖ Antman, S.S., “Nonlinear Problems of Elasticity,” Springer-Verlag, New York Inc, 1972.
- ❖ Baruh, H., “Analytical Dynamics,” McGraw Hill Companies Inc., Chapter-7,8, 1999.
- ❖ Cohen, H., and Muncaster, R.G., “The dynamics of pseudo-rigid bodies: general structure and exact solutions,” *J. Elast.* 14, pp. 127–154 L, 1984.
- ❖ Currano, L., “Experimental and Finite Element Analysis of Piezoelectrically Driven MEMS Actuators,” M.S. Thesis, Department of Mechanical Engineering, University of Maryland, College Park, 2002.
- ❖ DeVoe, D. L., “Thin Film Zinc Oxide Microsensors and Microactuators,” Ph.D. Thesis, Department of Mechanical Engineering, U.C. Berkeley, 1997.
- ❖ Eringen, A.C., “Theory of micro-polar elasticity,” Liebowitz, H. (Ed.), *Fracture – An Advanced Treatise*, vol. II. Academic Press, New York, pp. 621–693.F, 1968.

- ❖ Fabula.T, Wagner, H.-J., and Schmidt, B., “Triple-beam Resonant Silicon Force Sensor Based on Piezoelectric Thin Films,” *Sensors and Actuators A: Physical*, Vol. 42, pp. 257-280, 1994.
- ❖ Funk.K, T., Fabula, G., Flik and Larmer, F., “Piezoelectrical Driven Resonant Force Sensor: Fabrication and Cross Talk,” *Journal of Micromechanics and Microengineering*, Vol. 5, pp. 143-146, 1995.
- ❖ Green, A.E., Naghdi, P.M., and Wenner, M.L., “On the theory of rods I: derivations from the three-dimensional equations,” *Proc. Royal Soc. Lond. A* A337, pp. 451–483, 1974.
- ❖ Herbert, G., “Classical Mechanics,” Addison-Wesley Publishing Co., Inc., 1952.
- ❖ R. T. Howe and R.S. Muller, “Integrated Resonant-microbridge Vapor Sensor,” *IEEE International Electronic Devices Meeting*, San Francisco, California, December 10 12, pp. 213-216, 1984.
- ❖ A. Husain, J., Hone, H. W. C., Postma, X. M. H., Huang, T., Drake, M., Barbic, A., Scherer, and M. L. Roukes, “Nanowire-based Very-high-frequency Electromechanical Resonator,” *Applied Physics Letters*, Vol. 83, Issue 6, pp. 1240-1242, 2003.
- ❖ Jog, C.S, “Higher-order shell elements based on a Cosserat model, and their use in the topology design of structures,” *Computer Methods in Applied Mechanics and Engineering* 193(23-26):pp. 2191-2220.K, 2004.

- ❖ Kunin, I.A, “Elastic Media with Microstructure II,” Springer Verlag, Berlin, 1983.
- ❖ Krishnakumar,S and Foster,C.G, “ Axial load capacity of cylindrical shells with local geometric defects,” J. of Experimental Mechanics , volume 31, number 2, pp.104-110,1990.
- ❖ Kirchhoff , Euler, L., “Additamentum I de curvis elasticis, Methodus inveniendi lineas curvas maximi minimi proprietate gaudentes,”. In: Opera Omnia I, Vol. 24. Bousquet, Lausanne, pp. 231–297, 1744.
- ❖ Kumar,P, Li, L., Calhoun, Li., Boudreaux, P., and DeVoe, D., “Fabrication of Piezoelectric Al_{0.3}Ga_{0.7}As Microstructures,” *Sensors and Actuators A: Physical*, Vol. 115, pp. 96-103, 2004.
- ❖ Kreizig, E., “Advanced Engineering Mathematics,” John Wiley& Sons, Inc., Chapter-5,13, 2005.
- ❖ Li, H., and Balachandran, B., “Nonlinear Oscillations of Micromechanical Oscillators,” Proceedings of the ASME International Design Engineering Technical Conferences, Chicago, 2003.
- ❖ Liu, Zhengxing, Li, Dejian, “Numerical analysis of geometric imperfection influence on the safety of cylindrical shell,” *Computers and Structures*. Vol. 41, no. 3, pp. 547-551. 1991.

- ❖ Lin, L., Howe, R. T., and Pisano, A. P., “Microelectromechanical Filters for Signal Processing,” *Journal of Microelectromechanical Systems*, Vol. 7, No. 3, pp. 286-294, 1998.
- ❖ Mullem, C.J.V., Blom, F.R., Fluitman, J., and Elwenspoek, M., “Piezoelectrically Driven Silicon Beam Free Sensor,” *Sensors and Actuators A: Physical*, Vol. 26, pp. 279-283, 1991.
- ❖ Meirovitch, L., “Fundamentals of Vibration,” McGraw-Hill Book Co-Singapore, Chapter6, pp.268-273, 2001.
- ❖ Naghdi, P.M. and Rubin, M.B “Constrained theories of rods,” *J. Elasticity*. 14, pp. 343–361, 1984.
- ❖ Nguyen, C.T.-C., Wang, K., Wong, A.C., “VHF Free-Free Beam High-Q Micromechanical Resonators,” *Journal of Microelectromechanical Systems*, Vol.9, No.3, pp. 347-359, 2000.
- ❖ Nguyen, C.T.-C., and Wang, K., “High-order Micromechanical Electronic Filters,” *Proceedings of the 1997 IEEE International MEMS Workshop*, pp. 25-30, 1997.
- ❖ Nguyen, C.T.-C., and Howe, R. T., “An Integrated CMOS Micromechanical Resonator High-Q Oscillator,” *IEEE Journal of Solid-State Circuits*, Vol. 34, No.4, 1999.

- ❖ O'Reilly, M., and Vardi, P.C., "A unified treatment of constraints in the theory of a Cosserat point," *J. Math. Phys. (ZAMP)* 49, pp. 205–223, 1998.
- ❖ O'Reilly, M., Pisano, A.P., Wyatt, A., "Nonlinear dynamics of tether suspension," *Journal of Vibration and Acoustics*, Vol.126, pp.326-331, 2004.
- ❖ Pai, D. K., "STRANDS: Interactive Simulation of Thin Solids using Cosserat Models," *Eurographics*, Vol. 21, No.3, 2002.
- ❖ Prak, A., Elwenspoek M., and Fluitman, J., "Selective Mode Excitation and Detection of Micromachined Resonators," *Journal of Microelectromechanical Systems*, Vol.1, No.4, pp. 170-178, Dec. 1992.
- ❖ Piekarski, B., DeVoe, D., Dubey, M., Kaul, R., Conrad J., and Zeto, R., "Surface Micromachined Piezoelectric Resonant Beam Filters," *Sensors and actuators A: Physical*, Vol. 91, pp. 313-320, 2001.
- ❖ Paul, O., and Baltes,H., "Mechanical Behavior and Sound Generation Efficiency of Prestressed, Elastically Clamped and Thermomechanically Driven Thin Film Sandwiches," *Journal of Micromechanics and Microengineering*, Vol.9, pp.19-29, 1999.
- ❖ Postma, H. W. Ch., Kozinsky, I., Husain A., and Roukes, M. L., "Dynamic Range of Nanotube- and Nanowire-based Electromechanical Systems," *Applied Physics Letters*, Vol. 86, Issue 22, No.223105, 2005.

- ❖ Ramsey, H., “Elastic isotropic cylindrical shells,” *The Quarterly Journal of Mechanics and Applied Mathematics*, Volume 40, Number 3, pp 415-429, 1987.
- ❖ Rubin, M.B., “The theory of a Cosserat point and its application to the numerical solution of continuum problems,” *ASME J. Appl. Mech.* 52, pp. 368–372, 1985.
- ❖ Rubin, M.B., “Free vibration of a rectangular parallelepiped using the theory of a Cosserat point,” *ASME J. Appl. Mech.* 53, pp. 45–50, 1986.
- ❖ Rubin, M.B., “Numerical solution of nonlinear string problems using theory of a Cosserat point. *Int. J. Solids Struct.* 23, pp. 335–349, 1987.
- ❖ Rubin M.B., “Restrictions on nonlinear constitutive equations for elastic rods,” *J. Elast.* 44, pp. 9–36, 1996.
- ❖ Rubin, M. B., and Benveniste, Y., “A Cosserat Shell Model for Interphases in Elastic Media,” *J. Mech. Phys. Solids*, 52, 1023-1052, 2004.
- ❖ Rubin, M.B., “Cosserat Theories: shells, rods and points,” Kluwer Academic Publishers, Dordrecht, The Netherlands, 2000.
- ❖ Roessig, T., Howe, R.T., and Pisano, A.P., “Surface Micromachined Resonant Accelerometer,” *Proceedings of Transducers '97*, Vol. 2, pp. 859-862, 1997.
- ❖ Raskin, J. P., Brown, A. R., Khuri-Yakub, B., and Rebeiz, G. M., “A Novel Parametric-effect MEMS Amplifier,” *Journal of Microelectromechanical Systems*, Vol, 9, No. 4, pp. 528-537, Dec. 2000.

- ❖ Simo, J.C., “A finite strain beam formulation. The three-dimensional dynamic problem part I,” *Comp. Meth. Appl. Mech. Engng*, Vol 49, pp. 55–70, 1985.
- ❖ Simo, J.C., and Vu-Quoc, L., “A three-dimensional finite strain rod model part II. Computational aspects” *Comp. Meth. Appl. Mech. Engng*. 58, pp. 79–116, 1986
- ❖ Simo.J.C., Rifai, M.S., and Fox, D.D., “a stress resultant geometrically exact shell model part IV: variable thickness shells with through-the thickness stretching,” *Comp. Meth. Appl. Mech. Engng*. 81, pp. 91–126, 1990.
- ❖ Slawainowski J.J., “Newtonian dynamics of homogeneous strains,” *Arch. Mech*. 26, pp. 569–587, 1975.
- ❖ Slawainowski J.J., “The mechanics of the homogeneously-deformable body. Dynamical models with high symmetries,” *S. Angew. Math. Mech*. 62, pp. 229–240, 1982.
- ❖ Sansour and Bednarczyk, “The cosserat surface as a shell model theory and finite element formulation,” *Comput.methods Appl. Mech Engrg* 120, pp:1-32, 1995.
- ❖ Shaw, S.W., Turner, K.L., Rhoads, J.F., and Baskaran, R., "Parametrically Excited MEMS-Based Filters," *Proceedings of the IUTAM Symposium on Chaotic Dynamics and Control of Systems and Processes in Mechanics*, Rome, Italy, 2003.

- ❖ Turner, K. L., Miller, S. A., Hartwell, P.G., Macdonald, N.C., Strogartz , S.H., and Adams, S.G., “Five Parametric Resonances in a Microelectromechanical System,” *Nature*, Vol. 396, pp. 149-152, 1998.
- ❖ Valverde, Escalona, Dominguez, and Champneys, “Stability and Bifurcation Analysis of a Spinning Space Tether,” *J. Nonlinear Sci*, Vol. 16: pp. 507–542, 2006.
- ❖ Weisbord, L., “Single Beam Force Transducer with Integral Mounting Isolation,” US Patent #3470400, 1969.
- ❖ Wagner, B., Quenzer, H., Hoerschelmann, S., Lisek, T., and Juerss, M., "Bistable Microvalve with Pneumatically Coupled Membranes," in: *Proceedings of IEEE MEMS 1996 Conference*, pp.384-338, 1996.
- ❖ Wang, Charles H.-T., Dongsheng Liu, D.Q. Cao, “Computational Cosserat Dynamics in MEMS Component Modelling,” *Computational Mechanics*, 2004.

